ELSEVIER Volume 137, March 2021, 110465

Catalytic methane decomposition to boost the energy transition: Scientific and technological advancements

Luís Alves [1], Vítor Pereira [1], Tiago Lagarteira, Adélio Mendes

https://doi.org/10.1016/j.rser.2020.110465

Highlights

- Catalytic methane decomposition is a promising pathway for the energy transition.
- Catalysts and reactor designs have been optimized to increase reaction stability.
- Carbon is a valuable by-product with the potential creation of new markets.
- Catalyst regeneration must be employed and optimized for long-term stability.

Abstract

Decarbonization of the energy sector is a topic of paramount importance to avoid irreversible global warming. Hydrogen has been considered as the most suitable option to replace fossil fuels in industrial, residential and transport applications. However, hydrogen production has been almost limited to the reforming of hydrocarbons, which release large amounts of CO2, thus requiring several downstream purification processes.

Catalytic methane decomposition consists of the low-temperature cracking of methane, producing only COx-free hydrogen and solid carbon. This process has the unique potential to make the swift transition for a fully decarbonized economy and beyond: the methane decomposition of biomethane removes CO2 from the atmosphere at competitive costs. Yet, industrialization of catalytic methane decomposition has been hindered by the insufficient stability assigned to catalyst deactivation due to carbon clogging.

This article reviews not only the main accomplishments on methane decomposition since it was firstly reported, but also addresses technical barriers that have hindered its industrialization. Unlike other previous reviews that focused mainly on catalysts, more attention was put on the reactor design, catalyst regeneration strategies and processing of products (hydrogen purification and economic overview). The goal is to identify challenges and provide solutions for the industrialization paradigm that methane decomposition has faced up to now.

Elsevier Editorial System(tm) for Renewable & Sustainable Energy Reviews
Manuscript Draft

Manuscript Number: RSER-D-20-00761

Title: Catalytic methane decomposition to boost the energy transition: Scientific and technological advancements

Article Type: Review Article

Section/Category: Hydrogen

Keywords: catalytic methane decomposition; energy transition; hydrogen; COx-free; carbon; catalyst regeneration

Corresponding Author: Professor Adelio Mendes, PhD

Corresponding Author's Institution: FEUP

First Author: Luís Alves

Order of Authors: Luís Alves; Vítor Pereira; Tiago Lagarteira; Adelio Mendes, PhD

Abstract: Decarbonization of the energy sector is a topic of paramount importance to avoid irreversible global warming. Hydrogen has been considered as the most suitable option to replace fossil fuels in industrial, residential and transport applications. However, hydrogen production has been almost limited to the reforming of hydrocarbons, which release large amounts of CO2, thus requiring several downstream purification processes.
Catalytic methane decomposition consists of the low-temperature cracking of methane, producing only COx-free hydrogen and solid carbon. This process has the unique potential to make the swift transition for a fully decarbonized economy and beyond: the methane decomposition of biomethane removes CO2 from the atmosphere at competitive costs. Yet, industrialization of catalytic methane decomposition has been hindered by the insufficient stability assigned to catalyst deactivation due to carbon clogging.
This article reviews not only the main accomplishments on methane decomposition since it was firstly reported, but also addresses technical barriers that have hindered its industrialization. Unlike other previous reviews that focused mainly on catalysts, more attention was put on the reactor design, catalyst regeneration strategies and processing of products (hydrogen purification and economic overview). The goal is to identify challenges and provide solutions for the industrialization paradigm that methane decomposition has faced up to now.

Suggested Reviewers: Yogdan Li
Tianjin University
ydli@tju.edu.cn

Roberto Solimene
Istituto di Ricerche sulla Combustione
solimene@irc.cnr.it

Manoj Pudukudy
Universiti Kebangsaan Malaysia
manojpudukudy@gmail.com

Opposed Reviewers:

Porto, 06th of March 2020

Dear Editors,

Please find enclosed the manuscript *"Catalytic methane decomposition to boost the energy transition: Scientific and technological advancements"*. I would appreciate if you could consider this review article for publication in *Renewable and Sustainable Energy Reviews*.

Decarbonization of the energy sector is an urgent matter, requiring swift response to avoid irreversible climate changes. Renewable energy sources are expected to be the future of the energy sector, but their intermittency requires the development of efficient, versatile and cheap energy storage systems.

Catalytic methane decomposition (CMD) is one of the strongest contenders to fill the gap in the energy transition. The submitted manuscript is a thorough revision of the challenges and advancements of catalytic methane decomposition focusing on catalysts, reactor designs, catalyst regeneration and process economics. CMD is capable of transforming methane into H_2 and solid carbon without CO_x generation, producing clean fuel-cell grade H_2 while taking advantage of currently existing infrastructures. Furthermore, the decomposition of biomethane allows the cost effective removal of CO_2 from the atmosphere. As of now, catalyst deactivation, caused by carbon deposition over the catalyst surface, has hindered the industrialization of the process: regeneration of the deactivated catalyst is possible, but the most studied methods rely on gasification technics with high CO_x evolution. Our research group is currently working on a disruptive catalyst regeneration approach, which aims at loosening carbon deposits by partial methanation at the carbon-catalyst interface (at the expense of a small portion of the produced H_2). With this manuscript we intend to organize and summarize the current knowledge on CMD, in anticipation of our own developments on the technology.

The above-mentioned manuscript consists of original, unpublished work and has not been submitted to any other journal for review.

Sincerely,

Adélio Mendes

LEPABE – Laboratory for Process Engineering, Environment, Biotechnology and Energy
Rua do Dr. Roberto Frias, s/n – 4200-465 Porto Portugal
Tel.: 22 508 1687 Email: lepabe@fe.up.pt www.lepabe.fe.up.pt

Catalytic methane decomposition to boost the energy transition: Scientific and technological advancements

Luís Alves[1], Vítor Pereira[1],Tiago Lagarteira, Adélio Mendes[*]

LEPABE - Laboratory for Process Engineering, Environmental, Biotechnology and Energy, Faculty of Engineering, University of Porto, Rua Dr. Roberto Frias, 4200-465 Porto, Portugal

Abstract

Decarbonization of the energy sector is a topic of paramount importance to avoid irreversible global warming. Hydrogen has been considered as the most suitable option to replace fossil fuels in industrial, residential and transport applications. However, hydrogen production has been almost limited to the reforming of hydrocarbons, which release large amounts of CO_2, thus requiring several downstream purification processes.

Catalytic methane decomposition consists of the low-temperature cracking of methane, producing only CO_x-free hydrogen and solid carbon. This process has the unique potential to make the swift transition for a fully decarbonized economy and beyond: the methane decomposition of biomethane removes CO_2 from the atmosphere at competitive costs. Yet, industrialization of catalytic methane decomposition has been hindered by the insufficient stability assigned to catalyst deactivation due to carbon clogging.

This article reviews not only the main accomplishments on methane decomposition since it was firstly reported, but also addresses technical barriers that have hindered its industrialization. Unlike other previous reviews that focused mainly on catalysts, more attention was put on the reactor design, catalyst regeneration strategies and processing of products (hydrogen purification and economic overview). The goal is to

[*] This is to indicate the corresponding author.
Email address: mendes@fe.up.pt (A. Mendes)
[1] The first two authors contributed equally to this work.

identify challenges and provide solutions for the industrialization paradigm that methane decomposition has faced up to now.

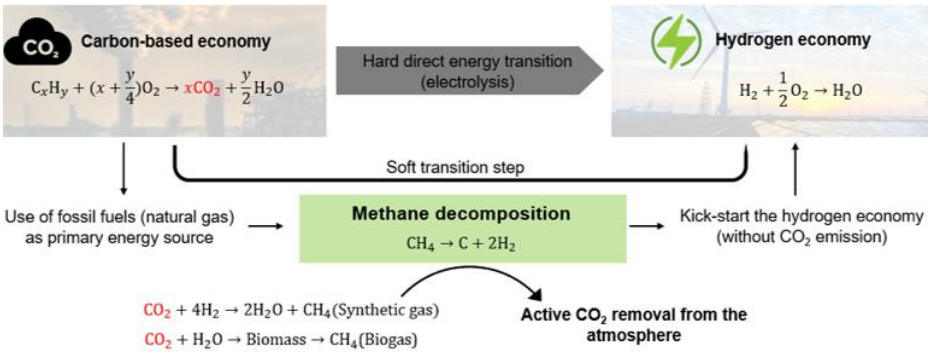

Highlights:

Catalytic methane decomposition is a promising pathway for the energy transition;

Catalysts and reactor designs have been optimized to increase reaction stability;

Carbon is a valuable by-product with the potential creation of new markets;

Catalyst regeneration must be employed and optimized for long-term stability.

Keywords: catalytic methane decomposition, energy transition, hydrogen, CO_x-free, carbon, catalyst regeneration

Word count: 9898 words

Abbreviations:

CMD	catalytic methane decomposition
AC	activated carbon
CNT	carbon nanotube
MWCNT	multi-walled carbon nanotube

SWCNT	single-walled carbon nanotube

Nomenclature:

Activity	hydrogen activity/production	$g_{H2} \cdot g_{cat}^{-1} \cdot h^{-1}$
Feed	methane feed stream	$dm^3_{CH4} \cdot g_{cat}^{-1} \cdot h^{-1}$ / $g_{CH4} \cdot g_{cat}^{-1} \cdot h^{-1}$
T	temperature	K
d_m	metal particle diameter	nm
X_{CH4}	average conversion	%
t	time on stream	h
$\frac{m_c}{W}$	carbon/catalyst ratio	$g_c \cdot g_{cat}^{-1}$
$-r_{CH4}$	reaction rate	$mol \cdot m^{-3} \cdot s^{-1}$
k	reaction rate coefficient	$mol \cdot m^{-3} \cdot Pa^{-0.5} \cdot s^{-1}$
P_{CH4}	methane partial pressure	Pa
E_c	elutriation rate	$g \cdot s^{-1}$
k_a	attrition constant	m^{-1}
$(U - U_{mf})$	fluidization excess velocity	$m \cdot s^{-1}$
W_c	carbon mass	g
$\Delta H^0_{298\,K}$	reaction enthalpy	$kJ \cdot mol^{-1}$

1. Introduction

Decarbonization is an urgent matter, as climate changes threaten to destabilize Earth's climate [1], altering Weather patterns and destroying current ecosystems, beyond recovery [2]. Competing with the need to stop carbon emissions,

is the ever-increasing demand for energy [3]. Figure 1 shows the CO_2 concentration history in the atmosphere, from 1958 to 2020, measured at the Mauna Loa Observatory [4].

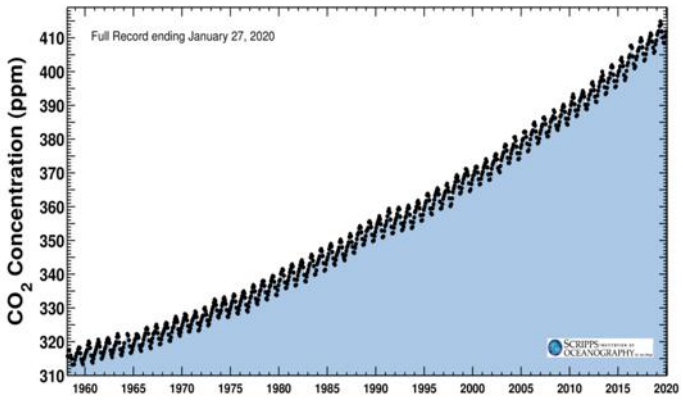

Figure 1 - Carbon dioxide concentration (ppm) from 1958 to 2020 (extracted from [4]).

Renewable energy sources have, for years, been the main focus of research to tackle CO_x production, being a central point of the Paris agreement [5]. While these technologies are widely accepted as the future for clean electricity production [6], certain limitations hamper the possibility of directly using their energy, namely, intermittency [7] and hard storability [8] make them only periodically available.

To address these issues, hydrogen has been proposed as a form of clean energy storage [9], ideally being produced by renewable-powered electrolysis [10]. Many initiatives are already in progress for the implementation of the so-called hydrogen-economy. For example, Hydrogen Europe [11] is a European hydrogen and fuel cell association that represents multiple industry companies and research organizations and is geared towards helping the foreseen energy transition, promoting research and development of hydrogen and fuel cell technologies. In a similar note,

the Hydrogen Council [12] was created from a coalition of CEOs from leading energy, transportation and industry companies, which promotes the investment on hydrogen-based technologies and reinforces, to policy-makers and general society, that hydrogen is the most viable alternative in the upcoming energy transition. However, hydrogen produced by electrolysis accounts only for 2 % of all produced molecular hydrogen (which does not exist abundantly in nature). Moreover, scale-up is yet challenging [13], with hydrogen production costs of 3.2-6.4 €·kg_{H2}^{-1} from solar energy and 2.3-4.6 €·kg_{H2}^{-1} from wind [14].

While water electrolysis remains uncompetitive [15], alternative processes for large scale hydrogen production must be used to start-up the development of structures capable of processing hydrogen as a fuel: storage [16], distribution [17] and usage (favorably fuel cells) [18]. Furthermore, geopolitical barriers to the transition towards clean energy sources have to be considered, as many countries are unwilling to fully transition their energy sector as long as there are fossil fuels within their borders [19–21]. As such, the production of hydrogen from fossil fuels renders a softer transition. Currently, from the 115 Mt of hydrogen produced yearly, 78 % are obtained from hydrocarbons and 18 % from coal [22]. The processes associated with these shares include: steam-reforming (equation (1)) [23], dry-reforming (equation (2)) [24], partial oxidation (equation (3)) [25], coal gasification (equation (4)) [26], and water gas shift reaction (equation (5)) [27]; and produce up to 830 Mt_{CO2}·yr^{-1} [18].

$$CH_4(g) + H_2O(g) \rightarrow 3H_2(g) + CO(g), \qquad \Delta H^0_{298\,K} = 206.2\ \mathrm{kJ \cdot mol^{-1}} \qquad (1)$$

$$CH_4(g) + CO_2(g) \rightarrow 2H_2(g) + 2CO(g), \qquad \Delta H^0_{298\,K} = 247\ \mathrm{kJ \cdot mol^{-1}} \qquad (2)$$

$$CH_4(g) + \frac{1}{2}O_2(g) \rightarrow 2H_2(g) + CO(g), \qquad \Delta H^0_{298\,K} = -72\ \text{kJ} \cdot \text{mol}^{-1} \tag{3}$$

$$C_nH_m(\text{coal}) + nH_2O(g) \rightarrow \left(n + \frac{m}{2}\right)H_2(g) + nCO(g), \qquad \text{Endothermic} \tag{4}$$

$$CO(g) + H_2O(g) \rightarrow CO_2(g) + H_2(g), \qquad \Delta H^0_{298\,K} = -41.09\ \text{kJ} \cdot \text{mol}^{-1} \tag{5}$$

Among these processes, steam-reforming is the cheapest and most used, with a cost of *ca.* 1.4 €·kg_{H2}^{-1} [28]. Dry-reforming, partial oxidation of methane and coal gasification processes are only competitive when CO_2 or coal are plentiful or when the use of an endothermic process is challenging [29], with production costs higher than 1.8 €·kg_{H2}^{-1} [14]. These processes release large amounts of CO_2, not only harming the environment but also risking their own viability, as the rapidly increasing tariffs on CO_2 emissions lead to the implementation of extensive down-stream treatments. As such, additional separation steps [30] and carbon capture and storage (CCS) [31] or carbon capture and valorization (CCV) [32] technologies have to be often considered.

Alternative, cost-effective, hydrogen production processes without releasing greenhouse effect gases are required [33]. Methane decomposition (equation (6)) [34] consists of cracking the methane molecule, producing CO_x-free hydrogen and solid carbon:

$$CH_4(g) \rightleftharpoons C(s) + 2H_2(g), \qquad \Delta H^0_{298\,K} = 74.8\ \text{kJ} \cdot \text{mol}^{-1} \tag{6}$$

The process is attractive for H_2 production since methane from natural gas is a fossil fuel with extensive and well-developed extraction, storage and distribution structures [35]. Moreover, if bio or synthetic methane are used as feed-streams, methane decomposition can be used to actively remove CO_2 from the atmosphere [36], as these

potential feed-streams originate directly (synthetic) [37] or indirectly (bio) [38] from CO_2. Operation costs are expected to be higher than those for steam-reforming (in the range of 1.8 €·kg_{H2}^{-1} [39]) but, H_2 is easily purified [40] (methane is the only other gas taking part in the reaction [41]). The only secondary product is solid carbon, contrasting with reforming processes where secondary products are gaseous, poisonous (particularly for fuel-cells[42]), hard to separate and contribute for greenhouse effects [43]. Since methane decomposition is an endothermic reaction, its energy requirements can be integrated with the heat released from fuel cells [44] or "Sabatier" reaction [45], increasing the overall energy efficiency of these processes.

Methane decomposition equilibrium conversion increases with the temperature since it is an endothermic reaction [46,47], but the uncatalyzed reaction kinetics is only reasonable at temperatures over 1300 °C [34], which is too high for becoming cost-effective [48]. The use of catalysts allows low-temperature operation: 450-650 °C [49], however, poor stability assigned to catalyst deactivation by carbon coverage has hindered industrial interest [50]. Carbon structures formed during the reaction may grow directly over the catalyst surface, covering the active sites (base-growth mechanism), or in the case of supported metal catalysts, carbon filaments can grow between the metal-support interface separating the metal from the support, permanently altering the catalyst (tip-growth mechanism) [51]. The growth mechanism for carbon particles impacts directly on the catalyst stability and it depends on several variables such as the catalyst itself, the reaction temperature, gas partial pressures and reactor design.

Many attempts have been proposed to increase stability, but none succeeded in more than a couple hundred hours of operation. Most reported approaches focus on

catalyst development [52–55] but, reactor design [56–60] and regeneration strategies [61] have also been receiving some attention. Our research group has, recently, performed a proof-of-concept experiment that delivers nearly full stability, largely outperforming the previous operation record of 210 h [62]. This result relies in an innovative cyclic regeneration step, consisting of the selective methanation of carbon at the carbon-catalyst interface [63]. This new approach has the potential for becoming the transition step between the current framework and the future renewable-powered hydrogen-economy. Another relevant challenge for CMD is the flow of carbon products into the market value-chain. There are already developed markets for carbon, such as nanotubes [64], activated carbon [65], carbon black [66], metallurgical coke [67] and carbon fillers [68].

To develop a compact, stable and thermally efficient low-temperature methane decomposition reactor, it is necessary to summarize past accomplishments and organize the disperse work on methane decomposition. Since most of the reviews focus mostly on the catalyst development, this work addresses other critical aspects for the methane decomposition process potential industrialization, such as, reactor design, operation strategies, catalyst regeneration and economical assessment.

2. First works on catalytic methane decomposition

The first works on catalytic methane decomposition (CMD) were published at the beginning of the 20th century [69,70]. Slater [69] reported iron and charcoal as the best catalysts among the materials tested (silica, alumina, magnesia, lime, barium oxide, wood charcoal, graphite, silicon carbide, graphite, iron, and copper). During

the following years, the focus was put on understanding the reaction mechanism [71]. Most authors proposed complex mechanisms based on the formation of methyl radicals [72] and larger hydrocarbons [73]. With the same purpose, during the 60s and following years, plasma and electric discharges were also used for assessing the reaction mechanism and similar conclusions were reported [74,75]. Plasma reactors were also used for producing carbon materials [76] and synthetic diamond [77]. During the 70s the formation of whiskers-like carbon nanomaterials in the CMD reaction with a nickel catalyst was reported for the first time [78].

In the 90s, there was an exponential increase in the number of publications about CMD, again focusing on the reaction mechanism. Some authors still argued that the reaction initiates with a methyl radical which causes multiple chain reactions [79], leading to the formation and consumption of C_2-C_6 hydrocarbons [80,81]; while other authors argued for the adsorption of methane in the catalyst surface, with consequent stepwise dehydrogenation and hydrogen desorption [82], followed by the carbon diffusion and deposition [83,84]. There is no consensus regarding the mechanism, but the latter gradually became the most accepted one [85]. Carbon deposition began to be the main focus of works, focusing on the growing rate [86], morphology [87] and type of carbon structures formed during CMD, such as nanofibers [88] and nanotubes [89]. It is reported that elemental carbon diffuses through the metal catalyst, and depending on the operation conditions and material interactions, carbon will either i) precipitate over the exposed face of the catalyst, generating carbon structures that grow from the base over the metal (strong metal-support interaction leads to base-growth) [90]; or ii) the catalyst will get partially or completely detached from the support (or from the bulk in the case of unsupported catalysts), raising the metal particle and growing from

the tip, where the metal is located (weak metal-support interaction leads to tip-growth) [91].

By the end of the 20th century, extensive research was devoted for developing processes to produce hydrogen with the required purity and quantity for the envisioned hydrogen-economy. In 2001, Muradov proposed, in a seminal report, the use of the methane decomposition reaction for decarbonization of the energy sector. The methane decomposition reaction displays very high selectivity and the product gas stream contains only hydrogen and unreacted methane, complying with standard ISO 14687, which requires CO concentration lower than 0.2 ppm [92]. However, by that time, the CMD processes displayed very low stability, just a few hours on stream, and moderate catalytic activities, in the range of 1 $g_{H2}{\cdot}g_{Cat}^{-1}{\cdot}h^{-1}$. Aiming to produce enough clean hydrogen to feed the hydrogen-economy, the stability of CMD catalysts became the main topic of research since then.

3. Metal catalysts

Transition metals are known to be the most active materials for the dissociation of hydrocarbons, due to their partially filled 3d orbitals, which allow the acceptance of electrons [51]. The temperature at which thermal decomposition of methane occurs is *ca.* 1300 °C (without any catalyst) due to the very strong C- H bond (440 $kJ{\cdot}mol^{-1}$). If metal catalysts are used, they decrease the temperature to the range of 450 °C to 750 °C [49]. Nickel, iron and cobalt are particularly active, being considered the most suitable metals to catalyze methane decomposition [93]. In the 90s, Ermakova *et al.* [94] reported 21.6 $g_{H2}{\cdot}g_{Cat}^{-1}{\cdot}h^{-1}$ of activity, during 6 h: the highest

yield at the time (*ca.* 385 $g_C \cdot g_{Ni}^{-1}$), at 550 °C with a 90 wt.% Ni/SiO_2 catalyst. For the first time, the CMD reaction was recognized as a promising pathway to produce CO_x-free hydrogen [95].

Nickel-based catalysts have the highest activity but are not stable at temperatures above 650 °C [96], while iron and cobalt-based catalysts, despite their lower activity, can withstand higher temperatures and produce carbon materials with higher market value [49]. Despite the efforts aimed at increasing activity and stability of monometallic catalysts, it was not possible so far to overcome deactivation, by coke formation, for pilot or industrial scales. Therefore, the combination of multiple metals started being used on catalysts, marking the development of the second generation of catalysts for CMD reaction.

Among the possible combinations of the most active metals, more attention was devoted on the combination of nickel and iron. The most significant difference between Fe and Ni-based catalysts is the maximum operating temperature. When combined, Ni-Fe catalysts can maintain activity at higher temperatures than Ni-based catalysts alone [97]. For Ni-based mixtures, the new structure consists of a Ni-Fe alloy, with no reported evidence of metallic iron [98]. Despite having lower activity than the monometallic catalysts, Ni-Fe alloy catalysts tend to display higher carbon diffusivity and therefore higher stability. Adding increasing concentrations of Fe to a Ni-based catalyst enhances stability until an optimal composition is reached. Wang *et al.* [62] used a $Ni-Fe/Al_2O_3$ with a molar ratio of 2Ni:1Fe:1Al for performing the CMD reaction at 650 °C. They reported a stable activity of *ca.* 0.9 $g_{H2} \cdot g_{Cat}^{-1} \cdot h^{-1}$ during 210 h. The authors attributed such high stability to the enhanced ratio between atomic carbon diffusivity through the catalyst particle and reaction rate, by adding Fe: in pure

Ni, at high temperature, methane cracking is faster than carbon diffusion (small ratio between diffusion and reaction rates), causing carbon accumulation at the surface (encapsulation/deactivation).

Iron is widely studied as a dopant in Ni-based catalysts, but most transition metals have also been studied. Arevalo *et al.* [99] utilized density functional theory (DFT) to study the decomposition of methane in stepped Ni and in stepped Ni doped with other transition metals. They reported the formation of a 5-coordinated bond between atomic carbon and the Ni layers, depicted in Figure 2 a), which both explains Ni reactivity towards carbon production and its ease of deactivation due to strongly adsorbed carbon blocking the active sites. When doped/alloyed with other transition metals this bond may weaken or strengthen, depending on the dopant. While metals like Au destroy the strong interaction between Ni and carbon, hampering CMD reaction, other metals like Fe, Co or Ru act as limiters, weakening the 5-coordinated without destroying it completely, as is depicted in Figure 2 b) Ru and c) Au. As such, Ni, when doped with the latter metals, tends to be less active than the pure metal, but shows enhanced stability.

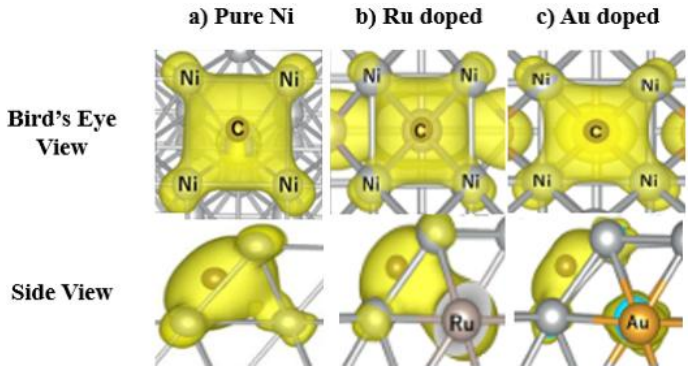

Figure 2 - Bird's eye and side view of carbon adsorbed in pure (a) and doped (b-Ru, c-Au) stepped Ni (adapted from [99]).

Another transition metal that is widely investigated as a promoter, predominantly on Ni-based catalysts, is copper [100]. Copper alone has low activity for the CMD reaction but several works have been using copper as a promoting agent in Ni-based metals [101]. These works report a large increase in the activity of the catalysts without fast deactivation [102]. As it can be observed in Table 1, Ni-Cu catalysts are able to achieve the highest activity among all catalysts tested for the CMD reaction. In most catalysts, for higher activities, stability is frequently very low, in the range of 3-5 h: with this type of Cu doped Ni-catalysts, more than 20 h on stream are often observed [103]. Shen and Lua [104] tested carbon nanotubes as a support for Ni-Cu catalysts. They were able to obtain a maximum activity of approximately 4.4 $g_{H2} \cdot g_{Cat}^{-1} \cdot h^{-1}$ and 30 h on stream, using a Ni-Cu/CNT catalyst at 700 °C, as shown in Figure 3.

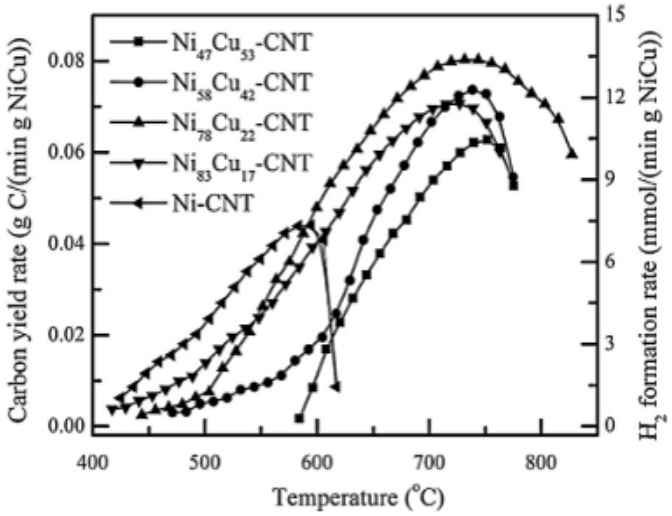

Figure 3 – Temperature-dependent activities of CNT-supported Ni-Cu-based catalysts (extracted from [104]).

Table 1 compares many of the best performing combinations of metal catalysts to date, accounting for: metal molar composition, reaction temperature (T), catalyst shape, metal particle diameter (d_m), methane feed, average activity, average conversion ($X_{\mathrm{CH_4}}$), time on stream (t) and mass ratio of carbon and catalyst at t ($\frac{m_C}{W}$). Catalysts are ordered from the highest $\frac{m_C}{W}$ to the lowest.

Other attempts to enhance the performance of CMD catalysts used noble metals as promoters, mainly platinum [105] and palladium [106]. Carbon diffusion is much faster on Pt and Pd than that on nickel, cobalt or iron [107]. This attribute improves the catalyst stability which results in lifetime increase [90,108]. As observed in

Table 2, doping metal catalysts with small amounts of either noble metal has a positive impact on the overall catalyst performance.

Table 1 - Comparing bi and trimetallic metal catalysts.

Catalyst	T / °C	Catalyst shape	d_m / nm	Feed / $g_{CH4}{\cdot}g_{Cat}^{-1}{\cdot}h^{-1}$	Activity / $g_{H2}{\cdot}g_{Cat}^{-1}{\cdot}h^{-1}$	X_{CH_4} / %	t / h	$\frac{m_C}{W}$ / $g_C{\cdot}g_{cat}^{-1}$
50Ni-25Fe/Al_2O_3[62]	650	Fine powder	40	8.58	0.892	42	>210	>562
75Ni-15Cu/ Al_2O_3[102]	625	n/a	20-25	64.29	3.241	20	54	525
82Ni-8Cu/ Al_2O_3[102]	625	n/a	20-25	64.29	2.791	17	62	515
60Ni-25Cu/SiO_2[109]	650	Fine powder	9	64.29	5.333	33	30	480
24Ni-6Cu/MgO[110]	665	Fine powder	38	51.43	3.378	26	45	456
62Fe-8Ni/Al_2O_3[93]	625	n/a	25-50	32.14	0.755	22	64	145
50Ni-10Fe-10Cu/Al_2O_3[108]	750	Slab	20	2.57	0.521	81	10	15.62
15Fe-3Ni/MgO[111]	700	Fine powder	3	2.14	0.386	72	3	3.47
30Fe-15Co/Al_2O_3[112]	700	Slab	5-40	2.14	0.380	71	3	3.42
30Fe-10Ni-5Co/Al_2O_3[112]	700	Slab	5-40	2.14	0.375	70	3	3.38
15Fe-6Co/MgO[111]	700	Fine powder	3	2.14	0.375	70	3	3.38
15Fe-6Mn/MgO[111]	700	Fine powder	5	2.14	0.375	70	3	3.38
30Fe-5Ni-10Co/Al_2O_3[112]	700	Slab	5-40	2.14	0.370	69	3	3.33
30Fe-7.5Ni-7.5Co/Al_2O_3[112]	700	Slab	5-40	2.14	0.359	67	3	3.23
25Ni-25Co/SBA-15[113]	700	Fine powder	20	3.57	0.171	19	5	2.57

Table 2 - Pt and Pd doping on metal catalysts used in CMD.

Catalyst	T / °C	Catalyst shape	d_m / nm	Feed / $g_{CH4}{\cdot}g_{Cat}^{-1}{\cdot}h^{-1}$	Activity / $g_{H2}{\cdot}g_{Cat}^{-1}{\cdot}h^{-1}$	X_{CH_4} / %	t / h	$\frac{m_C}{W}$ / $g_C{\cdot}g_{cat}^{-1}$
Ni/CeO_2[105]	700	Fine powder	50-100	3.21	0.183	23	6	3.30
0.2%wt Pt-Ni/CeO_2[105]	700	Fine powder	30-70	3.21	0.197	25	6	3.55
55Ni-15Cu[106]	600	Fine powder	20	5.14	0.746	58	10	22.37
55Ni-15Cu-4Pd[106]	600	Fine powder	25	5.14	0.771	60	10	23.14

3.1 Synthesis methods and catalyst supports

Beyond the metals used in CMD, optimization of the catalysts is also highly dependent on the synthesis methods [114] and the catalyst support [115]. Different preparation methods have been tested to optimize the lifetime of catalysts [116,117]. Echegoyen *et al.* [118] studied the influence of the preparation method on a Ni/MgO_2 catalyst. These authors prepared the catalysts by co-precipitation, impregnation and fusion. They reported that the major difference between the three catalysts was the particle size before and after the reaction. During the reaction, the co-precipitated and impregnated catalysts suffered sintering, which increased their metal particle size, while the opposite behavior was observed on the catalysts prepared by fusion. Hydrogen production increased in the following order: impregnated, co-precipitated and fused catalysts; particle size increased in the opposite order. Particle size is indeed one of the catalyst characteristics that influence their activity and mechanism of formation of carbon materials [119]. Li *et al.* [120] reported that the optimal crystallite size, for an unsupported nickel catalyst powder of 250-425 μm, is 10- 20 nm, resulting in an activity of approximately 1.57- 1.77 $g_{H2} \cdot g_{Cat}^{-1} \cdot h^{-1}$ (corresponding to a carbon yield of 354-398 $g_C \cdot g_{Ni}^{-1}$), which proved to be stable during approximately 70 h, at 500 °C. On the other hand, Wang *et al.* [121] analyzed the CMD reaction with a 23.3 wt.% Ni/SiO_2 catalyst, prepared with two different methods that resulted in different particle size distributions. They reported that particles with a size between 10-100 nm produced carbon nanofilaments and smaller particles (<10 nm) produced amorphous carbon that rapidly encapsulate the metal particles. Takenaka *et al.* [122] also claimed that particles with a size between

60- 100 nm had the greatest lifetime during the reaction when studying different loadings of metal in a Ni/SiO_2 catalyst.

For the production of supported metal catalysts, calcination and reduction steps are necessary [123]. The temperatures at which these processes are performed have a strong influence on the catalyst characteristics [124], mainly in terms of particle size and metal-support interaction [52,125]. Echegoyen *et al.* [126] studied the influence of the calcination temperature on a Ni/AlO_2 catalyst and found that the optimal calcination temperature was *ca.* 600 °C. They reported that increasing the calcination temperature hinders the reducibility of the catalyst not only due to the increase of particle size but also due to the formation of $NiAl_2O_4$ spinel phase: the reduction temperature is highly dependent on the type of metal, unreduced particle size and support [127]. Typically, higher reduction temperatures result in higher quantity of metal particles in the reduced state thus increasing the catalytic activity, since metal oxides do not catalyze the reaction [128]. Finally, reduction temperature also causes a decrease in the catalyst specific area which affects its activity and stability [129].

The catalyst support plays a relevant role in the catalytic activity, namely the loading and size of metallic particles and on the metal-support interaction. The most used catalyst supports are of SiO_2 or Al_2O_3. Takenaka *et al.* [115] tested several supports (SiO_2, TiO_2, graphite, ZrO_2, $SiO_2{\cdot}Al_2O_3$, Al_2O_3, $MgO{\cdot}SiO_2$, MgO), as depicted in Figure 4, and reported that SiO_2, TiO_2 and graphite are the supports with the highest carbon yields, at 500 °C: 199 $g_C{\cdot}g_{Ni}^{-1}$, 136 $g_C{\cdot}g_{Ni}^{-1}$ and 114 $g_C{\cdot}g_{Ni}^{-1}$, respectively. The remaining supports led to fast deactivation. The authors attributed

the lower activity to the formation of highly stable support phases with NiO during calcination, making the latter harder to reduce.

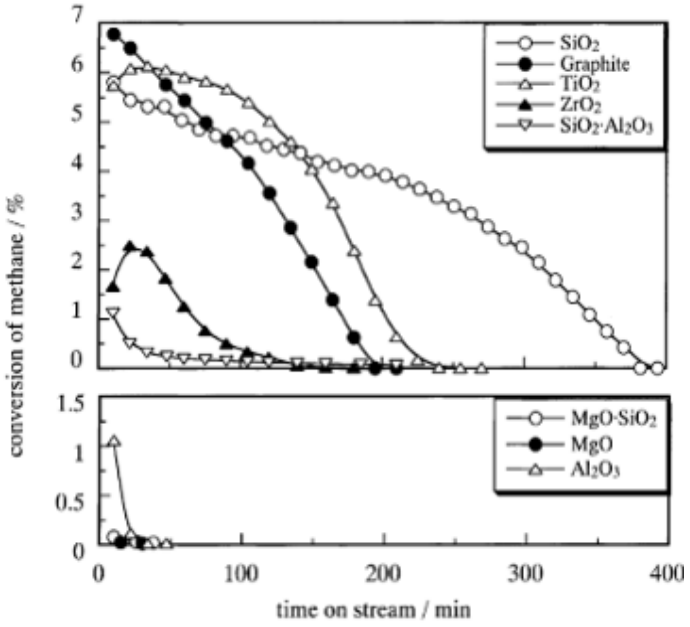

Figure 4 - Methane conversion on supported Ni catalysts in multiple supports, at 500 °C (extracted from [115]).

In a similar work [130], the same authors tested different supports (MgO, Al_2O_3, SiO_2, and TiO_2) on a cobalt-based catalyst, at 500 °C. In this case, the best performance was assigned to Co/Al_2O_3, with carbon yield of 56 $g_C \cdot g_{Co}^{-1}$. The Co catalyst supported on Al_2O_3 was easily reduced since no stable phases were formed, unlike for Ni-based ones, where the formation of stable $NiAl_2O_4$ spinel phase hinders reducibility. The same authors [115] also performed CMD using SiO_2 supports with different pore structures. SiO_2 with wider pores yielded the highest activity, of *ca.* 0.5 $g_{H2} \cdot g_{Cat}^{-1} \cdot h^{-1}$. This result suggests that pore size and volume of the catalyst support

are critical parameters for the growth of carbon structures, as small-sized pores get easily clogged [131,132].

La_2O_3 perovskite-type supports were also tested for the CMD reaction [133]. Maneerung *et al.* [134] compared $LaNiO_3$ perovskite with La_2O_3 for supporting Ni-based catalysts prepared by wet impregnation. The major differences between these two catalysts are the metal support interaction and the metal particle size distribution [135]. In the perovskite support, nickel particles are better attached and more dispersed [136]. This enhanced metal support interaction increases the sintering resistance of the catalyst and makes it capable of operating at higher temperatures, displaying a good stability up to 800 °C [137]. The size distribution of the catalyst particles, in the perovskite, is narrower, *ca.* 24 nm, resulting in higher uniformity of carbon nanomaterials [138].

Other supports that have been tested are carbon materials [139]. Otsuka *et al.* [140] used different carbon structures (graphitized carbon fibers, vapor-grown carbon fibers, graphite powder, activated carbon powder and carbon nanofibers laboratory-made from the decomposition of hydrocarbons) to support nickel catalyst particles prepared by impregnation. These authors reported that the highest activity was achieved using laboratory-synthesized carbon nanofibers. They stated that carbon materials with micropore structure had low activity due to the collision of the growing nanofibers with the pore walls. After optimizing the production of nanofibers and nickel loading, they were able to obtain an average activity of 1.8 $g_{H2} \cdot g_{Cat}^{-1} \cdot h^{-1}$ with a lifetime of *ca.* 20 h.

4. Carbon catalysts

Carbon materials have been investigated as catalysts for CMD [141] since they are cheaper and more resistant to poisoning, when compared to metals [49]. Several carbon structures have been tested, like activated carbon (AC) [142] and carbon black [143], which are the most investigated carbon materials for this reaction [50]. However, activation energy on ACs and carbon blacks (between 100 and 300 $kJ \cdot mol^{-1}$) [144] are considerably higher than those observed for metals (65-75 $kJ \cdot mol^{-1}$) [102]. For achieving appreciable activity, carbon catalysts are typically used at temperatures above 750 °C [50]. Carbon catalyst are, though, more stable than the metal catalysts when running at these high temperatures [145].

Guil-Lopez *et al.* [146] compared Ni and Fe-based catalysts, AC, carbon black, multi-walled carbon nanotubes (MWCNTs) and graphite, at 1100 °C. Metal catalysts show the highest initial activity, however, at this temperature, carbon catalysts generally show better stability, as can be illustrated in Figure 5. Among carbon catalysts, carbon black and AC showed the highest initial activity; carbon black was distinctly more stable. MWCNTs and graphite presented small initial activities, due to their more crystalline structure. Most authors correlate the amount of surface defects on carbon to its activity in CMD [50]. As for stability, MWCNTs are very stable, despite their small activity, while graphite deactivates rapidly. Carbon nanotubes generate graphitic carbon, increasing the number of walls and maintaining the original structure, while graphite gets gradually covered by less active carbon, causing gradual deactivation.

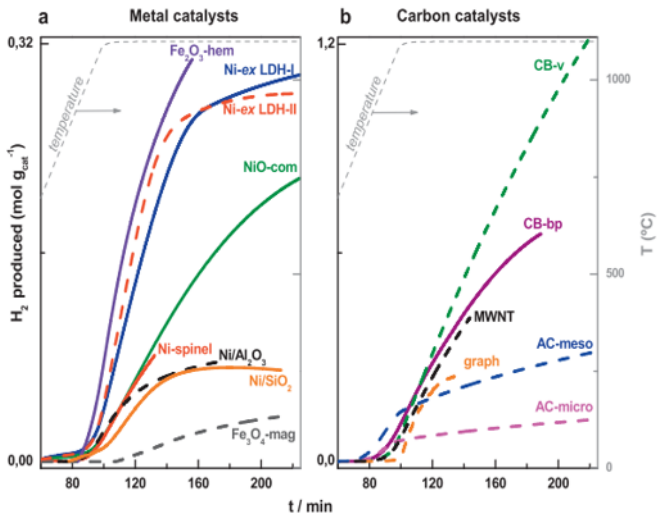

Figure 5 - Total hydrogen produced by each metal catalyst (a) and each carbon catalyst (b), along time on stream, at 1100 °C (extracted from [146]).

Muradov has made extensive research in CMD, mostly using carbon materials as catalysts [147]. One of these studies [148] compares AC, carbon black, acetylene black, glassy carbon, diamond powder, MWCNTs, graphite and fullerenes as catalysts, at 850 °C. AC catalysts displayed the highest initial activity, between 0.37 and 0.50 $g_{H2} \cdot g_{Cat}^{-1} \cdot h^{-1}$, which quickly dropped, reaching less than 25 % of the initial activities, after 90 min on stream. Carbon black and acetylene black catalysts were the most stable, maintaining constant activities between 0.03 and 0.20 $g_{H2} \cdot g_{Cat}^{-1} \cdot h^{-1}$ (increasing surface area and pore volume, catalysts become more active), during the tested time on stream (70 min). Fullerenes show both smaller activity and stability than AC and carbon black, but using fullerene soot it was possible to achieve both a high initial activity, 0.45 $g_{H2} \cdot g_{Cat}^{-1} \cdot h^{-1}$ (on par with AC), and high stability, 0.30 $g_{H2} \cdot g_{Cat}^{-1} \cdot h^{-1}$ during the entire experience (60 min). All other

carbon materials tested in this work show very small activity and stability, and were considered unsuitable to catalyze CMD.

Carbon catalysts have their advantages but ultimately metal catalysts are much more efficient, allowing low-temperature operation and easier optimization, by combining different metals and supports. Furthermore, carbon catalysts are generally harder to regenerate without damaging the catalyst itself, hindering long-term operation.

5. Catalytic Methane Decomposition at industrial scale

Alongside the development of catalysts, the CMD reactor design has been studied and optimized. It soon became clear that the formation of carbon materials, which ultimately causes the deactivation of the catalyst, is a major challenge concerning the reactor design [149]. Furthermore, catalyst optimization is mostly done at laboratory scale, rarely considering the need for industrial-scale synthesis of catalysts. Synthesis methods, calcination and reduction conditions often differ between scales: industrial catalysts are often pelletized [150] or impregnated in macrostructured supports [151] (in contrast to powders often used in small scale or batch operation), which impacts their performance [152]. Reactors must be designed for running the CMD reaction itself, while enabling possible energy integration with other processes nearby; for instance, the CMD running temperature and pressure should be designed so that they allow thermal integration with available industrial utilities [153].

The first studies regarding reactor design were performed in fixed-bed reactors [49,154], but this configuration was reported to be ineffective. Clogging [131,132] and pressure build-up [155] in the reactor were the main causes for a low production of hydrogen. Other alternatives started to be tested to avoid these problems; fluidized-bed reactors became the favored design. Alternatively, plasma reactors were also assessed and, more recently, new technologies comprising the use of molten metal reactors were reported.

5.1 Fluidized-bed reactors

Fluidized-bed reactors have multiple applications in metallurgical, petroleum and chemical industries [156]. The continuous flow of solids through the reaction zone enables the withdrawal of the carbon products. At an industrial scale, this is a major advantage since, in fixed-beds, the operation must be stopped to remove the formed carbon [157]. Moreover, high heat and mass transfer rates achieved with the fluidization of the reaction zone allow for: i) easy process optimization to maximize the catalyst lifetime; ii) maintaining a constant and homogeneous reactor temperature in the reaction volume [158,159].

5.1.1 Early reactors

A fluidized-bed CMD reactor was patented for the first time in the 1960s by the Universal Oil Products Company [160]. They used a Ni catalyst to produce hydrogen and carbon, which was combusted to regenerate the catalyst and provide

heat for the endothermic reaction. The initial research regarding a fluidized-bed reactor had the objective to improve the performance of the reactor or to extend the lifetime of the catalyst. Weizhong *et al.* [161] performed CMD, in a two-stage fluidized-bed reactor packed with Ni-Cu/Al_2O_3 catalyst. Each separate stage was kept at two different temperatures (500 and 850 °C). This reactor configuration increased the catalyst lifetime, compared to single-stage fluidized-bed reactors at the same temperature; the comparative results are depicted in Figure 6. With this configuration, the authors were able to maintain approximately 40 % conversion, using a feedstream of 4.68 $dm^3_{CH4} \cdot g_{cat}^{-1} \cdot h^{-1}$, for 17 h at 850 °C (1123 K). In the upper stage, the required high temperature for high conversion was maintained, while the lower temperature, at the lower reactor stage, enabled a stable operation for several hours.

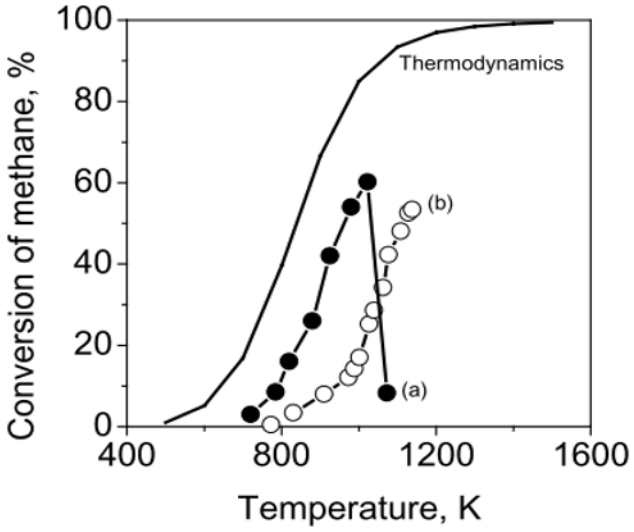

Figure 6 - Methane conversion at different temperatures: a) single-stage; b) two-stage (extracted from [161]).

Another modification to extend the lifetime of the catalyst was proposed by Shah *et al.* [162]. They implemented an alternating method between fixed-bed and fluidized-bed operations. CMD reaction proceeded in the fixed-bed reactor at 700 °C (0.6 $dm^3_{CH4} \cdot g_{cat}^{-1} \cdot h^{-1}$), which was periodically fluidized (6 $dm^3_{CH4} \cdot g_{cat}^{-1} \cdot h^{-1}$) to promote the detachment of carbon from the catalyst. Nevertheless, the periodically fluidized-bed reactor could not release enough carbon from the catalyst active sites and outperform the standard fixed-bed reactor, Figure 7.

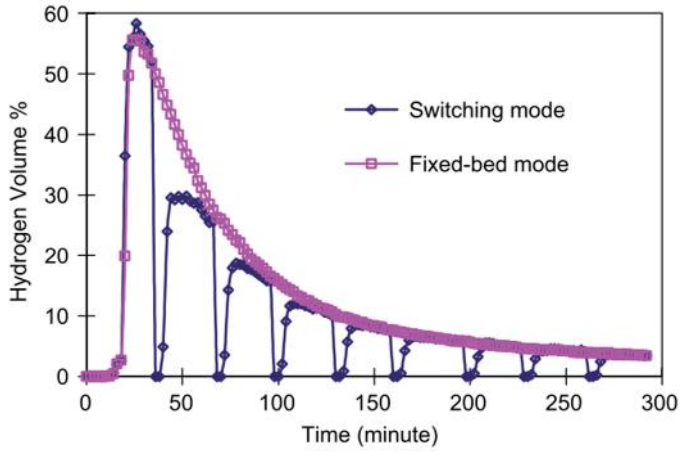

Figure 7 - Hydrogen yield in fixed-bed and switching mode, at 700 °C (extracted from [162]).

5.1.2 Reaction parameters and optimization

To optimize the fluidized-bed reactor design, several authors performed parametric studies on the major variables that influence the process, namely temperature, space velocity and feed composition. These authors concluded that methane conversion was always controlled by the intrinsic kinetics of the reaction

[163], similarly as reported for fixed-bed reactors [155]. An increase in reaction temperature tends to increase the conversion due to the endothermic nature of the CMD reaction: for Ni-based catalysts, there is an increase in activity until *ca.* 650 °C. Above that temperature, carbon production is faster than the diffusion through the metal particle (responsible for the creation of carbon structures) [164], leading to carbon accumulation at the surface of the catalyst, decrease of activity and early deactivation by full encapsulation of the active sites [165]. Iron-based catalysts can operate at higher temperatures, up to *ca.* 800 °C [166]. Although the reaction equilibrium conversion increase with the temperature, the reaction mechanism also changes and different carbon allotropes or amorphous carbon are formed. Often, an increase in the reaction kinetics leads to an overall smaller production of carbon and hydrogen during the catalyst lifetime, as higher reaction rates also lead to earlier deactivation [167].

Space velocity has a high impact, not only in the conversion but also on the quality of bed fluidization in a fluidized-bed reactor [168]. An increase in space velocity causes an improvement in the degree of fluidization of the bed, increasing the contact between the gas and the solid phase [169] and lowering the risk of defluidization. But, the formation of bubbles at higher space velocities decreases the overall conversion since bubbles flow through the reactor with minimum contact with the catalyst [170].

Suelves *et al.* [171] tested different space velocities (24-1200 $dm^3_{CH4} \cdot g_{cat}^{-1} \cdot h^{-1}$) in a fluidized-bed, at 700 °C, using Ni-Cu/Al_2O_3 catalyst, as seen in Figure 8. The authors reported an increase in the carbon capacity from 15.8 $g_C \cdot g_{cat}^{-1}$, using a space velocity of 24 $dm^3_{CH4} \cdot g_{cat}^{-1} \cdot h^{-1}$ during 3 h, to 141 $g_C \cdot g_{cat}^{-1}$,

using a space velocity of 1200 $dm^3_{CH4} \cdot g_{cat}^{-1} \cdot h^{-1}$; however, the latter completely deactivated after 2 h of experiment. The initial catalytic activity for both space velocities were 1.25 $g_{H2} \cdot g_{Cat}^{-1} \cdot h^{-1}$ and 16 $g_{H2} \cdot g_{Cat}^{-1} \cdot h^{-1}$, respectively. These results support their conclusion that the rate of carbon formation substantially increases with space velocity. As it is reported for higher temperatures, using excessive flow leads to carbon accumulation, as carbon diffusion limits the formation of carbon structures, thus causing a faster catalyst deactivation.

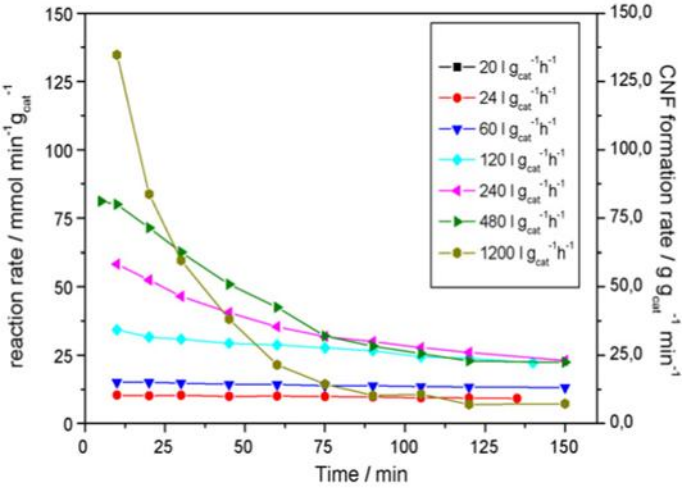

Figure 8 - Influence of GHSV on the evolution of hydrogen, at 700 °C (extracted from [171]).

Taking into account the purity of the inlet current, it has been also reported that the presence of hydrogen in the feed composition decreases the formation of encapsulating carbon, thus extending the catalyst lifetime [172]. The amount of hydrogen in the feed must be small since it influences the reaction equilibrium as it is one of the reaction products [173]. The presence of CO_2 at the feed stream was also studied since it is present in natural gas [174], synthetic gas [175] and biomass [176]

as sources of methane. Inaba *et al.* [177] studied CMD at 740 °C on a Fe/Al_2O_3 catalyst using feed streams of methane with different concentrations of CO_2, from 0 to 3 % (total feed stream of 6 $dm^3 \cdot g_{cat}^{-1} \cdot h^{-1}$). These authors concluded that for higher CO_2 concentration, >3 %, dry-reforming occurs instead of CMD [149]. However, for small CO_2 concentrations, 1-2 %, the stability of the catalyst was enhanced, as shown in Figure 9.

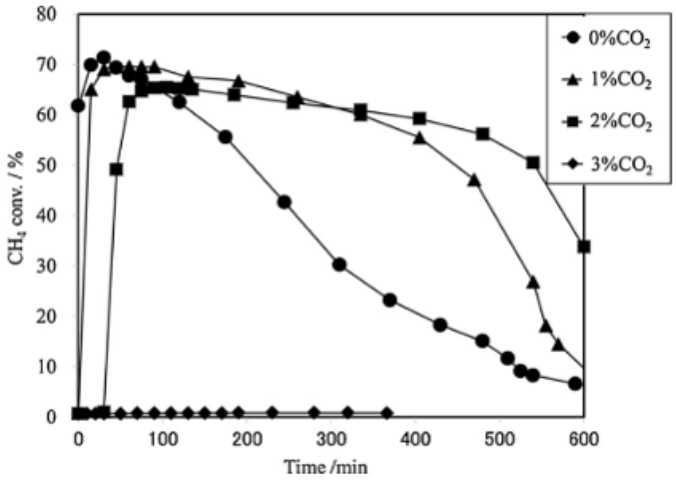

Figure 9 - Effect of CO_2 presence in the methane feed, at 740 °C (extracted from [177]).

5.1.3 Phenomenological modeling

Alongside the study of process parameters in fluidized-bed reactors, at laboratory scale, some authors developed phenomenological models to predict the behavior of this process at an industrial scale. Muradov *et al.* [57] developed a model to simulate a large-scale CMD unit for hydrogen production (21 $t \cdot day^{-1}$ of hydrogen),

using two fluidized-beds to alternately perform the cracking of methane and the regeneration of the activated carbon catalyst. In this process, carbon is moved from the cracking bed, either to be stored or to go for the second fluidized-bed to be oxidized to recover the catalytic activity (produced carbon is more amorphous than activated carbon, as such, it can be gasified without harming the catalyst too much) and to provide energy for the cracking reactor. They developed two different models for this process: in the first case, the reactor operates under a bubbling fluidized regime and in the second it operates under a turbulent fluidized regime. The objective was to scale-up a fluidized-bed reactor to meet the target production. The authors considered a CMD conversion, determined experimentally, of 38 %, at 850 °C, and the reaction kinetics expressed by equation (7):

$$-r_{CH_4} = kP_{CH_4}^{0.5} \quad (7)$$

where the CMD rate, $-r_{CH_4}$, in mol·m^{-3}·s^{-1}, is dictated by the methane partial pressure, P_{CH_4}, in Pa, and the reaction rate coefficient, k, in mol·m^{-3}·Pa$^{-0.5}$·s^{-1}. The reactor was designed based on the necessary carbon production rate to meet the energy requirements of the endothermic reaction, from the combustion of the produced carbon. The parameters estimated by the model are very close to values obtained experimentally, Figure 10.

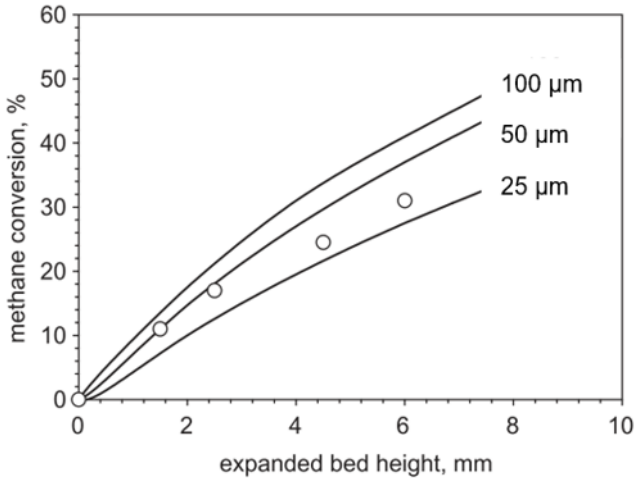

Figure 10 - Comparison of predicted and measured conversion as a function of expanded bed height, at 850 °C. Circles: experimental; Lines: modeling with 25, 50 and 100 µm particle sizes (extracted from [57]).

Ammendola *et al.* [178] developed a model for a CMD fluidized-bed reactor based on different concepts. This model takes into account three different phenomena: catalytic decomposition of methane over the metal catalyst, catalyst deactivation due to carbon deposition and the attrition-based removal of carbon deposited on the exterior surface of the bed particles, Figure 11.

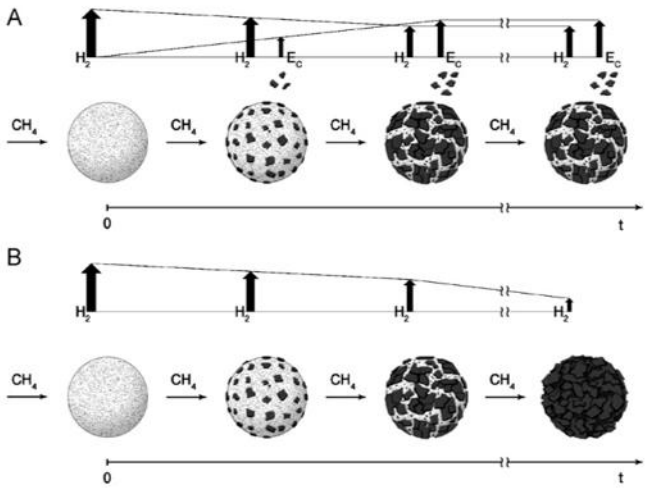

Figure 11 - Conceptual representation of a bed particle A - presence of attrition; B - absence of attrition (extracted from [178]).

To simulate the hydrodynamics of the fluidized-bed, the authors used a two-phase model, coupled with a semi-empirical correlation for bubble size as a function of bubble coalescence and volume change. Regarding the reaction kinetics, they assumed a first-order reaction with respect to methane. In addition, this model takes into account that carbon products may also catalyze the reaction (also first-order reaction with respect to methane). The catalytic deactivation was predicted assuming carbon deposition on the external and internal surface of the bed particles. The amount of carbon deposits was calculated as a function of time and the reaction rate, which is proportional to methane concentration. The methane concentration profile inside the particle was estimated through Thiele's number. The removal of carbon was based on the collision between bed particles, which makes the attached carbon

deposits, at their external surface, fall-off. The detached coke particles elutriated according to equation (8):

$$E_C = k_a(U - U_{mf})W_c \quad (8)$$

where carbon elutriation rate, E_C, in g·s^{-1}, is proportional to the attrition constant, k_a, in m^{-1}, to the fluidization excess velocity, $(U - U_{mf})$, in m·s^{-1}, and to the carbon mass, W_c, in g. Figure 12 compares the model results and experimental data, at 800 °C. The authors reported that for most experimental conditions, the model was able to predict the methane conversion within a relative error lower than ± 10 %. Moreover, for the tested operation conditions, the authors concluded that the contribution of attrition between particles, to renew the external catalyst activity, was very low (conversion change, between models considering attrition and models not considering it, was less than 1 %). But, from a sensitivity analysis, carbon attrition was found to play a key role in the regeneration of the external catalyst surface when the reaction rate is high (high temperature) or the catalyst particles are small-sized.

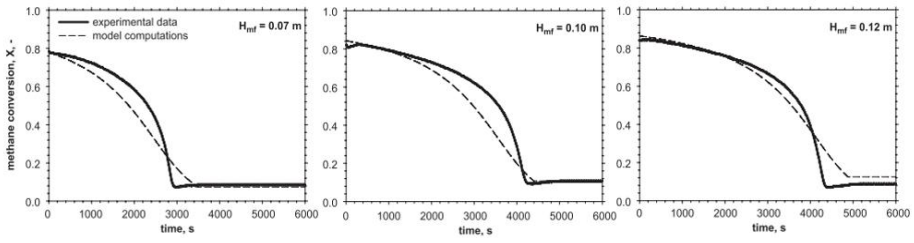

Figure 12 - Comparison of calculated and experimental conversions for different bed heights, at 800 °C (adapted from [178]).

5.2 Plasma reactors

By the end of the 20th century, the first studies on methane decomposition using plasma related technologies started to be developed [179]. Various plasma reactor configurations, namely, dielectric barrier discharge (DBD) [180,181], corona discharge [182–184], glow discharge [185,186], microwave [187,188], gliding arc [189,190] and spark discharge [191,192] have been used to investigate the conversion of methane. One of the biggest drawbacks of using plasma technology is the formation of heavier hydrocarbons (mainly C2 and C3), alongside hydrogen [193]. For example, Figure 13 depicts a simplified reactionary system, which considers the formation of hydrogen and C2 hydrocarbons, proposed by Kheirollahivash *et al.* [194]. According to these authors, the ratio between reactionary products (H_2, C_2H_6, C_2H_4 and C_2H_2) depends on the concentration of CH_x or H radicals.

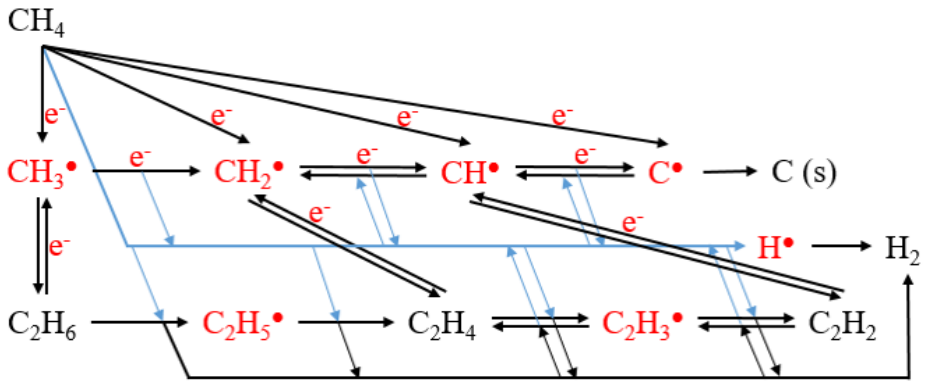

Figure 13 - Proposed reaction pathways for methane decomposition in plasma reactors (adapted from [194]).

Methane decomposition was conducted for the first time in a plasma reactor in 1998 [179]. Hsieh *et al.* [179] used a radio frequency plasma to study the conversion of methane; they used an argon/methane feed and studied the influence of methane concentration, pressure, total gas flow rate and input electric power. After conducting their experiments at different conditions, they were able to obtain methane conversions ranging from 30.2 % to 88.8 %. However, *ca.* 10 % to 30 % of methane was converted to C_2H_2, C_2H_4 and C_2H_6 instead of hydrogen and solid carbon. These results also demonstrate that methane conversion increases with the power input. On the other hand, it decreases for lower operational pressure, CH_4 concentration in the feed and total feed flow rate.

The use of a catalytic packed bed for the CMD reaction in the plasma reactors was later studied by other authors. Indarto [58] tested a DBD plasma reactor packed with mixed oxides of zinc and chromium catalysts, at ambient temperature, using a methane flow rate of 1.8 $dm^3_{CH4} \cdot g_{cat}^{-1} \cdot h^{-1}$, voltage of 10 kV and pulse frequency of 20 kHz. The power supply was increased to promote the formation of active species that could activate the catalyst surface. At the beginning, this reactor displayed higher conversion and higher hydrogen selectivity than the equivalent non-catalytic plasma reactor. However, after 8 h of operation, the conversion decreased to similar levels. Khalifeh *et al.* [195] also performed experiments with a packed bed plasma reactor at room temperature, using methane flow rates in the range of 0.15-2.4 $dm^3_{CH4} \cdot h^{-1}$, argon flow rates in the range of 1.5-12 $dm^3_{Ar} \cdot h^{-1}$, voltage in the range of 6-14 kV and frequency in the range of 0.9-10 kHz, testing three different configurations: plasma alone; packed bed with glass particles (9.7 g); and catalytic packed bed (5.9 g of Pt-Re/Al_2O_3). Figure 14 summarizes the results obtained by

these authors. Glass is a dielectric material that increases the stability of the DBD discharge: as such, packing the bed with glass particles increases the conversion of the process. The catalytic bed also increases conversion and allows the reactor to process higher methane flows [196].

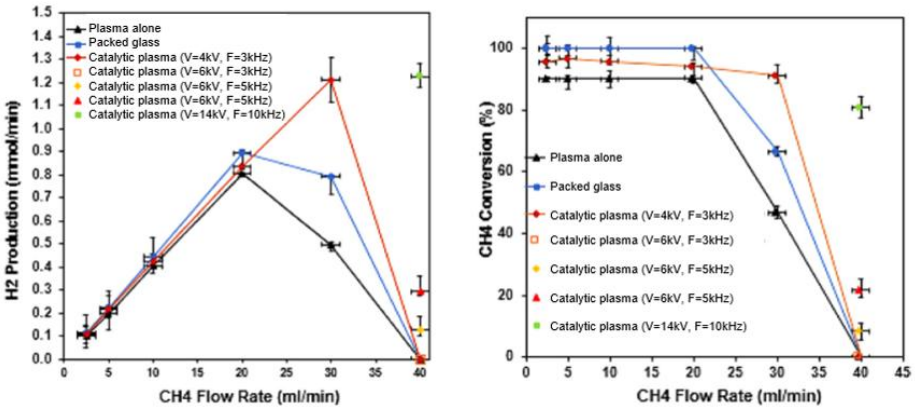

Figure 14 – Activity and conversion of plasma, glass packed plasma and catalytic plasma reactors, varying flowrates, voltage and pulse frequency (adapted from [195]).

Another alternative to increase the performance of plasma reactors was proposed by Mishra *et al.* [197]; they reported that argon could behave as a catalyst in a plasma reactor since it enhances the energy distribution of the pulse. During the chain reactions, if argon atoms remain excited, their reionization causes further decomposition, favoring the evolution of H_2 and solid carbon, increasing both conversion and selectivity.

Plasma reactors are an appealing alternative to the use of standard catalytic beds, but the low selectivity and required high power input affect the competitiveness of this endothermic process.

5.3 Molten metal reactors

An approach that has been receiving more attention is the use of molten metal reactors for the direct decomposition of methane. The original concept was proposed by Steinberg, in 1999 [198]. This approach exhibits two main advantages: high heat transfer between the molten metal and reaction gas and easy separation, by decantation, of the formed carbon from the molten metal medium. Also in the early 2000s, Serban *et al.* [59] studied a micro-reactor with a low melting point metal (lead or tin), granular or catalytic materials (silicon carbide, alumina) and a combination of both. The goal was to assess the best heat transfer medium. Lead and tin were initially used mainly due to their low melting point and absence of carbide formation. However, the conversion obtained was quite low, at a maximum of *ca.* 10 %, at 750 °C.

Upham *et al.* [199] developed then a similar molten metal reactor but used nickel (atomically dissolved in low melting point metals) to increase the reactivity of the reaction medium. To further optimize the reactor kinetics, the authors tested different low melting point metals (In, Ga, Bi, Sn, Pb) with different molar fractions of nickel. Their maximum conversion was obtained at 1065 °C with a molten alloy comprising 27 mol% of Ni dissolved in molten Bi in a 1.1 m long bubble column. While assessing the process stability, they were able to maintain operation during 170 h. In this period, the generated carbon accumulated at the top surface of the reactor in the form of powder, as depicted in Figure 15. After Raman and X-ray spectroscopy analysis, it was observed that the carbon deposits were mostly graphite. One of the most important observations during their work was that the active metals

were atomically dispersed and negatively charged; the catalytic activity was assigned to this negative charge.

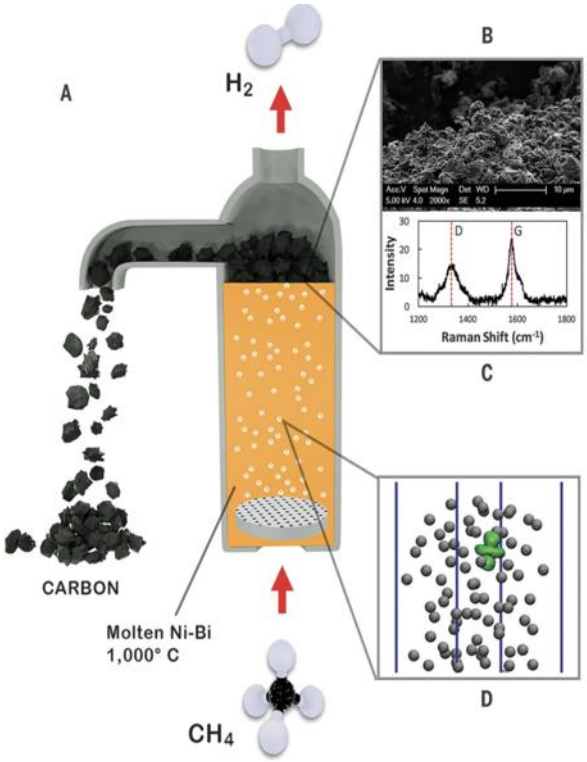

Figure 15 – Schematics of a molten metal reactor (adapted from [199]).

The high temperature of operation needed to carry out the methane decomposition in a molten metal reactor affects the implementation of such reactors. Temperatures near the range of non-catalytic methane decomposition are needed to achieve sizable production of hydrogen, implying the same drawbacks of pure thermolysis (reactor wear and high energy intensity).

6. Regeneration

The fast deactivation of methane decomposition catalysts has hindered the use of this process to produce CO_x-free hydrogen. Extensive work has been done for optimizing the catalyst composition and morphology and the reactor design, but even the most stable catalysts only last up to a few hundred hours. Carbon deposition [200] and morphology changes of the metal particles [201] will eventually stop the catalytic process. Several authors suggested the possibility of regenerating the spent catalyst. Regeneration consists of removing carbon deposits by gasifying and/or oxidizing them either completely or partially.

The carbon deposits can grow over the catalyst (base-growth) or between the catalyst and the support (tip-growth) [90,91]. Tip-grown carbon separates the catalyst from the support and, as such, turns the catalyst regeneration impossible. So, regeneration is possible, and may theoretically allow the process to go-on indefinably, as long as the deposits are base-grown. The carbon deposits must be directly gasified by a gasifying agent and/or the gasification should be catalyzed by the CMD catalyst.

6.1 Oxygen gasification

The first efforts for regenerating methane decomposition catalysts were centered in the combustion of the carbon deposits [202]:

$$\mathrm{C\,(s)} + \mathrm{O_2\,(g)} \rightarrow \mathrm{CO_2\,(g)}, \qquad \Delta H^0_{298\,\mathrm{K}} = -393.4\ \mathrm{kJ \cdot mol^{-1}} \quad (9)$$

Depending on the oxygen concentration and reaction conditions, partial oxidation of carbon can also take place [149]:

$$\mathrm{C\ (s)} + \frac{1}{2}\mathrm{O_2\ (g)} \rightarrow \mathrm{CO\ (g)}, \qquad \Delta H^0_{298\ \mathrm{K}} = -110.5\ \mathrm{kJ \cdot mol^{-1}} \tag{10}$$

As early as 1966, Pohlenz *et al.* [160] designed a methane decomposition reactor that worked in cycles of CMD and carbon combustion. The approach is simple but nullifies one of the main benefits of the process, which is the production of hydrogen without producing CO_x [203]. More recently, studies [204,205] on cyclic production of hydrogen and regeneration by oxidation were performed reporting full activity recovery between cycles for Ni catalyst and partial regeneration for Co-based catalysts. Figure 16 depicts the hydrogen produced and the initial reaction rate of Ni and Co catalyst with cyclic regeneration: both production and regeneration at 500 °C.

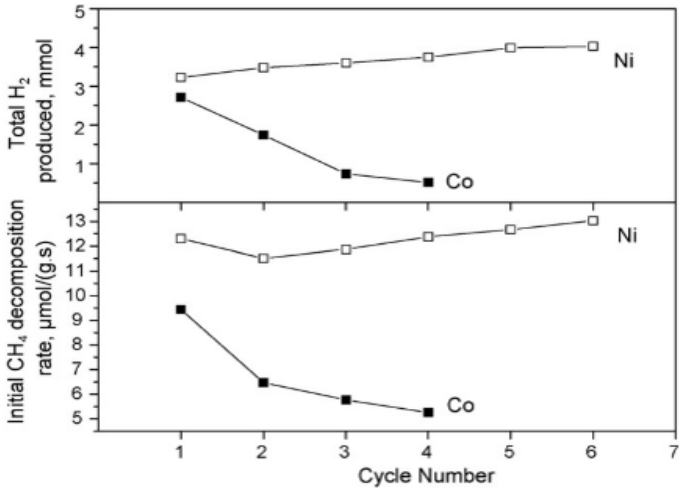

Figure 16 – Total quantity of hydrogen produced per cycle (top) and initial decomposition rate in each cycle (bottom), at 500 °C (extracted from [205]).

6.2 Steam gasification

At the turn of the century, as environmental concerns became a topic of major relevance, researchers started looking into ways to regenerate the catalysts while avoiding the combustion of carbon [206]. Steam is long known to gasify coke [207], so it can be used to regenerate the catalyst [149]:

$$\mathrm{C\,(s)} + \mathrm{H_2O\,(g)} \rightarrow \mathrm{CO\,(g)} + \mathrm{H_2\,(g)}, \qquad \Delta H^0_{298\,\mathrm{K}} = -131.2\ \mathrm{kJ \cdot mol^{-1}} \qquad (11)$$

The CO formed can be further oxidized to CO_2 [208,209], by water gas shift reaction. As for combustion, this regeneration also releases carbon in its oxidized form [210]. But in this case, additional hydrogen is produced, increasing the H_2/CO_x ratio of the process [211].

Zhang and Amiridis [212] performed the CMD reaction at 550 °C, using silica supported nickel. They reported complete deactivation of the catalyst after 200 minutes on stream and attributed the loss of activity to the clogging of the porous catalyst. In follow-up work, Aiello *et al.* [211] attempted to regenerate the same catalyst with steam, achieving ten production/regeneration cycles with small activity loss between cycles. Łamacz [213,214] studied this regeneration in CeO_2-supported Ni catalyst at 550 °C (then increased up to 700 °C) and reported that regeneration time and H_2/CO_x ratios are dependent on the used amount of steam. Using higher steam rate input, a faster regeneration is achieved, as depicted in Figure 17. With a steam flowrate (GHSV) of 2000 $g \cdot g_{Cat}^{-1} \cdot h^{-1}$, regeneration lasted 650 min, while with a steam flowrate of 8000 $g \cdot g_{Cat}^{-1} \cdot h^{-1}$, regeneration took only 205 min. Moreover, for higher steam partial pressure, water gas shift reaches higher conversions producing more hydrogen.

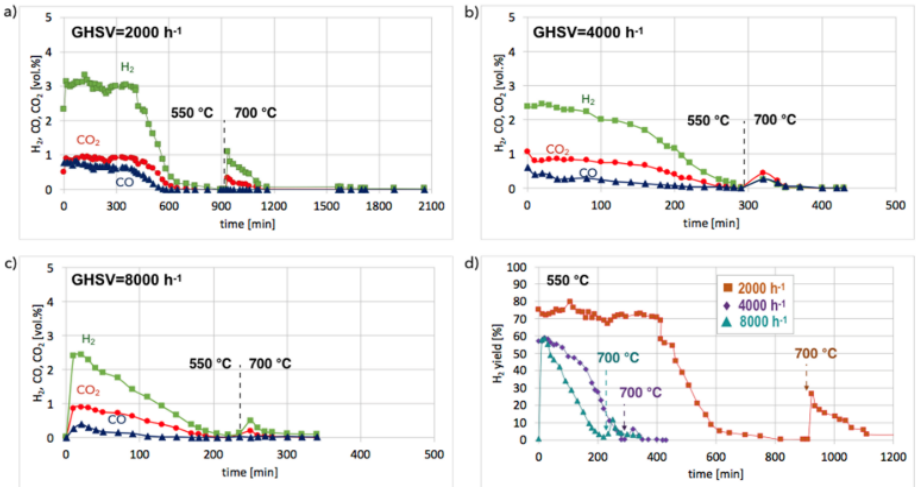

Figure 17 – Outlet hydrogen, carbon dioxide and carbon monoxide concentration during regeneration, using several GHSV, at 550 °C, then increased to 700 °C (extracted from [214]).

6.3 Carbon dioxide gasification

Carbon dioxide can be used for gasifying the coke deposits [215,216]:

$$C\,(s) + CO_2(g) \rightleftharpoons 2CO\,(g), \qquad \Delta H^0_{298\,K} = 172.4\ \text{kJ} \cdot \text{mol}^{-1} \qquad (12)$$

Ammendola *et al.* [61] used this methodology to regenerate carbon catalysts used in methane decomposition, as oxygen and steam were often aggressive oxidants to the catalyst. Abbas and Daud [217] studied the cyclic CO_2 gasification to regenerate an activated carbon (AC) catalyst at different temperatures. These authors showed that higher temperatures result in a more complete catalyst regeneration; at 900 and 950 °C the regeneration was only partial, with a significant activity drop between cycles,

but at 1000 °C the loss of activity between cycles was considerably smaller. Temperature programmed CO_2 oxidation (TPCO2) analysis of the pristine catalyst revealed that for temperatures ≤1000 °C the catalyst suffers a mass loss of <30 % over 50 min. While carbon catalysts can be oxidized by carbon dioxide, the highly amorphous carbon produced by CMD is much easier to oxidize. These authors were then able to consistently remove the produced coke, while reporting only an acceptable catalytic activity decrease (<10 % after 6 cycles).

Carbon dioxide gasification is also reported in metal catalysts, as oxygen and steam may oxidize metal catalysts [218–221]:

$$\mathrm{Ni\,(s)} + \frac{1}{2}\mathrm{O_2(g)} \rightleftharpoons \mathrm{NiO\,(s)}, \qquad \Delta H^0_{298\,\mathrm{K}} = -240.28\ \mathrm{kJ \cdot mol^{-1}} \tag{13}$$

$$\mathrm{Ni\,(s)} + \mathrm{H_2O\,(g)} \rightleftharpoons \mathrm{NiO\,(s)} + \mathrm{H_2\,(g)}, \qquad \Delta H^0_{298\,\mathrm{K}} = 45.22\ \mathrm{kJ \cdot mol^{-1}} \tag{14}$$

These reactions hamper the follow-up CMD reaction process, as the catalyst will be re-reduced by methane, with release of CO [221–223]:

$$\mathrm{NiO\,(s)} + \mathrm{CH_4\,(g)} \rightarrow \mathrm{Ni\,(s)} + \mathrm{CO\,(g)} + \mathrm{2H_2\,(g)}, \qquad \Delta H^0_{298\,\mathrm{K}} = 160{,}98\ \mathrm{kJ \cdot mol^{1}} \tag{15}$$

Xia *et al.* [224] studied Fe/Al_2O_3, to produce hydrogen in a fluidized-bed reactor, in cycles of production and regeneration using carbon dioxide, at 750 °C. After the first regeneration cycle, 5 cycles were performed with barely any activity loss between cycles, as illustrated in Figure 18. These authors concluded, however, that some carbon species could not be removed by a weak oxidant such as carbon dioxide, like CNTs, but less crystalline carbon was consistently removed.

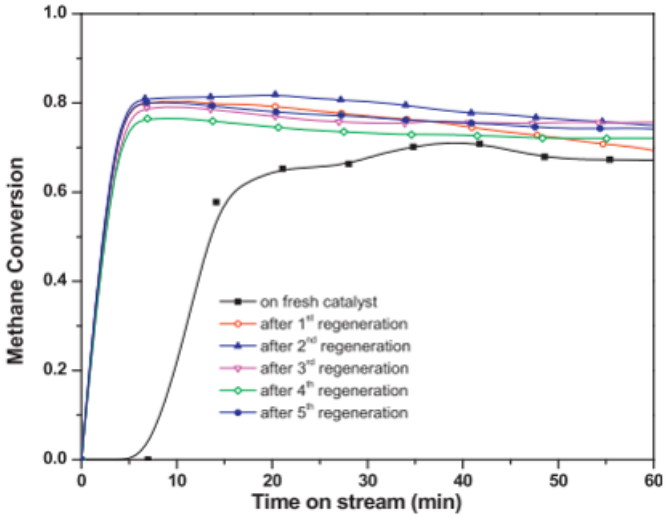

Figure 18 - Methane conversion with time on stream, at 750 °C, after each regeneration step (extracted from [224]).

6.4 Hydrogen gasification

Since the several steps of methane decomposition are known to be reversible [56], it has been considered that hydrogen may be used to gasify the carbon deposits [225], by the reverse of the CMD reaction [226]:

$$\mathrm{C\,(s) + H_2\,(g) \rightleftharpoons CH_4\,(g)}, \qquad \Delta H^0_{298\,\mathrm{K}} = -74.8\ \mathrm{kJ \cdot mol^{-1}} \tag{16}$$

The carbon hydrogenation would completely eliminate the evolution of CO_x during regeneration, allowing for the design of reactors without any direct emission of greenhouse effect gases [39].

It is well established that hydrogen can methanize coal in conditions similar to those used for CMD [227–229]. As for the coke from the methane decomposition,

H_2-reduction has been performed on used catalysts to evaluate the reducibility of the deposits. Hardiman *et al.* [230] studied the coke deposited during the propane steam reforming over Co-Ni/Al_2O_3 by temperature programmed oxidation and reduction (TPO and H_2-TPR). These authors observed that the maximum removal of carbon with oxygen was completed faster and at a lower temperature (550 °C) than with hydrogen (650 °C). However, since the catalyst was partially oxidized after TPO, it required a new reduction, which resulted in catalyst surface defects. Hydrogen is a weaker gasifier than oxygen, but as hydrogen is a reducing agent, it does not corrode the already reduced catalyst.

Figueiredo [231] studied the gasification of coke formed by several processes involving hydrocarbon pyrolysis, in temperature programmed and isothermal regimes. Even though hydrogen was reported to gasify carbon considerably slower than oxygen, steam, and carbon dioxide without using catalysts [232], hydrogen was very effective in the presence of transition metal catalysts. Ni is a particularly studied catalyst for this process [233–235]. Total methanation of the deposited carbon requires the same amount of hydrogen that produced these deposits. As such, the regeneration method needs to be localized. Since Ni is shown to catalyze both CMD and the reverse reaction, and non-catalytic gasification is slow [232], gasification of the carbon should occur selectively, at the interface between the formed carbon structures and the catalyst [236]. This way, as long as there is good contact between the gas phase and the carbon-catalyst interface, only a fraction of the produced hydrogen has to be used to completely separate the carbon materials from the catalyst, without destroying said materials [235].

To the best knowledge of the authors, hydrogen gasification for the regeneration of the CMD catalysts was first proposed by [63]. These authors disclose the cyclic regeneration of a nickel-based catalyst using a small fraction of the produced hydrogen, *ca*. 5 %. Hydrogen gasification is probably the most suitable option to achieve the ambitious goal of cyclic catalyst regeneration and then have a methane decomposition catalyst stable for several thousands of hours. A stable catalyst for the CMD process will allow a fast transition to full decarbonized energy.

7. Reaction products

When pure methane is fed, only hydrogen and carbon are produced during CMD [41]. As such, the outbound gas stream is composed exclusively of hydrogen and unreacted methane. The separation of these compounds is easily achievable by PSA [40]; the maximum methane concentration allowed for PEMFC is 2 ppm [237]. When natural gas is used as feed, substances other than methane are present, such as CO_2, heavier hydrocarbons and sulfur compounds, but these substances can be easily removed by PSA either down-stream or up-stream of the reactor [92].

Alternatively, palladium membranes can be used to separate hydrogen, with high purity and recovery [238]. Pd is particularly selective towards hydrogen, allowing considerable hydrogen flow even for small pressure gradients, while blocking any other gas [239]. The main issue with such a separation process rests on the high costs of Pd membranes and their fragility [240]. Electrochemical pumping using solid electrolyte membranes can replicate the behavior of Pd, using electricity to forcefully pump hydrogen in the form of protons through the membrane-electrode

assembly. Electrochemical pumping can proceed even in counter-gradient, but more electrical energy is needed when pressure gradients are lower [241].

Any of the considered separation processes can be implemented to treat the outbound stream of a CMD reactor. The use of membranes, either Pd or electrochemical, allows for the development of membrane reactors. Such a configuration may be composed of any of the previously discussed designs coupled with a membrane that blocks any gases other than hydrogen to leave the reactor [242]. The reaction must be periodically stopped to remove carbon and, in case of any impurities in the inlet methane feed, the reactor requires a periodical purge [243]. Ishiara *et al.* [244] reported one of the earliest membrane reactors used for CMD, observing conversions far higher than the chemical equilibrium, based on the inlet concentrations [245].

7.1 Carbon materials

Different carbon allotropes can be produced during the catalytic methane decomposition, depending on operation conditions and catalysts used to carry out the reaction [91]. The decomposition of methane has long been used with metal catalysts for the production of carbon nanomaterials [246,247]. When carbon is used as a catalyst, the formation of mostly amorphous carbon products is reported [248].

The most typical carbon structures, reported in CMD over supported metals, are filamentous. Awadallah *et al.* [249] studied cobalt supported on several combinations of binary Zr-M oxide (M = Mg, Al, Si, La or Ce) supports, at temperatures between 500 and 700 °C, and reported the formation of MWCNTs in all

catalysts. In supports with low interaction with the active phase (M = Al, Si or La), they also reported the formation of graphite nanosheets/nanospheres (onion-like), *i.e.* multiple graphite nanosheets encapsulating the metal particles [250]. Zhang *et al.* [251] reported the production of MWCNTs and nanospheres, in CeO_2-supported Ni catalyst with a 400-700 °C ramp. They claim that the nanosheets suffer structural changes with the time-on-stream becoming base-grown MWCNTs (high interaction between metal and support [252]). Nanospheres are observed mostly at higher temperatures (*e.g.* in molten metal reactors [199]), but large catalyst particles tend to generate carbon nanospheres in a wide range of temperatures [253]. Examples of the obtained structures are depicted in Figure 19:

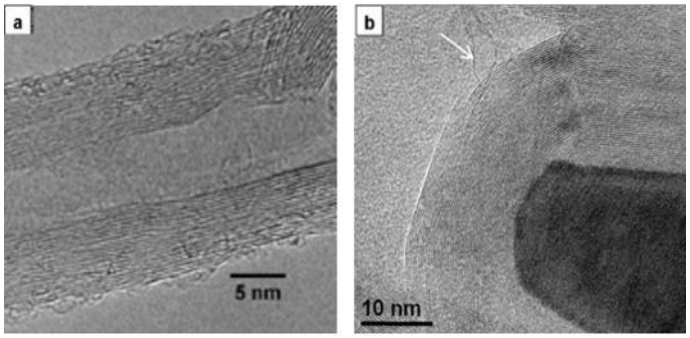

Figure 19 - a) MWCNT (adapted from [138]) and b) onion-like carbon nanosheets (adapted from [104]).

Other types of filamentous carbon structures can be observed, namely: single wall carbon nanotubes (SWCNTs); solid fibers: herringbone/cup-stacked (graphene sheets that form the fiber have an acute angle with the fiber axis [254]) or platelet/plate-stacked (graphene sheets that form the fiber have a 90° angle with the

fiber axis [255]); irregular/fishbone nanotubes (semi-hollow nanotube, with punctual graphite sheets connecting the interior walls [138]).

SWCNTs are produced by CMD using metals catalysts at high temperature, in the range of 1000 °C [256]. Solid herringbone fibers and fishbone nanotubes are typically generated by tip-growth mechanisms (the catalyst is at the tip of the growing filament) in supported metal catalysts, with small particle size (less than 40 nm), weak metal-support interaction [246,257,258], and at temperatures between 500 (mostly fibers) and 700 °C (mostly hollow tubes) [117,118,138]. Figure 20 depicts a herringbone solid fiber and a fishbone nanotube, with α/2 angles with the filament axis:

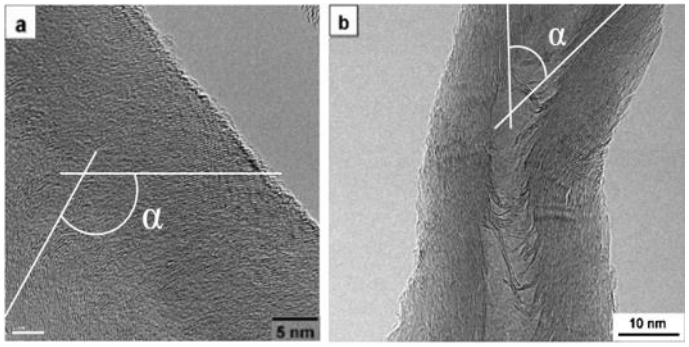

Figure 20 – a) Herringbone fiber (adapted from [258]) and b) fishbone nanotubes (adapted from [118]).

Platelet fibers are mostly base-grown in Ni-Cu particles with a diameter larger than 100 nm: several nanofibers grow from the same catalyst particle in different directions, the so-called octopus-conformation. For smaller size metal particles, Ni-Cu catalysts form fishbone nanotubes that, at high temperatures (~650 °C), drip off as pear-shaped metal drops. These structures are caused by the

quasi-liquid state of Ni-Cu catalysts at reaction temperature [254,259]. Figure 21 depicts an octopus-shaped catalyst particle and an encapsulated fragment of metal inside a fishbone nanotube [260].

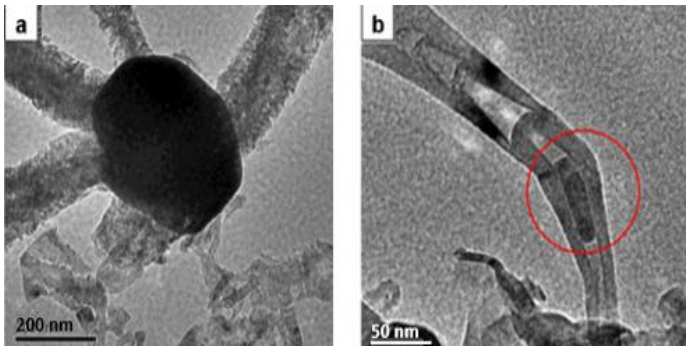

Figure 21 - a) Octopus-shaped nanofibers and b) fragmentation caused by quasi-liquid state (extracted from [260]).

When carbon catalysts are used, the formation of carbon filaments is rare, although some authors report such structures in catalysts with high pore volume [50]. Most commonly amorphous carbon is formed, which is active for CMD [248], keeping the reaction running even after the initially exposed surface becomes completely covered [261].

7.2 Economic overview

The current hydrogen market is dominated by methane reforming processes, with production costs of 1.4 €·kg_{H2}^{-1} [28] for steam methane reforming and *ca.* 1.8 €·kg_{H2}^{-1} [14] for other reforming processes. Large amounts of CO_2 are produced by reforming reactions, not only harming the environment but also requiring the

implementation of extensive down-stream treatments, as the tariffs on CO_2 emissions are rapidly increasing. Additional separation steps [30] and carbon capture and storage (CCS) [31] or carbon capture and valorization (CCV) [32] technologies have to be considered. Currently, CCS has a price range of 90-160 €·t_{CO2}^{-1} [262]; with such a cost, steam methane reforming with CCS would have production costs in the range of 1.9-2.3 €·kg_{H2}^{-1}. Hydrogen produced by CMD, using natural gas, has an expected production cost in the range of 1.8 €·kg_{H2}^{-1} [39]. As methane decomposition does not produce CO_x, as long as regulations are sufficiently strict, it will be cheaper than the current *status quo* technologies.

CMD also has the potential to be used as a competitive process to actively remove CO_2 from the atmosphere. Using biogas, priced in the range of 7.81 €·$kmol_{CH4}^{-1}$ [263], CMD can produce hydrogen with production costs of *ca.* 2.2 €·kg_{H2}^{-1}. As biogas is indirectly generated from atmospheric CO_2 (1:1 ratio), this process can actively reduce greenhouse effect while only increasing hydrogen production costs by 0.4 €·kg_{H2}^{-1}. The CMD of biomethane mimics Nature, as it removes CO_2 from the atmosphere and deposits it as coal; CMD process does this just for 37 €·t_{CO2}^{-1}, which compares very favorably with 27 to 83 €·t_{CO2}^{-1} indicated by IRENA [14] just for removing/capturing the CO_2 from the atmosphere.

Even if hydrogen production is considered to be the main product of the CMD, the properties of the generated carbon are of paramount importance, as its economic value can improve the competitiveness of the CMD process as a widely spread technology [39]. One of the most demanding applications for carbon particles is as fillers. Fillers are traditionally used to lower production prices of materials, but functional fillers represent an ever-increasing market where carbon is playing an

important role, offering unique characteristics (thermal/electric conductivity, lightness, mechanical resistance) while still being relatively cheap [264]. Specifically, carbon is used as functional filler in paints [265], asphalt [68,266], bricks [267] and other building materials [268], rubber [269] and in plastic composites [270]. If crystalline carbon structures are formed, they can be valorized in more profitable applications such as catalysts [271]; supports [272]; adsorbents [273–275]; or thermal [276–278]/electro [279–281] conductors.

8. Conclusions

Catalytic methane decomposition can play an important role in the future of the energy sector, being used as a soft transition step towards renewable sources: kick-starting the hydrogen-economy, by producing CO_x-free hydrogen from fossil fuel. Furthermore, active removal of CO_2 from the atmosphere can be achieved, if synthetic or biogas are decomposed. CMD still faces many challenges, particularly in the matter of long-term stable operation. But, much work has been done to curve this drawback, with extensive development of catalysts, reactor designs and regeneration strategies.

Transition metals are normally used as catalysts for the methane decomposition reaction. Ni, Fe and Co-based catalysts show the highest activity among mono-metallic catalysts, allowing for low-temperature operation of CMD processes. Combining these metals among themselves or with other metals (Cu, Pd, Pt, other transition metals) greatly improves the catalytic performance, with some combinations of catalysts reaching hundreds of hours of stable hydrogen production.

Carbon catalysts, such as activated carbon and carbon black, can also be used to catalyze this reaction. While these catalysts have their advantages, metals are easier to optimize (by combining different metals and supports) and demonstrated higher catalytic activity. Moreover, carbon catalysts are harder to regenerate without being damaged, hindering long-term operation.

While CMD is not yet industrially competitive, increased attention has been given to reactor designs such as fluidized-bed, plasma and molten metal reactors. Among these, fluidized-bed design is most promising since plasma technology lacks selectivity towards hydrogen production and molten metal reactors are still a recent technology, needing further development, as the current process is very energy-intensive (requiring temperatures only slightly lower than the non-catalytic methane decomposition).

Low stability is the main factor that hinders the industrialization of CMD, with catalysts inevitably getting deactivated by carbon accumulation. Regeneration was appointed as a possible strategy achieving long-term operation. Theoretically, as long as the carbon deposits are base-grown and the carbon can be directly gasified and/or the carbon-metal interface is exposed (and the catalyst also catalyzes the gasification), regeneration can extend the operation indefinably. The future of CMD depends on the development of efficient regeneration strategies. Oxygen, steam, carbon dioxide and hydrogen are all usable as gasifying agents to regenerate catalysts. When Ni-based catalysts are used, the cyclic regeneration of the catalyst can be achieved promoting the selective carbon hydrogenation at the catalyst/coke particle interface; the coke particles drop from the catalyst surface rendering it active again.

Since both methane decomposition and carbon hydrogenation are extremely selective reactions, this approach produces no side products.

Carbon materials vary considerably depending on operation conditions and catalysts: the most reported carbon products include amorphous carbon (mostly on carbon catalysts) and graphitic nanomaterials (mostly filamentous carbon on metal catalysts). Carbon products can be recovered and exploited for profit, increasing the economic interest of the process. There are already established markets for carbon materials, but with the increasing search for inexpensive carbon materials in many industrial and commercial applications, new markets will emerge to accommodate the predicted carbon influx.

Acknowledgments

This work was financially supported by: Base Funding - UIDB/00511/2020 of the Laboratory for Process Engineering, Environment, Biotechnology and Energy – LEPABE - funded by national funds through the FCT/MCTES (PIDDAC). Vítor Pereira acknowledges the Portuguese Foundation of Science and Technology (FCT) support for their PhD grant SFRH/BD/143218/2019.

References

[1] Marzeion B, Kaser G, Maussion F, Champollion N. Limited influence of climate change mitigation on short-term glacier mass loss. Nat Clim Chang 2018;8:305–8. https://doi.org/10.1038/s41558-018-0093-1.

[2] Figueres C, Schellnhuber HJ, Whiteman G, Rockström J, Hobley A,

Rahmstorf S. Three years to safeguard our climate. Nature 2017;546:593–5. https://doi.org/10.1038/546593a.

[3] Iftikhar Y, Wang Z, Zhang B, Wang B. Energy and CO2 emissions efficiency of major economies: A network DEA approach. Energy 2018;147:197–207. https://doi.org/10.1016/j.energy.2018.01.012.

[4] CO2 concentration n.d. https://scripps.ucsd.edu/programs/keelingcurve/ (accessed January 27, 2020).

[5] UNFCCC. eHandbook n.d. https://unfccc.int/resource/bigpicture/ (accessed January 6, 2020).

[6] Przychodzen W, Przychodzen J. Determinants of renewable energy production in transition economies: A panel data approach. Energy 2020;191:116583. https://doi.org/10.1016/j.energy.2019.116583.

[7] Ridjan I, Mathiesen BV, Connolly D. Synthetic fuel production costs by means of solid oxide electrolysis cells. Energy 2014;76:104–13. https://doi.org/10.1016/j.energy.2014.04.002.

[8] Lund H, Østergaard PA, Connolly D, Mathiesen BV. Smart energy and smart energy systems. Energy 2017;137:556–65. https://doi.org/10.1016/j.energy.2017.05.123.

[9] Züttel A, Remhof A, Borgschulte A, Friedrichs O. Hydrogen: The future energy carrier. Philos Trans R Soc A Math Phys Eng Sci 2010;368:3329–42. https://doi.org/10.1098/rsta.2010.0113.

[10] Connolly D, Mathiesen B V., Ridjan I. A comparison between renewable transport fuels that can supplement or replace biofuels in a 100% renewable energy system. Energy 2014;73:110–25. https://doi.org/10.1016/j.energy.2014.05.104.

[11] Hydrogen Europe. Home | Hydrogen n.d.

[12] Hydrogen Council. Hydrogen Council – A global CEO-level initiative with a united vision for hydrogen n.d.

[13] Wang J. Barriers of scaling-up fuel cells: Cost, durability and reliability. Energy 2015;80:509–21. https://doi.org/10.1016/j.energy.2014.12.007.

[14] IRENA. Hydrogen: a renewable energy perspective. Tokyo: 2019.

[15] Tseng P, Lee J, Friley P. A hydrogen economy: Opportunities and challenges.

Energy 2005;30:2703–20. https://doi.org/10.1016/j.energy.2004.07.015.

[16] Guelpa E, Bischi A, Verda V, Chertkov M, Lund H. Towards future infrastructures for sustainable multi-energy systems: A review. Energy 2019;184:2–21. https://doi.org/10.1016/j.energy.2019.05.057.

[17] Rudy W, Zbikowski M, Teodorczyk A. Detonations in hydrogen-methane-air mixtures in semi confined flat channels. Energy 2016;116:1479–83. https://doi.org/10.1016/j.energy.2016.06.001.

[18] International Energy Agency. The future of hydrogen. 2019.

[19] Clark D. Why can't we quit fossil fuels. Guard 2013;Wed 17 Apr.

[20] Farand C. Countries' fossil fuel production plans inconsistent with Paris Agreement. Clim Home News 2019;November 2.

[21] Bayens C. "Utter hypocrisy": Government refuses to stop spending billions on fossil fuel projects across world. Independent 2019;Wednesday.

[22] da Silva Veras T, Mozer TS, da Costa Rubim Messeder dos Santos D, da Silva César A. Hydrogen: Trends, production and characterization of the main process worldwide. Int J Hydrogen Energy 2017;42:2018–33. https://doi.org/10.1016/j.ijhydene.2016.08.219.

[23] Xu J, Froment GF. Methane steam reforming, methanation and water-gas shift: I. Intrinsic kinetics. AIChE J 1989;35:88–96. https://doi.org/10.1002/aic.690350109.

[24] Andraos S, Abbas-Ghaleb R, Chlala D, Vita A, Italiano C, Laganà M, et al. Production of hydrogen by methane dry reforming over ruthenium-nickel based catalysts deposited on Al2O3, MgAl2O4, and YSZ. Int J Hydrogen Energy 2019;44:25706–16. https://doi.org/10.1016/j.ijhydene.2019.08.081.

[25] Dissanayake D, Rosynek MP, Kharas KCC, Lunsford JH. Partial oxidation of methane to carbon monoxide and hydrogen over a Ni/Al2O3 catalyst. J Catal 1991;132:117–27. https://doi.org/10.1016/0021-9517(91)90252-Y.

[26] Lin S, Harada M, Suzuki Y, Hatano H. Hydrogen production from coal by separating carbon dioxide during gasification. Fuel 2002;81:2079–85. https://doi.org/10.1016/S0016-2361(02)00187-4.

[27] Holladay JD, Hu J, King DL, Wang Y. An overview of hydrogen production technologies. Catal Today 2009;139:244–60.

https://doi.org/10.1016/j.cattod.2008.08.039.

[28] Jones G, Jakobsen JG, Shim SS, Kleis J, Andersson MP, Rossmeisl J, et al. First principles calculations and experimental insight into methane steam reforming over transition metal catalysts. J Catal 2008;259:147–60. https://doi.org/10.1016/j.jcat.2008.08.003.

[29] Verma A, Olateju B, Kumar A. Greenhouse gas abatement costs of hydrogen production from underground coal gasification. Energy 2015;85:556–68. https://doi.org/10.1016/j.energy.2015.03.070.

[30] Beaver MG, Caram HS, Sircar S. Sorption enhanced reaction process for direct production of fuel-cell grade hydrogen by low temperature catalytic steam-methane reforming. J Power Sources 2010;195:1998–2002. https://doi.org/10.1016/j.jpowsour.2009.10.015.

[31] Gunderson R, Stuart D, Petersen B. The fossil fuel industry's framing of carbon capture and storage: Faith in innovation, value instrumentalization, and status quo maintenance. J Clean Prod 2020;252:119767. https://doi.org/10.1016/j.jclepro.2019.119767.

[32] Olajire AA. Valorization of greenhouse carbon dioxide emissions into value-added products by catalytic processes. J CO2 Util 2013;3–4:74–92. https://doi.org/10.1016/j.jcou.2013.10.004.

[33] Chein RY, Hsu WH. Thermodynamic analysis of syngas production via chemical looping dry reforming of methane. Energy 2019;180:535–47. https://doi.org/10.1016/j.energy.2019.05.083.

[34] Ping JN, Fairlie DM. X.-The Methane Equilibrium. J Chem Soc 1912;101:91–103.

[35] Navarro RM, Peña MA, Fierro JLG. Hydrogen production reactions from carbon feedstocks: Fossil fuels and biomass. Chem Rev 2007;107:3952–91. https://doi.org/10.1021/cr0501994.

[36] Lebarbier VM, Dagle RA, Kovarik L, Albrecht KO, Li X, Li L, et al. Sorption-enhanced synthetic natural gas (SNG) production from syngas: A novel process combining CO methanation, water-gas shift, and CO2 capture. Appl Catal B Environ 2014;144:223–32. https://doi.org/10.1016/j.apcatb.2013.06.034.

[37] Bermejo-López A, Pereda-Ayo B, González-Marcos JA, González-Velasco JR. Mechanism of the CO2 storage and in situ hydrogenation to CH4. Temperature and adsorbent loading effects over Ru-CaO/Al2O3 and Ru-Na2CO3/Al2O3 catalysts. Appl Catal B Environ 2019;256:117845. https://doi.org/10.1016/j.apcatb.2019.117845.

[38] Jensen IG, Skovsgaard L. The impact of CO2-costs on biogas usage. Energy 2017;134:289–300. https://doi.org/10.1016/j.energy.2017.06.019.

[39] Zhang X, Kätelhön A, Sorda G, Helmin M, Rose M, Bardow A, et al. CO2 mitigation costs of catalytic methane decomposition. Energy 2018;151:826–38. https://doi.org/10.1016/j.energy.2018.03.132.

[40] Papadias DD, Ahmed S, Kumar R, Joseck F. Hydrogen quality for fuel cell vehicles - A modeling study of the sensitivity of impurity content in hydrogen to the process variables in the SMR-PSA pathway. Int J Hydrogen Energy 2009;34:6021–35. https://doi.org/10.1016/j.ijhydene.2009.06.026.

[41] LI Y, ZHANG B, XIE X, LIU J, XU Y, SHEN W. Novel Ni catalysts for methane decomposition to hydrogen and carbon nanofibers. J Catal 2006;238:412–24. https://doi.org/10.1016/j.jcat.2005.12.027.

[42] Tsotridis G, Pilenga A, Marco G De, Malkow T. EU Harmonised Test Protocols for PEMFC MEA Testing in Single Cell Configuration for Automotive Applications. 2015.

[43] Lajunen A, Lipman T. Lifecycle cost assessment and carbon dioxide emissions of diesel, natural gas, hybrid electric, fuel cell hybrid and electric transit buses. Energy 2016;106:329–42. https://doi.org/10.1016/j.energy.2016.03.075.

[44] Vielstich W. Ideal and effective efficiencies of cell reactions and comparison to carnot cycles. Handb. Fuel Cells, Chichester, UK: John Wiley & Sons, Ltd; 2010, p. 1–5. https://doi.org/10.1002/9780470974001.f101004.

[45] Falbo L, Martinelli M, Visconti CG, Lietti L, Bassano C, Deiana P. Kinetics of CO2 methanation on a Ru-based catalyst at process conditions relevant for Power-to-Gas applications. Appl Catal B Environ 2018;225:354–63. https://doi.org/10.1016/j.apcatb.2017.11.066.

[46] Cantelo RC. The Thermal Decomposition of Methane. J Phys Chem

1924;28:1036–48. https://doi.org/10.1021/j150244a003.

[47] Cantelo RC. The Thermal Decomposition of Methane. II. J Phys Chem 1926;30:899–901. https://doi.org/10.1021/j150265a004.

[48] Ko PL, Lina A, Ambard A. A Review of Wear Scar Patterns of Nuclear Power Plant Components. Flow-Induced Vib., ASMEDC; 2003, p. 97–106. https://doi.org/10.1115/PVP2003-2079.

[49] Ashik UPM, Wan Daud WMA, Abbas HF. Production of greenhouse gas free hydrogen by thermocatalytic decomposition of methane – A review. Renew Sustain Energy Rev 2015;44:221–56. https://doi.org/10.1016/j.rser.2014.12.025.

[50] Zhang J, Li X, Chen H, Qi M, Zhang G, Hu H, et al. Hydrogen production by catalytic methane decomposition: Carbon materials as catalysts or catalyst supports. Int J Hydrogen Energy 2017;42:19755–75. https://doi.org/10.1016/j.ijhydene.2017.06.197.

[51] Li Y, Li D, Wang G. Methane decomposition to COx-free hydrogen and nano-carbon material on group 8-10 base metal catalysts: A review. Catal Today 2011;162:1–48. https://doi.org/10.1016/j.cattod.2010.12.042.

[52] Sikander U, Samsudin MF, Sufian S, KuShaari KZ, Kait CF, Naqvi SR, et al. Tailored hydrotalcite-based Mg-Ni-Al catalyst for hydrogen production via methane decomposition: Effect of nickel concentration and spinel-like structures. Int J Hydrogen Energy 2019;44:14424–33. https://doi.org/10.1016/j.ijhydene.2018.10.224.

[53] Kuvshinov DG, Kurmashov PB, Bannov AG, Popov M V., Kuvshinov GG. Synthesis of Ni-based catalysts by hexamethylenetetramine-nitrates solution combustion method for co-production of hydrogen and nanofibrous carbon from methane. Int J Hydrogen Energy 2019;44:16271–86. https://doi.org/10.1016/j.ijhydene.2019.04.179.

[54] Hasnan NSN, Timmiati SN, Pudukudy M, Yaakob Z, Lim KL, Taufiq-Yap YH. Catalytic decomposition of methane into hydrogen and carbon nanotubes over mesostructured silica nanoparticle-supported nickel catalysts. J Porous Mater 2019. https://doi.org/10.1007/s10934-019-00819-6.

[55] Cunha AF, Órfão JJM, Figueiredo JL. Catalytic decomposition of methane on

Raney-type catalysts. Appl Catal A Gen 2008;348:103–12. https://doi.org/10.1016/j.apcata.2008.06.028.

[56] Saraswat SK, Sinha B, Pant KK, Gupta RB. Kinetic Study and Modeling of Homogeneous Thermocatalytic Decomposition of Methane over a Ni-Cu-Zn/Al2O3 Catalyst for the Production of Hydrogen and Bamboo-Shaped Carbon Nanotubes. Ind Eng Chem Res 2016;55:11672–80. https://doi.org/10.1021/acs.iecr.6b03145.

[57] MURADOV N, CHEN Z, SMITH F. Fossil hydrogen with reduced emission: Modeling thermocatalytic decomposition of methane in a fluidized bed of carbon particles. Int J Hydrogen Energy 2005;30:1149–58. https://doi.org/10.1016/j.ijhydene.2005.04.005.

[58] Indarto A. Hydrogen production from methane in a dielectric barrier discharge using oxide zinc and chromium as catalyst. J Chinese Inst Chem Eng 2008;39:23–8. https://doi.org/10.1016/j.jcice.2007.10.001.

[59] Serban M, Lewis MA, Marshall CL, Doctor RD. Hydrogen Production by Direct Contact Pyrolysis of Natural Gas. Energy & Fuels 2003;17:705–13. https://doi.org/10.1021/ef020271q.

[60] ABANADES S, FLAMANT G. Production of hydrogen by thermal methane splitting in a nozzle-type laboratory-scale solar reactor. Int J Hydrogen Energy 2005;30:843–53. https://doi.org/10.1016/j.ijhydene.2004.09.006.

[61] Ammendola P, Chirone R, Ruoppolo G, Russo G. Regeneration strategies of deactivated catalysts for thermo-catalytic decomposition process in a fluidized bed reactor. Combust Sci Technol 2008;180:869–82. https://doi.org/10.1080/00102200801894174.

[62] Wang G, Jin Y, Liu G, Li Y. Production of Hydrogen and Nanocarbon from Catalytic Decomposition of Methane over a Ni–Fe/Al 2 O 3 Catalyst. Energy & Fuels 2013;27:4448–56. https://doi.org/10.1021/ef3019707.

[63] Mendes A, Pedrero C, Catarino M. Catalytic Methane Decomposition and Catalyst Regeneration, Methods and uses thereof, 2018.

[64] Value Market Research. Global Carbon Nanotubes Market Report By Type (Multi-Walled Carbon Nanotubes, Single-Walled Carbon Nanotubes And Others), By End-User Industry (Electronics, Aerospace & Defense,

Automotive, Textile, Healthcare, Energy And Others) And By Regions - Industry. 2020.

[65] Transparency Market Research. Activated Carbon Market - Global Industry Analysis, Value, Share, Growth, Trends, and Forecast 2018 - 2026. 2019.

[66] Dannenberg EM, Paquin L, Gwinnell H. Carbon Black. Kirk-Othmer Encycl. Chem. Technol., Hoboken, NJ, USA: John Wiley & Sons, Inc.; 2000. https://doi.org/10.1002/0471238961.0301180204011414.a01.

[67] Luo M, Li Y, Jin S, Sang S, Zhao L, Li Y. Microstructures and mechanical properties of Al 2O 3-C refractories with addition of multi-walled carbon nanotubes. Mater Sci Eng A 2012;548:134–41. https://doi.org/10.1016/j.msea.2012.04.001.

[68] Wu S, Mo L, Shui Z, Chen Z. Investigation of the conductivity of asphalt concrete containing conductive fillers. Carbon N Y 2005;43:1358–63. https://doi.org/10.1016/j.carbon.2004.12.033.

[69] Slater WE. XV.—The influence of different surfaces on the decomposition of methane. J Chem Soc, Trans 1916;109:160–4. https://doi.org/10.1039/CT9160900160.

[70] Cantelo RC. The Thermal Decomposition of Methane. J Phys Chem 1924;28:1036–48. https://doi.org/10.1021/j150244a003.

[71] Belchetz L. The thermal catalytic decomposition of methane. vol. 30. 1933.

[72] Stewart PH, Smith GP, Golden DM. The pressure and temperature dependence of methane decomposition. Int J Chem Kinet 1989;21:923–45. https://doi.org/10.1002/kin.550211005.

[73] Roscoe JM, Thompson MJ. Thermal decomposition of methane: Autocatalysis. Int J Chem Kinet 1985;17:967–90. https://doi.org/10.1002/kin.550170905.

[74] Manton JE, Tickner AW. The decomposition of methane by low-energy electrons. Can J Chem 1960;38:858–68.

[75] Tickner AW. The decomposition of methane in the negative glow. Can J Chem 1961;39:87–95.

[76] Prince ET. Intrinsic stress in hydrogenated amorphous carbon prepared by rf plasma decomposition of methane. J Appl Phys 1991;70:4903–8.

https://doi.org/10.1063/1.349035.

[77] Okeke L, St ri H. Plasma-chemical decomposition of methane during diamond synthesis. Plasma Chem Plasma Process 1991;11:489–99. https://doi.org/10.1007/BF01447161.

[78] Rostrup-Nielsen JR. Equilibria of decomposition reactions of carbon monoxide and methane over nickel catalysts. J Catal 1972;27:343–56. https://doi.org/10.1016/0021-9517(72)90170-4.

[79] Billaud F, Gueret C, Weill J. Thermal decomposition of pure methane at 1263 K. Experiments and mechanistic modelling. Thermochim Acta 1992;211:303–22. https://doi.org/10.1016/0040-6031(92)87029-A.

[80] Olsvik O, Billaud F. Modelling of the decomposition of methane at 1273 K in a plug flow reactor at low conversion. J Anal Appl Pyrolysis 1993;25:395–405. https://doi.org/10.1016/0165-2370(93)80058-8.

[81] Solymosi F, Cserhyi J. Decomposition of CH4 over supported Ir catalysts. Catal Letters 1994;1:561–9.

[82] Demicheli MC, Ponzi EN, Ferretti OA, Yeramian AA. Kinetics of carbon formation from CH4-H2mixtures on nickel-alumina catalyst. Chem Eng J 1991;46:129–36. https://doi.org/10.1016/0300-9467(91)87004-T.

[83] Alstrup I, Tavares MT, Bernardo CA, Sørensen O, Rostrup-Nielsen JR. Carbon formation on nickel and nickel-copper alloy catalysts. Mater Corros 1998;49:367–72. https://doi.org/10.1002/(SICI)1521-4176(199805)49:5<367::AID-MACO367>3.0.CO;2-M.

[84] Alstrup I, Tavares MT. Kinetics of Carbon Formation from CH4 + H2 on Silica-Supported Nickel and Ni-Cu Catalysts. J Catal 1993;139:513–24. https://doi.org/10.1006/jcat.1993.1045.

[85] Ayillath Kutteri D, Wang I-W, Samanta A, Li L, Hu J. Methane decomposition to tip and base grown carbon nanotubes and CO x -free H 2 over mono- and bimetallic 3d transition metal catalysts. Catal Sci Technol 2018;8:858–69. https://doi.org/10.1039/C7CY01927K.

[86] Snoeck JW, Froment GF, Fowles M. Filamentous carbon formation and gasification: Thermodynamics, driving force, nucleation, and steady-state

growth. J Catal 1997;169:240–9. https://doi.org/10.1006/jcat.1997.1634.

[87] Ermakova MA, Ermakov DY, Plyasova LM, Kuvshinov GG. XRD studies of evolution of catalytic nickel nanoparticles during synthesis of filamentous carbon from methane. Catal Letters 1999;62:93–7. https://doi.org/10.1023/A:1019079929435.

[88] Kato T, Matsumoto T, Saito T, Hayashi J-I, Kusakabe K, Morooka S. Effect of carbon source on formation of vapor-grown carbon fiber. Carbon N Y 1993;31:937–40. https://doi.org/10.1016/0008-6223(93)90195-G.

[89] Avdeeva L., Kochubey D., Shaikhutdinov S. Cobalt catalysts of methane decomposition: accumulation of the filamentous carbon. Appl Catal A Gen 1999;177:43–51. https://doi.org/10.1016/S0926-860X(98)00250-6.

[90] Pudukudy M, Yaakob Z, Akmal ZS. Direct decomposition of methane over Pd promoted Ni/SBA-15 catalysts. Appl Surf Sci 2015;353:127–36. https://doi.org/10.1016/j.apsusc.2015.06.073.

[91] Syed Muhammad AF, Awad A, Saidur R, Masiran N, Salam A, Abdullah B. Recent advances in cleaner hydrogen productions via thermo-catalytic decomposition of methane: Admixture with hydrocarbon. Int J Hydrogen Energy 2018;43:18713–34. https://doi.org/10.1016/j.ijhydene.2018.08.091.

[92] Yang Q, Su Q, Wang G, Wen D, Zhang Y, Bao H, et al. Production of hybrid phage displaying secreted aspartyl proteinase epitope of Candida albicans and its application for the diagnosis of disseminated candidiasis. Mycoses 2007;50:165–71. https://doi.org/10.1111/j.1439-0507.2006.01349.x.

[93] Reshetenko T V, Avdeeva LB, Ushakov VA, Moroz EM, Shmakov AN, Kriventsov V V, et al. Coprecipitated iron-containing catalysts (Fe-Al2O3, Fe-Co-Al2O3, Fe-Ni-Al2O3) for methane decomposition at moderate temperatures Part II. Evolution of the catalysts in reaction. Appl Catal A Gen 2004;270:87–99. https://doi.org/10.1016/j.apcata.2004.04.026.

[94] Ermakova M., Ermakov DY, Kuvshinov G. Effective catalysts for direct cracking of methane to produce hydrogen and filamentous carbon. Appl Catal A Gen 2000;201:61–70. https://doi.org/10.1016/S0926-860X(00)00433-6.

[95] MURADOV N. How to produce hydrogen from fossil fuels without CO2 emission. Int J Hydrogen Energy 1993;18:211–5.

https://doi.org/10.1016/0360-3199(93)90021-2.

[96] Takenaka S, Ogihara H, Otsuka K. Structural change of Ni species in Ni/SiO2 catalyst during decomposition of methane. J Catal 2002;208:54–63. https://doi.org/10.1006/jcat.2002.3523.

[97] Wang W, Wang H, Yang Y, Jiang S. Ni-SiO2and Ni-Fe-SiO2catalysts for methane decomposition to prepare hydrogen and carbon filaments. Int J Hydrogen Energy 2012;37:9058–66. https://doi.org/10.1016/j.ijhydene.2012.03.003.

[98] Bayat N, Rezaei M, Meshkani F. Methane decomposition over Ni–Fe/Al2O3 catalysts for production of COx-free hydrogen and carbon nanofiber. Int J Hydrogen Energy 2016;41:1574–84. https://doi.org/10.1016/j.ijhydene.2015.10.053.

[99] Arevalo RL, Aspera SM, Escaño MCS, Nakanishi H, Kasai H. Tuning methane decomposition on stepped Ni surface: The role of subsurface atoms in catalyst design. Sci Rep 2017;7. https://doi.org/10.1038/s41598-017-14050-3.

[100] Monzón A, Latorre N, Ubieto T, Royo C, Romeo E, Villacampa JI, et al. Improvement of activity and stability of Ni–Mg–Al catalysts by Cu addition during hydrogen production by catalytic decomposition of methane. Catal Today 2006;116:264–70. https://doi.org/10.1016/j.cattod.2006.05.085.

[101] Bayat N, Rezaei M, Meshkani F. Methane dissociation to COx-free hydrogen and carbon nanofiber over Ni-Cu/Al2O3 catalysts. Fuel 2017;195:88–96. https://doi.org/10.1016/j.fuel.2017.01.039.

[102] Reshetenko T V, Avdeeva LB, Ismagilov ZR, Chuvilin AL, Ushakov VA. Carbon capacious Ni-Cu-Al2O3catalysts for high-temperature methane decomposition. Appl Catal A Gen 2003;247:51–63. https://doi.org/10.1016/S0926-860X(03)00080-2.

[103] Saraswat SK, Pant KK. Synthesis of hydrogen and carbon nanotubes over copper promoted Ni/SiO2 catalyst by thermocatalytic decomposition of methane. J Nat Gas Sci Eng 2013;13:52–9. https://doi.org/10.1016/j.jngse.2013.04.001.

[104] Shen Y, Lua AC. Synthesis of Ni and Ni – Cu supported on carbon nanotubes

for hydrogen and carbon production by catalytic decomposition of methane. Appl Catal B, Environ 2015;164:61–9. https://doi.org/10.1016/j.apcatb.2014.08.038.

[105] Pudukudy M, Yaakob Z, Jia Q, Sobri Takriff M. Catalytic decomposition of undiluted methane into hydrogen and carbon nanotubes over Pt promoted Ni/CeO 2 catalysts. New J Chem 2018;42:14843–56. https://doi.org/10.1039/C8NJ02842G.

[106] Rategarpanah A, Meshkani F, Wang Y, Arandiyan H, Rezaei M. Thermocatalytic conversion of methane to highly pure hydrogen over Ni–Cu/MgO·Al2O3 catalysts: Influence of noble metals (Pt and Pd) on the catalytic activity and stability. Energy Convers Manag 2018;166:268–80. https://doi.org/10.1016/j.enconman.2018.04.033.

[107] Yokoyama H, Numakura H, Koiwa M. The solubility and diffusion of carbon in palladium. Acta Mater 1998;46:2823–30. https://doi.org/10.1016/S1359-6454(97)00458-8.

[108] Bayat N, Rezaei M, Meshkani F. Hydrogen and carbon nanofibers synthesis by methane decomposition over Ni-Pd/Al2O3catalyst. Int J Hydrogen Energy 2016;41:5494–503. https://doi.org/10.1016/j.ijhydene.2016.01.134.

[109] Ashok J, Reddy PS, Raju G, Subrahmanyam M, Venugopal A. Catalytic Decomposition of Methane to Hydrogen and Carbon Nanofibers over Ni−Cu−SiO 2 Catalysts. Energy & Fuels 2009;23:5–13. https://doi.org/10.1021/ef8003976.

[110] Wang H, Baker RTK. Decomposition of methane over a Ni-Cu-MgO catalyst to produce hydrogen and carbon nanofibers. J Phys Chem B 2004;108:20273–7. https://doi.org/10.1021/jp040496x.

[111] Al-Fatesh AS, Barama S, Ibrahim AA, Barama A, Khan WU, Fakeeha A. Study of Methane Decomposition on Fe/MgO-Based Catalyst Modified by Ni, Co, and Mn Additives. Chem Eng Commun 2017;204:739–49. https://doi.org/10.1080/00986445.2017.1311254.

[112] Al-Fatesh AS, Fakeeha AH, Khan WU, Ibrahim AA, He S, Seshan K. Production of hydrogen by catalytic methane decomposition over alumina supported mono-, bi- and tri-metallic catalysts. Int J Hydrogen Energy

2016;41:22932–40. https://doi.org/10.1016/j.ijhydene.2016.09.027.

[113] Pudukudy M, Yaakob Z, Akmal ZS. Direct decomposition of methane over SBA-15 supported Ni, Co and Fe based bimetallic catalysts. Appl Surf Sci 2015;330:418–30. https://doi.org/10.1016/j.apsusc.2015.01.032.

[114] Yu Z, Hu X, Jia P, Zhang Z, Dong D, Hu G, et al. Steam reforming of acetic acid over nickel-based catalysts: The intrinsic effects of nickel precursors on behaviors of nickel catalysts. Appl Catal B Environ 2018;237:538–53. https://doi.org/10.1016/j.apcatb.2018.06.020.

[115] Takenaka S, Ogihara H, Yamanaka I, Otsuka K. Decomposition of methane over supported-Ni catalysts: Effects of the supports on the catalytic lifetime. Appl Catal A Gen 2001;217:101–10. https://doi.org/10.1016/S0926-860X(01)00593-2.

[116] Ashok J, Raju G, Reddy PS, Subrahmanyam M, Venugopal A. Catalytic decomposition of CH4 over NiO–Al2O3–SiO2 catalysts: Influence of catalyst preparation conditions on the production of H2. Int J Hydrogen Energy 2008;33:4809–18. https://doi.org/10.1016/j.ijhydene.2008.06.004.

[117] Lázaro MJ, Echegoyen Y, Suelves I, Palacios JM, Moliner R. Decomposition of methane over Ni-SiO2 and Ni-Cu-SiO2 catalysts: Effect of catalyst preparation method. Appl Catal A Gen 2007;329:22–9. https://doi.org/10.1016/j.apcata.2007.06.014.

[118] Echegoyen Y, Suelves I, Lázaro MJ, Sanjuán ML, Moliner R. Thermo catalytic decomposition of methane over Ni-Mg and Ni-Cu-Mg catalysts. Effect of catalyst preparation method. Appl Catal A Gen 2007;333:229–37. https://doi.org/10.1016/j.apcata.2007.09.012.

[119] Chen D, Christensen KO, Ochoa-Fernández E, Yu Z, Tøtdal B, Latorre N, et al. Synthesis of carbon nanofibers: effects ofNi crystal size during methane decomposition. J Catal 2005;229:82–96. https://doi.org/10.1016/j.jcat.2004.10.017.

[120] Li Y, Zhang B, Xie X, Liu J, Xu Y, Shen W. Novel Ni catalysts for methane decomposition to hydrogen and carbon nanofibers. J Catal 2006;238:412–24. https://doi.org/10.1016/j.jcat.2005.12.027.

[121] Wang P, Tanabe E, Ito K, Jia J, Morioka H, Shishido T, et al. Filamentous

carbon prepared by the catalytic pyrolysis of CH4 on Ni/SiO2. Appl Catal A Gen 2002;231:35–44. https://doi.org/10.1016/S0926-860X(01)00906-1.

[122] Takenaka S, Kobayashi S, Ogihara H, Otsuka K. Ni/SiO2catalyst effective for methane decomposition into hydrogen and carbon nanofiber. J Catal 2003;217:79–87. https://doi.org/10.1016/S0021-9517(02)00185-9.

[123] Ping D, Wang C, Dong X, Dong Y. Co-production of hydrogen and carbon nanotubes on nickel foam via methane catalytic decomposition. Appl Surf Sci 2016;369:299–307. https://doi.org/10.1016/j.apsusc.2016.02.074.

[124] Fakeeha AH, Ibrahim AA, Khan WU, Seshan K, Al Otaibi RL, Al-Fatesh AS. Hydrogen production via catalytic methane decomposition over alumina supported iron catalyst. Arab J Chem 2018;11:405–14. https://doi.org/10.1016/j.arabjc.2016.06.012.

[125] Chai S-P, Sharif Zein SH, Mohamed AR. The effect of catalyst calcination temperature on the diameter of carbon nanotubes synthesized by the decomposition of methane. Carbon N Y 2007;45:1535–41. https://doi.org/10.1016/j.carbon.2007.03.020.

[126] Echegoyen Y, Suelves I, Lázaro MJ, Moliner R, Palacios JM. Hydrogen production by thermocatalytic decomposition of methane over Ni-Al and Ni-Cu-Al catalysts: Effect of calcination temperature. J Power Sources 2007;169:150–7. https://doi.org/10.1016/j.jpowsour.2007.01.058.

[127] Gao F, Walter ED, Washton NM, Szanyi J, Peden CHF. Synthesis and evaluation of Cu/SAPO-34 catalysts for NH3-SCR 2: Solid-state ion exchange and one-pot synthesis. Appl Catal B Environ 2015;162:501–14. https://doi.org/10.1016/j.apcatb.2014.07.029.

[128] Abdul Ghani A, Torabi F, Ibrahim H. Autothermal reforming process for efficient hydrogen production from crude glycerol using nickel supported catalyst: Parametric and statistical analyses. Energy 2018;144:129–45. https://doi.org/10.1016/j.energy.2017.11.132.

[129] Ermakova MA, Ermakov DY. Ni/SiO2and Fe/SiO2catalysts for production of hydrogen and filamentous carbon via methane decomposition. Catal Today 2002;77:225–35. https://doi.org/10.1016/S0920-5861(02)00248-1.

[130] Takenaka S, Ishida M, Serizawa M, Tanabe E, Otsuka K. Formation of

Carbon Nanofibers and Carbon Nanotubes through Methane Decomposition over Supported Cobalt Catalysts. J Phys Chem B 2004;108:11464–72. https://doi.org/10.1021/jp048827t.

[131] PINILLA J, MOLINER R, SUELVES I, LAZARO M, ECHEGOYEN Y, PALACIOS J. Production of hydrogen and carbon nanofibers by thermal decomposition of methane using metal catalysts in a fluidized bed reactor. Int J Hydrogen Energy 2007;32:4821–9. https://doi.org/10.1016/j.ijhydene.2007.08.013.

[132] Jang HT, Cha WS. Hydrogen production by the thermocatalytic decomposition of methane in a fluidized bed reactor. Korean J Chem Eng 2007;24:374–7. https://doi.org/10.1007/s11814-007-5037-9.

[133] Al-Fatesh AS, Abu-Dahrieh J, Ibrahim AA, Fakeeha AH, Khan WU. Coproduction of hydrogen and carbon filaments from methane decomposition over Fe/La<inf>2</inf>O<inf>3</inf>catalysts. J Chem Soc Pakistan 2016;38:1104–11.

[134] Maneerung T, Hidajat K, Kawi S. LaNiO3perovskite catalyst precursor for rapid decomposition of methane: Influence of temperature and presence of H2in feed stream. Catal Today 2011;171:24–35. https://doi.org/10.1016/j.cattod.2011.03.080.

[135] Pudukudy M, Yaakob Z, Takriff MS. Methane decomposition into COx free hydrogen and multiwalled carbon nanotubes over ceria, zirconia and lanthana supported nickel catalysts prepared via a facile solid state citrate fusion method. Energy Convers Manag 2016;126:302–15. https://doi.org/10.1016/j.enconman.2016.08.006.

[136] Rivas ME, Fierro JLG, Guil-López R, Peña MA, La Parola V, Goldwasser MR. Preparation and characterization of nickel-based mixed-oxides and their performance for catalytic methane decomposition. Catal Today 2008;133–135:367–73. https://doi.org/10.1016/j.cattod.2007.12.045.

[137] Ye RP, Gong W, Sun Z, Sheng Q, Shi X, Wang T, et al. Enhanced stability of Ni/SiO2 catalyst for CO2 methanation: Derived from nickel phyllosilicate with strong metal-support interactions. Energy 2019;188:116059. https://doi.org/10.1016/j.energy.2019.116059.

[138] Gallego J, Sierra G, Mondragon F, Barrault J, Batiot-Dupeyrat C. Synthesis of MWCNTs and hydrogen from ethanol catalytic decomposition over a Ni/La2O3catalyst produced by the reduction of LaNiO3. Appl Catal A Gen 2011;397:73–81. https://doi.org/10.1016/j.apcata.2011.02.017.

[139] Srilatha K, Viditha V, Srinivasulu D, Ramakrishna SUB, Himabindu V. Hydrogen production using thermocatalytic decomposition of methane on Ni30/activated carbon and Ni30/carbon black. Environ Sci Pollut Res 2016;23:9303–11. https://doi.org/10.1007/s11356-015-5112-4.

[140] Otsuka K, Ogihara H, Takenaka S. Decomposition of methane over Ni catalysts supported on carbon fibers formed from different hydrocarbons. Carbon N Y 2003;41:223–33. https://doi.org/10.1016/S0008-6223(02)00308-1.

[141] Venkateswaran R, Back MH, Scacchi G. The dual nature of carbon: Catalyst and inhibitor. Carbon N Y 1994;32:911–9. https://doi.org/10.1016/0008-6223(94)90048-5.

[142] Moliner R, Suelves I, Lázaro MJ, Moreno O. Thermocatalytic decomposition of methane over activated carbons: Influence of textural properties and surface chemistry. Int J Hydrogen Energy 2005;30:293–300. https://doi.org/10.1016/j.ijhydene.2004.03.035.

[143] Lee EK, Lee SY, Han GY, Lee BK, Lee TJ, Jun JH, et al. Catalytic decomposition of methane over carbon blacks for CO 2-free hydrogen production. Carbon N Y 2004;42:2641–8. https://doi.org/10.1016/j.carbon.2004.06.003.

[144] Serrano DP, Botas JÁ, Pizarro P, Gómez G. Kinetic and autocatalytic effects during the hydrogen production by methane decomposition over carbonaceous catalysts. Int J Hydrogen Energy 2013;38:5671–83. https://doi.org/10.1016/j.ijhydene.2013.02.112.

[145] Ryu BH, Lee SY, Lee DH, Han GY, Lee TJ, Yoon KJ. Catalytic characteristics of various rubber-reinforcing carbon blacks in decomposition of methane for hydrogen production. Catal Today 2007;123:303–9. https://doi.org/10.1016/j.cattod.2007.02.001.

[146] Guil-lopez R, Botas JA, Fierro JLG, Serrano DP. Comparison of metal and

carbon catalysts for hydrogen production by methane decomposition. "Applied Catal A, Gen 2011;396:40–51. https://doi.org/10.1016/j.apcata.2011.01.036.

[147] Muradov N. Thermocatalytic CO2-Free Production of Hydrogen from Hydrocarbon Fuels. 2000. https://doi.org/NREL/CP-570-28890.

[148] Muradov N. Catalysis of methane decomposition over elemental carbon. Catal Commun 2001;2:89–94. https://doi.org/10.1016/S1566-7367(01)00013-9.

[149] Charisiou ND, Douvartzides SL, Siakavelas GI, Tzounis L, Sebastian V, Stolojan V, et al. The Relationship between Reaction Temperature and Carbon Deposition on Nickel Catalysts Based on Al2O3, ZrO2 or SiO2 Supports during the Biogas Dry Reforming Reaction. Catalysts 2019;9:676. https://doi.org/10.3390/catal9080676.

[150] Moradi M, Moussavi G, Yaghmaeian K, Yazdanbakhsh A, Srivastava V, Sillanpää M. Synthesis of novel Ag-doped S-MgO nanosphere as an efficient UVA/LED-activated photocatalyst for non-radical oxidation of diclofenac: Catalyst preparation and characterization and photocatalytic mechanistic evaluation. Appl Catal B Environ 2020;260:118128. https://doi.org/10.1016/j.apcatb.2019.118128.

[151] Panić S, Kukovecz Á, Boskovic G. Design of catalytic carbon nanotube-based reactor for water denitration – The impact of active metal confinement. Appl Catal B Environ 2018;225:207–17. https://doi.org/10.1016/j.apcatb.2017.11.078.

[152] Wang J, Zhu W, Yang S, Wang W, Zhou Y. Catalytic wet air oxidation of phenol with pelletized ruthenium catalysts. Appl Catal B Environ 2008;78:30–7. https://doi.org/10.1016/j.apcatb.2007.08.014.

[153] Kolios G, Gritsch A, Morillo A, Tuttlies U, Bernnat J, Opferkuch F, et al. Heat-integrated reactor concepts for catalytic reforming and automotive exhaust purification. Appl Catal B Environ 2007;70:16–30. https://doi.org/10.1016/j.apcatb.2006.01.030.

[154] Ashik UPM, Wan Daud WMA, ichiro Hayashi J. A review on methane transformation to hydrogen and nanocarbon: Relevance of catalyst characteristics and experimental parameters on yield. Renew Sustain Energy

Rev 2017;76:743–67. https://doi.org/10.1016/j.rser.2017.03.088.

[155] Lee KK, Han GY, Yoon KJ, Lee BK. Thermocatalytic hydrogen production from the methane in a fluidized bed with activated carbon catalyst. Catal Today 2004;93–95:81–6. https://doi.org/10.1016/j.cattod.2004.06.080.

[156] Azimi SS, Kalbasi M. Three-phase modeling of dehydrogenation of isobutane to isobutene in a fluidized bed reactor: Effect of operating conditions on the energy consumption. Energy 2018;149:250–61. https://doi.org/10.1016/j.energy.2018.02.012.

[157] Gokon N, Kumaki S, Miyaguchi Y, Bellan S, Kodama T, Cho H. Development of a 5kW th internally circulating fluidized bed reactor containing quartz sand for continuously-fed coal-coke gasification and a beam-down solar concentrating system. Energy 2019;166:1–16. https://doi.org/10.1016/j.energy.2018.10.036.

[158] Effendi A, Zhang ZG, Hellgardt K, Honda K, Yoshida T. Steam reforming of a clean model biogas over Ni/Al2O3 in fluidized- and fixed-bed reactors. Catal Today 2002;77:181–9. https://doi.org/10.1016/S0920-5861(02)00244-4.

[159] Yang S, Wang H, Wei Y, Hu J, Chew JW. Eulerian-Lagrangian simulation of air-steam biomass gasification in a three-dimensional bubbling fluidized gasifier. Energy 2019;181:1075–93. https://doi.org/10.1016/j.energy.2019.06.003.

[160] Pohlenz JB, Heights A, Scott NH, J P, N S. Method for Hydrogen Production by Catalytic Decomposition of a Gaseous Hydrocarbon Stream. US3284161, 1966.

[161] Weizhong Q, Tang L, Zhanwen W, Fei W, Zhifei L, Guohua L, et al. Production of hydrogen and carbon nanotubes from methane decomposition in a two-stage fluidized bed reactor. Appl Catal A Gen 2004;260:223–8. https://doi.org/10.1016/j.apcata.2003.10.018.

[162] Shah N, Ma S, Wang Y, Huffman GP. Semi-continuous hydrogen production from catalytic methane decomposition using a fluidized-bed reactor. Int J Hydrogen Energy 2007;32:3315–9. https://doi.org/10.1016/j.ijhydene.2007.04.040.

[163] Ammendola P, Chirone R, Ruoppolo G, Russo G. Production of hydrogen

from thermo-catalytic decomposition of methane in a fluidized bed reactor. Chem Eng J 2009;154:287–94. https://doi.org/10.1016/j.cej.2009.03.048.

[164] Rahman MS, Croiset E, Hudgins RR. Catalytic Decomposition of Methane for Hydrogen Production. Top Catal 2006;37:137–45. https://doi.org/10.1007/s11244-006-0015-8.

[165] Tanggarnjanavalukul C, Donphai W, Witoon T, Chareonpanich M, Limtrakul J. Deactivation of nickel catalysts in methane cracking reaction: Effect of bimodal meso–macropore structure of silica support. Chem Eng J 2015;262:364–71. https://doi.org/10.1016/j.cej.2014.09.112.

[166] Shah N, Panjala D, Huffman GP. Hydrogen Production by Catalytic Decomposition of Methane 2001. https://doi.org/10.1021/ef0101964.

[167] Villacampa JI, Royo C, Romeo E, Montoya JA, Del Angel P, Monzón A. Catalytic decomposition of methane over Ni-Al2O3 coprecipitated catalysts. Appl Catal A Gen 2003;252:363–83. https://doi.org/10.1016/S0926-860X(03)00492-7.

[168] Nuernberg GB, Fajardo H V., Mezalira DZ, Casarin TJ, Probst LFD, Carreño NLV. Preparation and evaluation of Co/Al2O3 catalysts in the production of hydrogen from thermo-catalytic decomposition of methane: Influence of operating conditions on catalyst performance. Fuel 2008;87:1698–704. https://doi.org/10.1016/j.fuel.2007.08.005.

[169] Pinilla JL, Suelves I, Lázaro MJ, Moliner R, Palacios JM. Parametric study of the decomposition of methane using a NiCu/Al2O3catalyst in a fluidized bed reactor. Int J Hydrogen Energy 2010;35:9801–9. https://doi.org/10.1016/j.ijhydene.2009.10.008.

[170] Torres D, de Llobet S, Pinilla JL, Lázaro MJ, Suelves I, Moliner R. Hydrogen production by catalytic decomposition of methane using a Fe-based catalyst in a fluidized bed reactor. J Nat Gas Chem 2012;21:367–73. https://doi.org/10.1016/S1003-9953(11)60378-2.

[171] Suelves I, Pinilla JL, Lázaro MJ, Moliner R, Palacios JM. Effects of reaction conditions on hydrogen production and carbon nanofiber properties generated by methane decomposition in a fixed bed reactor using a NiCuAl catalyst. J Power Sources 2009;192:35–42.

https://doi.org/10.1016/j.jpowsour.2008.11.096.

[172] Wang J, Jin L, Li Y, Wang M, Hu H. Effect of hydrogen additive on methane decomposition to hydrogen and carbon over activated carbon catalyst. Int J Hydrogen Energy 2018;43:17611–9. https://doi.org/10.1016/j.ijhydene.2018.07.179.

[173] Piao L, Li Y, Chen J, Chang L, Lin JYS. Methane decomposition to carbon nanotubes and hydrogen on an alumina supported nickel aerogel catalyst. Catal Today 2002;74:145–55. https://doi.org/10.1016/S0920-5861(01)00540-5.

[174] Uniongas. Chemical composition of natural gas n.d. https://www.uniongas.com/about-us/about-natural-gas/chemical-composition-of-natural-gas (accessed February 4, 2020).

[175] Bock S, Zacharias R, Hacker V. Experimental study on high-purity hydrogen generation from synthetic biogas in a 10 kW fixed-bed chemical looping system. RSC Adv 2019;9:23686–95. https://doi.org/10.1039/c9ra03123e.

[176] Charisiou ND, Tzounis L, Sebastian V, Hinder SJ, Baker MA, Polychronopoulou K, et al. Investigating the correlation between deactivation and the carbon deposited on the surface of Ni/Al2O3 and Ni/La2O3-Al2O3 catalysts during the biogas reforming reaction. Appl Surf Sci 2019;474:42–56. https://doi.org/10.1016/j.apsusc.2018.05.177.

[177] Inaba M, Zhang Z, Matsuoka K, Soneda Y. Optimization of the reaction conditions for Fe-catalyzed decomposition of methane and characterization of the produced nanocarbon fibers. Catal Today 2019;332:11–9. https://doi.org/10.1016/j.cattod.2018.11.014.

[178] AMMENDOLA P, CHIRONE R, RUOPPOLO G, RUSSO G, SOLIMENE R. Some issues in modelling methane catalytic decomposition in fluidized bed reactors. Int J Hydrogen Energy 2008;33:2679–94. https://doi.org/10.1016/j.ijhydene.2008.03.033.

[179] Hsieh L Te, Lee WJ, Chen CY, Chang MB, Chang HC. Converting methane by using an RF plasma reactor. Plasma Chem Plasma Process 1998;18:215–39. https://doi.org/10.1023/A:1021650516043.

[180] Tu X, Gallon HJ, Twigg M V., Gorry PA, Whitehead JC. Dry reforming of

methane over a Ni/Al 2 O 3 catalyst in a coaxial dielectric barrier discharge reactor. J Phys D Appl Phys 2011;44:274007. https://doi.org/10.1088/0022-3727/44/27/274007.

[181] Tu X, Whitehead JC. Plasma-catalytic dry reforming of methane in an atmospheric dielectric barrier discharge: Understanding the synergistic effect at low temperature. Appl Catal B Environ 2012;125:439–48. https://doi.org/10.1016/j.apcatb.2012.06.006.

[182] Aleknaviciute I, Karayiannis TG, Collins MW, Xanthos C. Methane decomposition under a corona discharge to generate COx-free hydrogen. Energy 2013;59:432–9. https://doi.org/10.1016/j.energy.2013.06.059.

[183] Zhao G-B, John S, Zhang J-J, Wang L, Muknahallipatna S, Hamann JC, et al. Methane conversion in pulsed corona discharge reactors. Chem Eng J 2006;125:67–79. https://doi.org/10.1016/j.cej.2006.08.008.

[184] Li MW, Xu GH, Tian YL, Chen L, Fu HF. Carbon Dioxide Reforming of Methane Using DC Corona Discharge Plasma Reaction. J Phys Chem A 2004;108:1687–93. https://doi.org/10.1021/jp037008q.

[185] Cheng D, Zhu X, Ben Y, He F, Cui L, Liu C. Carbon dioxide reforming of methane over Ni/Al2O3 treated with glow discharge plasma. Catal Today 2006;115:205–10. https://doi.org/10.1016/j.cattod.2006.02.063.

[186] Li D, Li X, Bai M, Tao X, Shang S, Dai X, et al. CO2 reforming of CH4 by atmospheric pressure glow discharge plasma: A high conversion ability. Int J Hydrogen Energy 2009;34:308–13. https://doi.org/10.1016/j.ijhydene.2008.10.053.

[187] Heintze M, Magureanu M, Kettlitz M. Mechanism of C2 hydrocarbon formation from methane in a pulsed microwave plasma. J Appl Phys 2002;92:7022–31. https://doi.org/10.1063/1.1521518.

[188] Wang YF, Tsai CH, Chang WY, Kuo YM. Methane steam reforming for producing hydrogen in an atmospheric-pressure microwave plasma reactor. Int J Hydrogen Energy 2010;35:135–40. https://doi.org/10.1016/j.ijhydene.2009.10.088.

[189] Tu X, Whitehead JC. Plasma dry reforming of methane in an atmospheric pressure AC gliding arc discharge: Co-generation of syngas and carbon

nanomaterials. Int J Hydrogen Energy 2014;39:9658–69. https://doi.org/10.1016/j.ijhydene.2014.04.073.

[190] Bo Z, Yan J, Li X, Chi Y, Cen K. Plasma assisted dry methane reforming using gliding arc gas discharge: Effect of feed gases proportion. Int J Hydrogen Energy 2008;33:5545–53. https://doi.org/10.1016/j.ijhydene.2008.05.101.

[191] Malik MA, Hughes D, Malik A, Xiao S, Schoenbach KH. Study of the Production of Hydrogen and Light Hydrocarbons by Spark Discharges in Diesel, Kerosene, Gasoline, and Methane. Plasma Chem Plasma Process 2013;33:271–9. https://doi.org/10.1007/s11090-012-9429-1.

[192] Li X-S, Zhu B, Shi C, Xu Y, Zhu A-M. Carbon dioxide reforming of methane in kilohertz spark-discharge plasma at atmospheric pressure. AIChE J 2011;57:2854–60. https://doi.org/10.1002/aic.12472.

[193] Mishra L, Shibata K, Ito H. Conversion of methane to hydrogen via pulsed corona discharge. J Nat Gas 2004;13:82–6.

[194] Kheirollahivash M, Rashidi F, Moshrefi MM. Hydrogen Production from Methane Decomposition Using a Mobile and Elongating Arc Plasma Reactor. Plasma Chem Plasma Process 2019;39:445–59. https://doi.org/10.1007/s11090-018-9950-y.

[195] Khalifeh O, Taghvaei H, Mosallanejad A, Rahimpour MR, Shariati A. Extra pure hydrogen production through methane decomposition using nanosecond pulsed plasma and Pt–Re catalyst. Chem Eng J 2016;294:132–45. https://doi.org/10.1016/j.cej.2016.02.077.

[196] Nishida Y, Cheng C-Z, Iwasaki K. Hydrogen Production From Hydrocarbons With Use of Plasma Discharges Under High Pressure Condition. IEEE Trans Plasma Sci 2014;42:3674–80. https://doi.org/10.1109/TPS.2014.2337351.

[197] Mishra LN, Shibata K, Ito H, Yugami N, Nishida Y. Pulsed Corona Discharge as a Source of Hydrogen and Carbon Nanotube Production. IEEE Trans Plasma Sci 2004;32:1727–33. https://doi.org/10.1109/TPS.2004.831591.

[198] Steinberg M. Fossil fuel decarbonization technology for mitigating global warming. Int J Hydrogen Energy 1999;24:771–7. https://doi.org/10.1016/S0360-3199(98)00128-1.

[199] Upham DC, Agarwal V, Khechfe A, Snodgrass ZR, Gordon MJ, Metiu H, et al. Catalytic molten metals for the direct conversion of methane to hydrogen and separable carbon. Science (80-) 2017;358:917–21. https://doi.org/10.1126/science.aao5023.

[200] Wang HY, Lua AC. Deactivation and kinetic studies of unsupported Ni and Ni-Co-Cu alloy catalysts used for hydrogen production by methane decomposition. Chem Eng J 2014;243:79–91. https://doi.org/10.1016/j.cej.2013.12.100.

[201] Charisiou ND, Siakavelas G, Tzounis L, Sebastian V, Monzon A, Baker MA, et al. An in depth investigation of deactivation through carbon formation during the biogas dry reforming reaction for Ni supported on modified with CeO2 and La2O3 zirconia catalysts. Int J Hydrogen Energy 2018;43:18955–76. https://doi.org/10.1016/j.ijhydene.2018.08.074.

[202] Khiari B, Jeguirim M, Bennici S, Limousy L. Char combustion. Elsevier Inc.; 2019. https://doi.org/10.1016/b978-0-12-814893-8.00005-5.

[203] Parkinson B, Tabatabaei M, Upham DC, Ballinger B, Greig C, Smart S, et al. Hydrogen production using methane: Techno-economics of decarbonizing fuels and chemicals. Int J Hydrogen Energy 2018;43:2540–55. https://doi.org/10.1016/j.ijhydene.2017.12.081.

[204] Fakeeha AH, Barama S, Ibrahim AA, Al-Otaibi RL, Barama A, Abasaeed AE, et al. In situ regeneration of alumina-supported Cobalt–iron catalysts for hydrogen production by catalytic methane decomposition. Catalysts 2018;8. https://doi.org/10.3390/catal8110567.

[205] Li J, Smith KJ. Methane decomposition and catalyst regeneration in a cyclic mode over supported Co and Ni catalysts. Appl Catal A Gen 2008;349:116–24. https://doi.org/10.1016/j.apcata.2008.07.011.

[206] Muradov NZ, Veziroğlu TN. "Green" path from fossil-based to hydrogen economy: An overview of carbon-neutral technologies. Int J Hydrogen Energy 2008;33:6804–39. https://doi.org/10.1016/j.ijhydene.2008.08.054.

[207] Gilliland ER, Harriott P. Reactivity of Deposited Carbon. Ind Eng Chem 1954;46:2195–202. https://doi.org/10.1021/ie50538a052.

[208] Alamolhoda S, Vitale G, Hassan A, Nassar NN, Pereira Almao P.

Development and characterization of novel combinations of Ce-Ni-MFI solids for water gas shift reaction. Can J Chem Eng 2019;97:140–51. https://doi.org/10.1002/cjce.23201.

[209] Lazzaroni E, Elsholkami M, Martelli E, Elkamel A. Design and simulation of a petcoke gasification polygeneration plant integrated with a bitumen extraction and upgrading facility and net energy analysis. Energy 2017;141:880–91. https://doi.org/10.1016/j.energy.2017.09.072.

[210] Barbarias I, Artetxe M, Lopez G, Arregi A, Santamaria L, Bilbao J, et al. Catalyst performance in the HDPE pyrolysis-reforming under reaction-regeneration cycles. Catalysts 2019;9. https://doi.org/10.3390/catal9050414.

[211] Aiello R, Fiscus JE, zur Loye H-C, Amiridis MD. Hydrogen production via the direct cracking of methane over Ni/SiO2: catalyst deactivation and regeneration. Appl Catal A Gen 2000;192:227–34. https://doi.org/10.1016/S0926-860X(99)00345-2.

[212] Zhang T, Amiridis MD. Hydrogen production via the direct cracking of methane over silica-supported nickel catalysts. Appl Catal A Gen 1998;167:161–72. https://doi.org/10.1016/S0926-860X(97)00143-9.

[213] Łamacz A. CNT and H2 Production During CH4 Decomposition over Ni/CeZrO2. I. A Mechanistic Study. ChemEngineering 2019;3:26. https://doi.org/10.3390/chemengineering3010026.

[214] Łamacz A, Łabojko G. CNT and H2 Production during CH4 Decomposition over Ni/CeZrO2. II. Catalyst Performance and Its Regeneration in a Fluidized Bed. ChemEngineering 2019;3:25. https://doi.org/10.3390/chemengineering3010025.

[215] Chang JS, Park SE, Yoo JW, Park JN. Catalytic behavior of supported KNiCa catalyst and mechanistic consideration for carbon dioxide reforming of methane. J Catal 2000;195:1–11. https://doi.org/10.1006/jcat.2000.2978.

[216] Matsukata M, Matsushita T, Ueyama K. A novel hydrogen/syngas production process: Catalytic activity and stability of Ni/SiO2. Chem Eng Sci 1996;51:2769–74. https://doi.org/10.1016/0009-2509(96)00150-9.

[217] Abbas HF, Daud WMAW. Thermocatalytic decomposition of methane for hydrogen production using activated carbon catalyst: Regeneration and

characterization studies. Int J Hydrogen Energy 2009;34:8034–45. https://doi.org/10.1016/j.ijhydene.2009.08.014.

[218] O'Neill HSC. Free energies of formation of NiO, CoO, Ni2SiO4 and Co2SiO4. Am Mineral 1987;72:280–91.

[219] Agaev TN, Garibov AA, Guseinov VI, Melikova SZ, Tagiev MM, Dzhafarova SZ. Kinetics of the Radiation-Catalytic and Catalytic Decomposition of Water on a Surface of Nano-Zirconium. Russ J Phys Chem A 2019;93:44–7. https://doi.org/10.1134/S0036024419010023.

[220] L'vov B V., Galwey AK. The mechanism and kinetics of NiO reduction by hydrogen Thermochemical approach. J Therm Anal Calorim 2012;110:601–10. https://doi.org/10.1007/s10973-011-2000-0.

[221] Hu YH. Solid-solution catalysts for CO2 reforming of methane. Catal Today 2009;148:206–11. https://doi.org/10.1016/j.cattod.2009.07.076.

[222] Matsumura Y, Nakamori T. Steam reforming of methane over nickel catalysts at low reaction temperature. Appl Catal A Gen 2004;258:107–14. https://doi.org/10.1016/j.apcata.2003.08.009.

[223] Alizadeh R, Jamshidi E, Ale-Ebrahim H. Kinetic study of nickel oxide reduction by methane. Chem Eng Technol 2007;30:1123–8. https://doi.org/10.1002/ceat.200700067.

[224] Xia J, Reddy L, Ju W, Gary D, Del-gallo P, Basset J, et al. Optimization of a fluidized bed reactor for methane decomposition over Fe / Al 2 O 3 catalysts : Activity and regeneration studies. Int J Hydrogen Energy 2019. https://doi.org/10.1016/j.ijhydene.2019.10.058.

[225] Blackwood JD, McTaggart FK. Reactions of carbon with atomic gases. Aust J Chem 1959;12:533–42. https://doi.org/10.1071/CH9590533.

[226] Figueiredo JL, Bernardo CA, Chludzinski JJ, Baker RTK. The reversibility of filamentous carbon growth and gasification. J Catal 1988;110:127–38. https://doi.org/10.1016/0021-9517(88)90303-X.

[227] Blackwood JD, McCarthy DJ. The Mechanism of Hydrogenation of Coal to Methane. Aust J Chem 1966;19:797–813. https://doi.org/10.1071/CH9660797.

[228] Blackwood JD. The kinetics of the system carbon-hydrogen-methane 1962.

[229] Blackwood JD, McCarthy DJ, Cullis BD. The Carbon-Hydrogen Reaction with Cokes and Chars. Aust J Chem 1967;20:3–6.

[230] Hardiman KM, Cooper CG, Adesina AA, Lange R. Post-mortem characterization of coke-induced deactivated alumina-supported Co-Ni catalysts. Chem Eng Sci 2006;61:2565–73. https://doi.org/10.1016/j.ces.2005.11.021.

[231] Figueiredo JL. Reactivity of coke deposited on metal surfaces. Mater Corros - Werkstoffe Und Korrosion 1999;50:696–9. https://doi.org/10.1002/(SICI)1521-4176(199912)50:12<696::AID-MACO696>3.0.CO;2-I.

[232] Bernardo CA, Trimms DL. Trimm, Kinetics of gasification of carbondeposited on nickel catalysts, 1979 1979;17.

[233] Audier M, Coulon M, Bonnetain L. Hydrogenation of catalytic carbons obtained by CO disproportionation or CH4 decomposition on nickel. Carbon N Y 1979;17:391–4. https://doi.org/10.1016/0008-6223(79)90052-6.

[234] Nishiyama Y, Tamai Y. Deposition of carbon and its hydrogenation catalyzed by nickel. Carbon N Y 1976;14:13–7. https://doi.org/10.1016/0008-6223(76)90075-0.

[235] Figueiredo JL, Trimm DL. Gasification of carbon deposits on nickel catalysts. J Catal 1975;40:154–9. https://doi.org/10.1016/0021-9517(75)90241-9.

[236] Zhang J, Schneider A, Inden G. Cementite decomposition and coke gasification in He and H2-He gas mixtures. Corros Sci 2004;46:667–79. https://doi.org/10.1016/S0010-938X(03)00177-X.

[237] U.S. Department of Energy, Ohi JM, Vanderborgh N, Voecks G. Hydrogen Fuel Quality Specifications for Polymer Electrolyte Fuel Cells in Road Vehicles. Safety, Codes Stand Progr 2016:1–72. https://doi.org/10.1111/j.1439-0507.2006.01349.x.

[238] Matsumura Y, Ishibe H. Selective steam reforming of methanol over silica-supported copper catalyst prepared by sol-gel method. Appl Catal B Environ 2009;86:114–20. https://doi.org/10.1016/j.apcatb.2008.08.007.

[239] Basile A, Tereschenko GF, Orekhova N V., Ermilova MM, Gallucci F, Iulianelli A. An experimental investigation on methanol steam reforming with

oxygen addition in a flat Pd-Ag membrane reactor. Int J Hydrogen Energy 2006;31:1615–22. https://doi.org/10.1016/j.ijhydene.2005.12.013.

[240] Basile A, Gallucci F, Tosti S. Synthesis, Characterization, and Applications of Palladium Membranes. Membr. Sci. Technol., vol. 13, 2008, p. 255–323. https://doi.org/10.1016/S0927-5193(07)13008-4.

[241] Athanassiou C, Pekridis G, Kaklidis N, Kalimeri K, Vartzoka S, Marnellos G. Hydrogen production in solid electrolyte membrane reactors (SEMRs). Int J Hydrogen Energy 2007;32:38–54. https://doi.org/10.1016/j.ijhydene.2006.06.031.

[242] Chen Y, Wang Y, Xu H, Xiong G. Efficient production of hydrogen from natural gas steam reforming in palladium membrane reactor. Appl Catal B Environ 2008;81:283–94. https://doi.org/10.1016/j.apcatb.2007.10.024.

[243] Kyriakou V, Garagounis I, Vourros A, Vasileiou E, Manerbino A, Coors WG, et al. Methane steam reforming at low temperatures in a BaZr0.7Ce0.2Y0.1O2.9 proton conducting membrane reactor. Appl Catal B Environ 2016;186:1–9. https://doi.org/10.1016/j.apcatb.2015.12.039.

[244] Ishihara T, Miyashita Y, Iseda H, Takita Y. Decomposition of Methane over Ni/SiO 2 Catalysts with Membrane Reactor for the Production of Hydrogen. Chem Lett 1995;24:93–4. https://doi.org/10.1246/cl.1995.93.

[245] Sheu EJ, Mokheimer EMA, Ghoniem AF. A review of solar methane reforming systems. Int J Hydrogen Energy 2015;40:12929–55. https://doi.org/10.1016/j.ijhydene.2015.08.005.

[246] Kunadian I, Andrews R, Qian D, Pinar Mengüç M. Growth kinetics of MWCNTs synthesized by a continuous-feed CVD method. Carbon N Y 2009;47:384–95. https://doi.org/10.1016/j.carbon.2008.10.022.

[247] Fujita JI, Hiyama T, Hirukawa A, Kondo T, Nakamura J, Ito SI, et al. Near room temperature chemical vapor deposition of graphene with diluted methane and molten gallium catalyst. Sci Rep 2017;7. https://doi.org/10.1038/s41598-017-12380-w.

[248] Nishii H, Miyamoto D, Umeda Y, Hamaguchi H, Suzuki M, Tanimoto T, et al. Catalytic activity of several carbons with different structures for methane decomposition and by-produced carbons. Appl Surf Sci 2019;473:291–7.

https://doi.org/10.1016/j.apsusc.2018.12.073.

[249] Awadallah AE, Aboul-Enein AA, Mahmoud AH, Abd El Rehim SS, El-Ziaty AK, Aboul-Gheit AK. Methane decomposition into CO x -free hydrogen and carbon nanomaterials over ZrO 2 –M (M = MgO, Al 2 O 3 , SiO 2 , La 2 O 3 or CeO 2) binary oxides supported cobalt catalysts. Fullerenes Nanotub Carbon Nanostructures 2019;27:128–36. https://doi.org/10.1080/1536383X.2018.1523147.

[250] Musamali R, Isa YM. Decomposition of Methane to Carbon and Hydrogen: A Catalytic Perspective. Energy Technol 2019;7. https://doi.org/10.1002/ente.201800593.

[251] Zhang C, Zhang W, Drewett NE, Wang X, Yoo SJ, Wang H, et al. Integrating Catalysis of Methane Decomposition and Electrocatalytic Hydrogen Evolution with Ni/CeO 2 for Improved Hydrogen Production Efficiency. ChemSusChem 2019;12:1000–10. https://doi.org/10.1002/cssc.201802618.

[252] Gonzalez I, De Jesus JC, Cañizales E, Delgado B, Urbina C. Comparison of the surface state of Ni nanoparticles used for methane catalytic decomposition. J Phys Chem C 2012;116:21577–87. https://doi.org/10.1021/jp302372r.

[253] Carneiro OC, Kim MS, Yim JB, Rodriguez NM, Baker RTK. Growth of graphite nanofibers from the iron-copper catalyzed decomposition of CO/H2 mixtures. J Phys Chem B 2003;107:4237–44. https://doi.org/10.1021/jp022364e.

[254] Monthioux M, Noé L, Dussault L, Dupin JC, Latorre N, Ubieto T, et al. Texturising and structurising mechanisms of carbon nanofilaments during growth. J Mater Chem 2007;17:4611–8. https://doi.org/10.1039/b707742d.

[255] Rodriguez NM, Chambers A, Baker RTK. Catalytic Engineering of Carbon Nanostructures. Langmuir 1995;11:3862–6. https://doi.org/10.1021/la00010a042.

[256] Cassell AM, Raymakers JA, Kong J, Dai H. Large Scale CVD Synthesis of Single-Walled Carbon Nanotubes. J Phys Chem B 1999;103:6484–92. https://doi.org/10.1021/jp990957s.

[257] Chai SP, Lee KY, Ichikawa S, Mohamed AR. Synthesis of carbon nanotubes

by methane decomposition over Co-Mo/Al2O3: Process study and optimization using response surface methodology. Appl Catal A Gen 2011;396:52–8. https://doi.org/10.1016/j.apcata.2011.01.038.

[258] Pinilla JL, Suelves I, Lázaro MJ, Moliner R, Palacios JM. Influence of nickel crystal domain size on the behaviour of Ni and NiCu catalysts for the methane decomposition reaction. Appl Catal A Gen 2009;363:199–207. https://doi.org/10.1016/j.apcata.2009.05.009.

[259] Dussault L, Dupin JC, Guimon C, Monthioux M, Latorre N, Ubieto T, et al. Development of Ni-Cu-Mg-Al catalysts for the synthesis of carbon nanofibers by catalytic decomposition of methane. J Catal 2007;251:223–32. https://doi.org/10.1016/j.jcat.2007.06.022.

[260] Lua AC, Wang HY. Decomposition of methane over unsupported porous nickel and alloy catalyst. Appl Catal B Environ 2013;132–133:469–78. https://doi.org/10.1016/j.apcatb.2012.12.014.

[261] Bai Z, Li W, Bai J, Li B, Chen H. The effects of textural properties and surface chemistry of activated carbon on its catalytic performance in methane decomposition for hydrogen production. Energy Sources, Part A Recover Util Environ Eff 2012;34:1145–53. https://doi.org/10.1080/15567031003663174.

[262] Global CCS institute n.d. https://www.globalccsinstitute.com.

[263] Simon F. Europeans confront biomethane cost reduction challenge. EURACTIV 2019.

[264] Guo Y, Ruan K, Yang X, Ma T, Kong J, Wu N, et al. Constructing fully carbon-based fillers with a hierarchical structure to fabricate highly thermally conductive polyimide nanocomposites. J Mater Chem C 2019;7:7035–44. https://doi.org/10.1039/c9tc01804b.

[265] Leong CK, Chung DDL. Improving the electrical and mechanical behavior of electrically conductive paint by partial replacement of silver by carbon black. J Electron Mater 2006;35:118–22. https://doi.org/10.1007/s11664-006-0193-y.

[266] WU S, LIU X, YE Q, LI N. Self-monitoring electrically conductive asphalt-based composite containing carbon fillers. Trans Nonferrous Met Soc China 2006;16:s512–6. https://doi.org/10.1016/s1003-6326(06)60246-x.

[267] Amin MS, El-Gamal SMA, Hashem FS. Fire resistance and mechanical properties of carbon nanotubes - Clay bricks wastes (Homra) composites cement. Constr Build Mater 2015;98:237–49. https://doi.org/10.1016/j.conbuildmat.2015.08.074.

[268] A V, M S. Usage of Carbon nanotubes and nano fibers in cement and concrete: A review. Int J Eng Technol 2017;9:564–9. https://doi.org/10.21817/ijet/2017/v9i2/170902045.

[269] Rattanasom N, Saowapark T, Deeprasertkul C. Reinforcement of natural rubber with silica/carbon black hybrid filler. Polym Test 2007;26:369–77. https://doi.org/10.1016/j.polymertesting.2006.12.003.

[270] Mittal G, Dhand V, Rhee KY, Park SJ, Lee WR. A review on carbon nanotubes and graphene as fillers in reinforced polymer nanocomposites. J Ind Eng Chem 2015;21:11–25. https://doi.org/10.1016/j.jiec.2014.03.022.

[271] Serp P, Figueiredo JL, editors. Carbon Materials for Catalysis. Hoboken, NJ, USA: John Wiley & Sons, Inc.; 2008. https://doi.org/10.1002/9780470403709.

[272] Abotsi GMK, Scaroni AW. A review of carbon-supported hydrodesulfurization catalysts. Fuel Process Technol 1989;22:107–33. https://doi.org/10.1016/0378-3820(89)90028-3.

[273] Kisiela AM, Czajka KM, Moroń W, Rybak W, Andryjowicz C. Unburned carbon from lignite fly ash as an adsorbent for SO2 removal. Energy 2016;116:1454–63. https://doi.org/10.1016/j.energy.2016.02.143.

[274] Cui Q, Tao G, Chen H, Guo X, Yao H. Environmentally benign working pairs for adsorption refrigeration. Energy 2005;30:261–71. https://doi.org/10.1016/j.energy.2004.05.005.

[275] Yaumi AL, Bakar MZA, Hameed BH. Reusable nitrogen-doped mesoporous carbon adsorbent for carbon dioxide adsorption in fixed-bed. Energy 2017;138:776–84. https://doi.org/10.1016/j.energy.2017.07.130.

[276] Zhang Y, Heo YJ, Son YR, In I, An KH, Kim BJ, et al. Recent advanced thermal interfacial materials: A review of conducting mechanisms and parameters of carbon materials. Carbon N Y 2019;142:445–60. https://doi.org/10.1016/j.carbon.2018.10.077.

[277] Kwon YK, Kim P. Unusually high thermal conductivity in carbon nanotubes. High Therm Conduct Mater 2006:227–65. https://doi.org/10.1007/0-387-25100-6_8.

[278] Prasher RS, Hu XJ, Chalopin Y, Mingo N, Lofgreen K, Volz S, et al. Turning carbon nanotubes from exceptional heat conductors into insulators. Phys Rev Lett 2009;102:1–4. https://doi.org/10.1103/PhysRevLett.102.105901.

[279] Novák I, Krupa I, Janigová I. Hybrid electro-conductive composites with improved toughness, filled by carbon black. Carbon N Y 2005;43:841–8. https://doi.org/10.1016/j.carbon.2004.11.019.

[280] Han J, Wang H, Yue Y, Mei C, Chen J, Huang C, et al. A self-healable and highly flexible supercapacitor integrated by dynamically cross-linked electro-conductive hydrogels based on nanocellulose-templated carbon nanotubes embedded in a viscoelastic polymer network. Carbon N Y 2019;149:1–18. https://doi.org/10.1016/j.carbon.2019.04.029.

[281] Keshavarz AH, Mohseni M, Montazer M. Electro-conductive modification of polyethylene terephthalate fabric with nano carbon black and washing fastness improvement by dopamine self-polymerized layer. J Appl Polym Sci 2019;136:1–8. https://doi.org/10.1002/app.48035.

Figure 1

Click here to download high resolution image

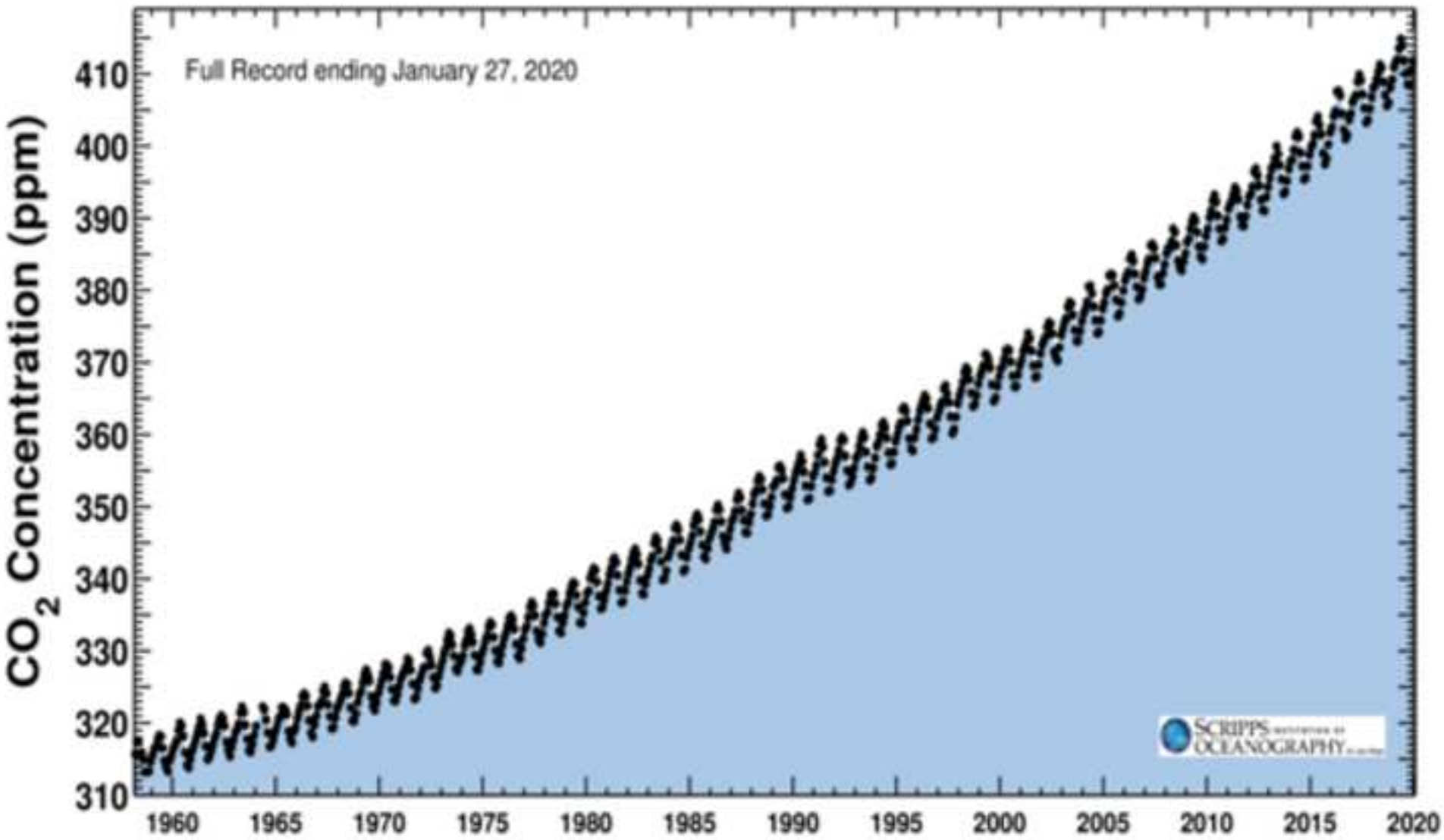

Figure 2
Click here to download high resolution image

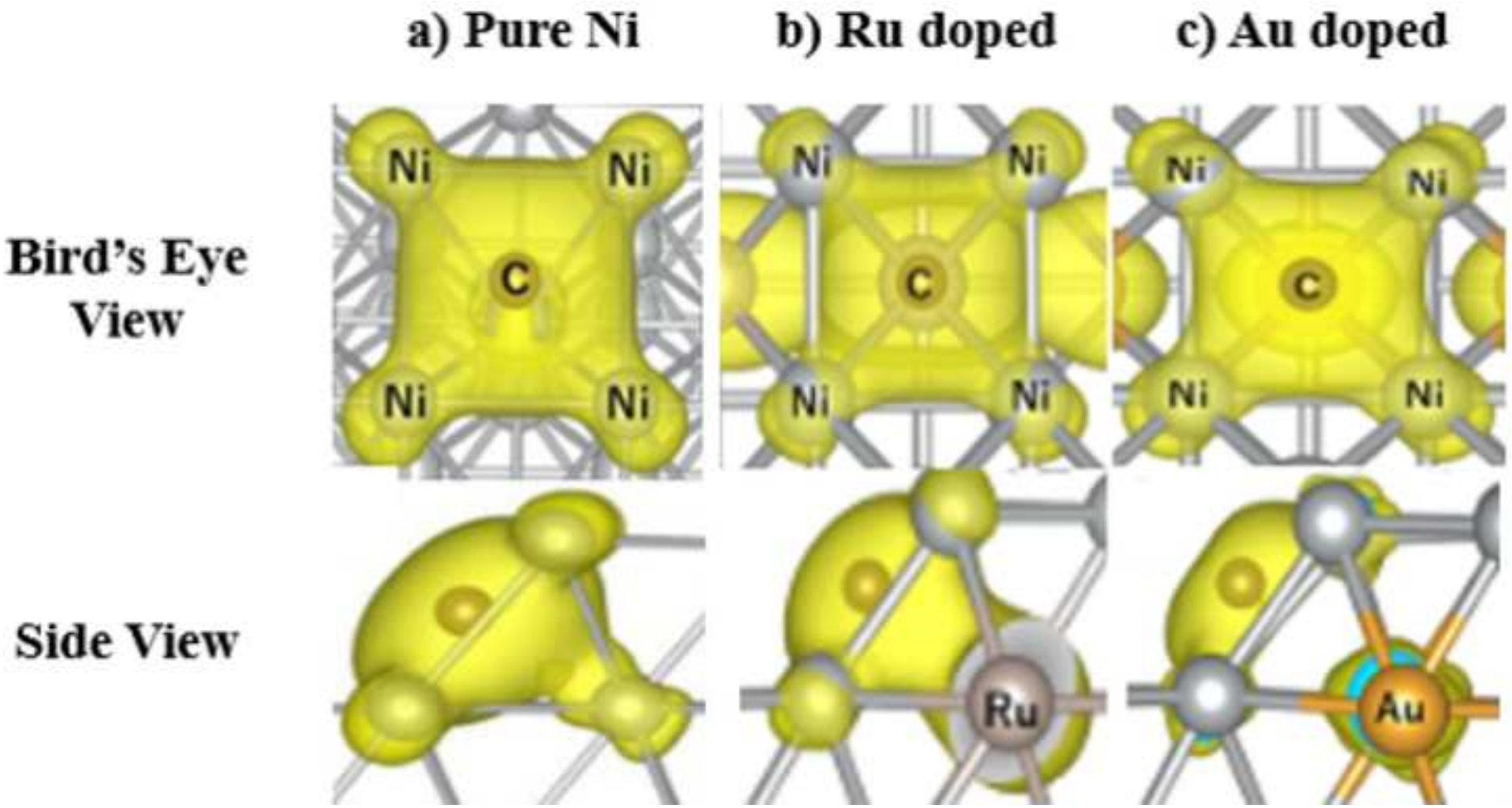

Figure 3

Click here to download high resolution image

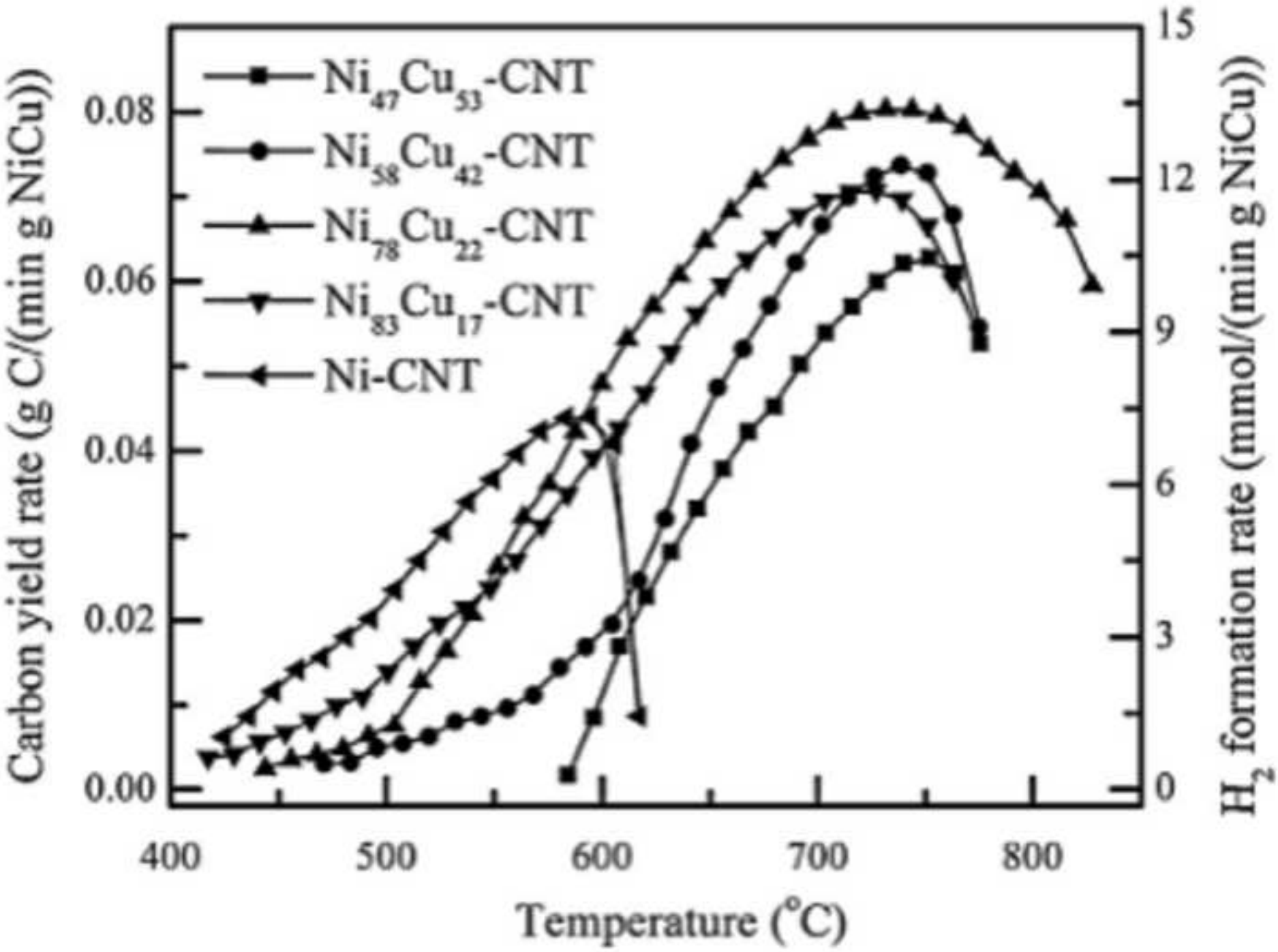

Figure 4

Click here to download high resolution image

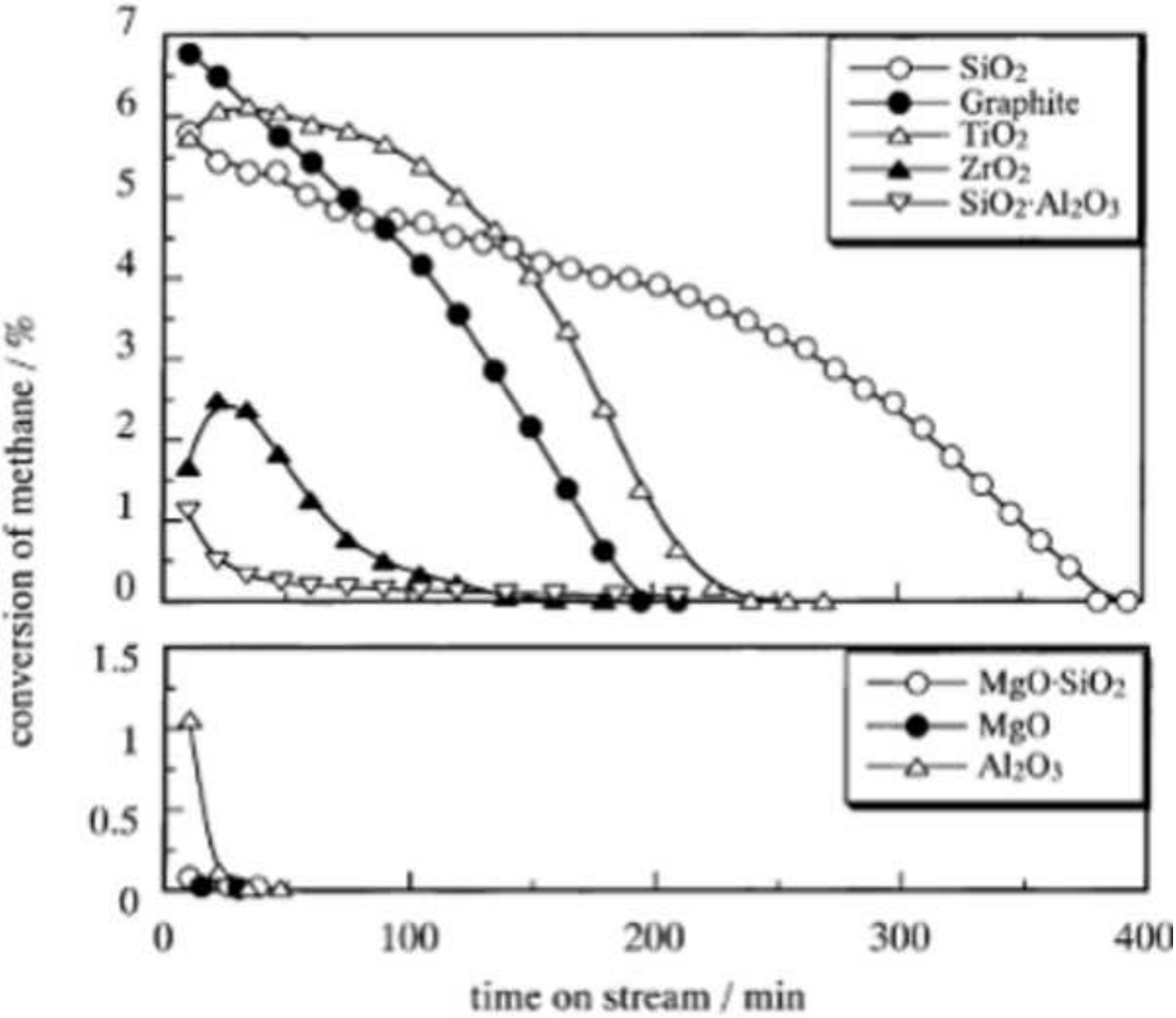

Figure 5

Click here to download high resolution image

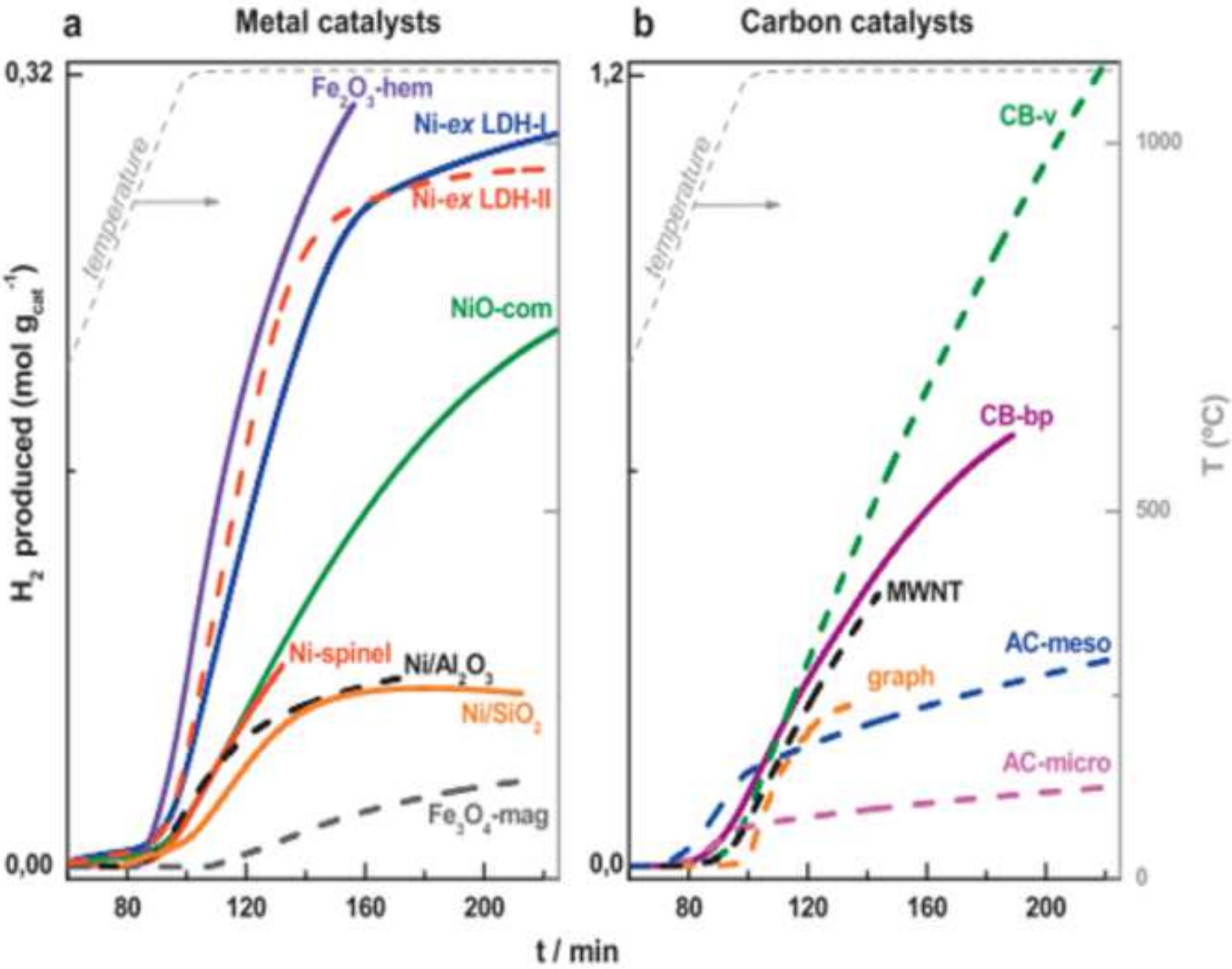

Figure 6

Click here to download high resolution image

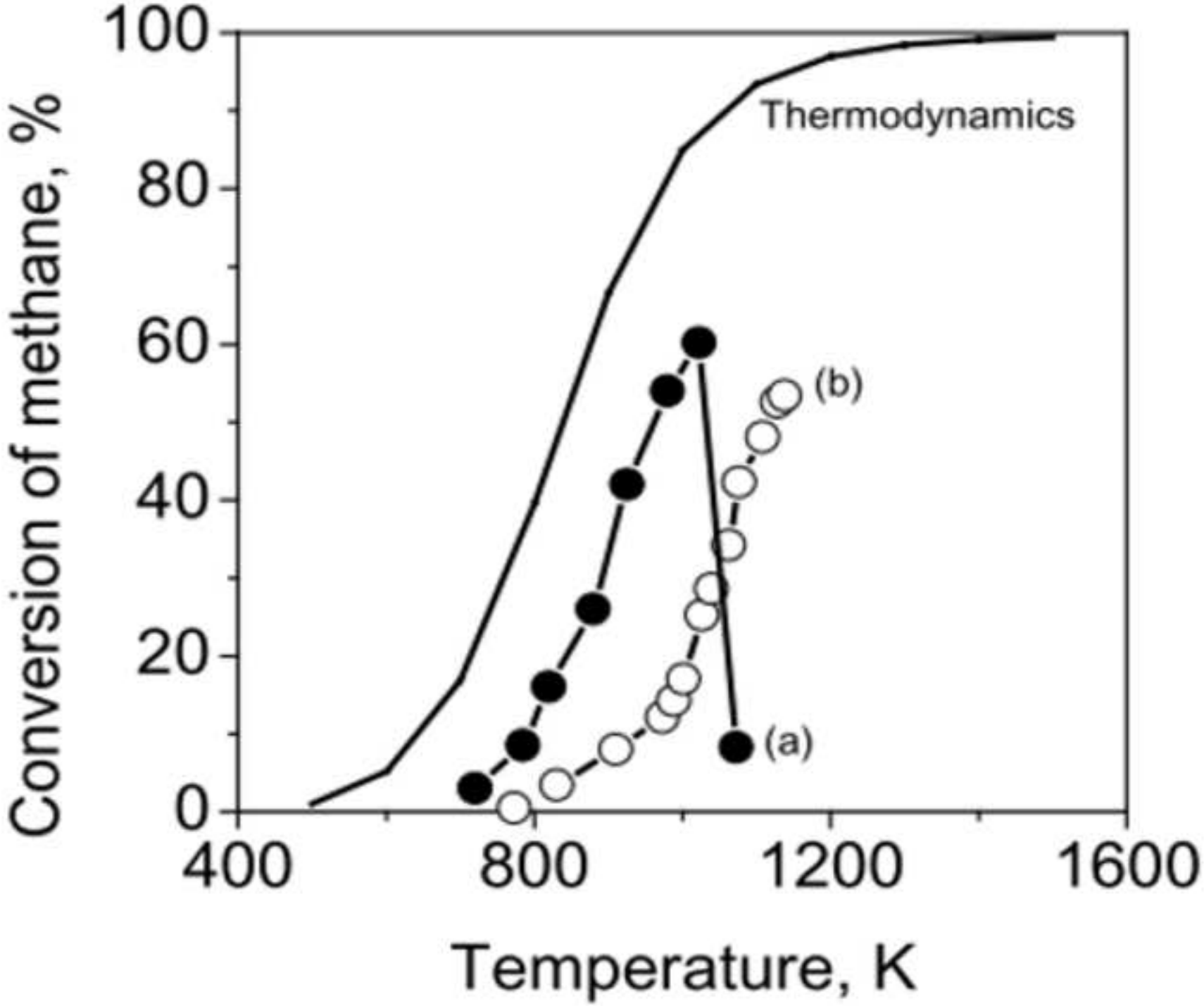

Figure 7

Click here to download high resolution image

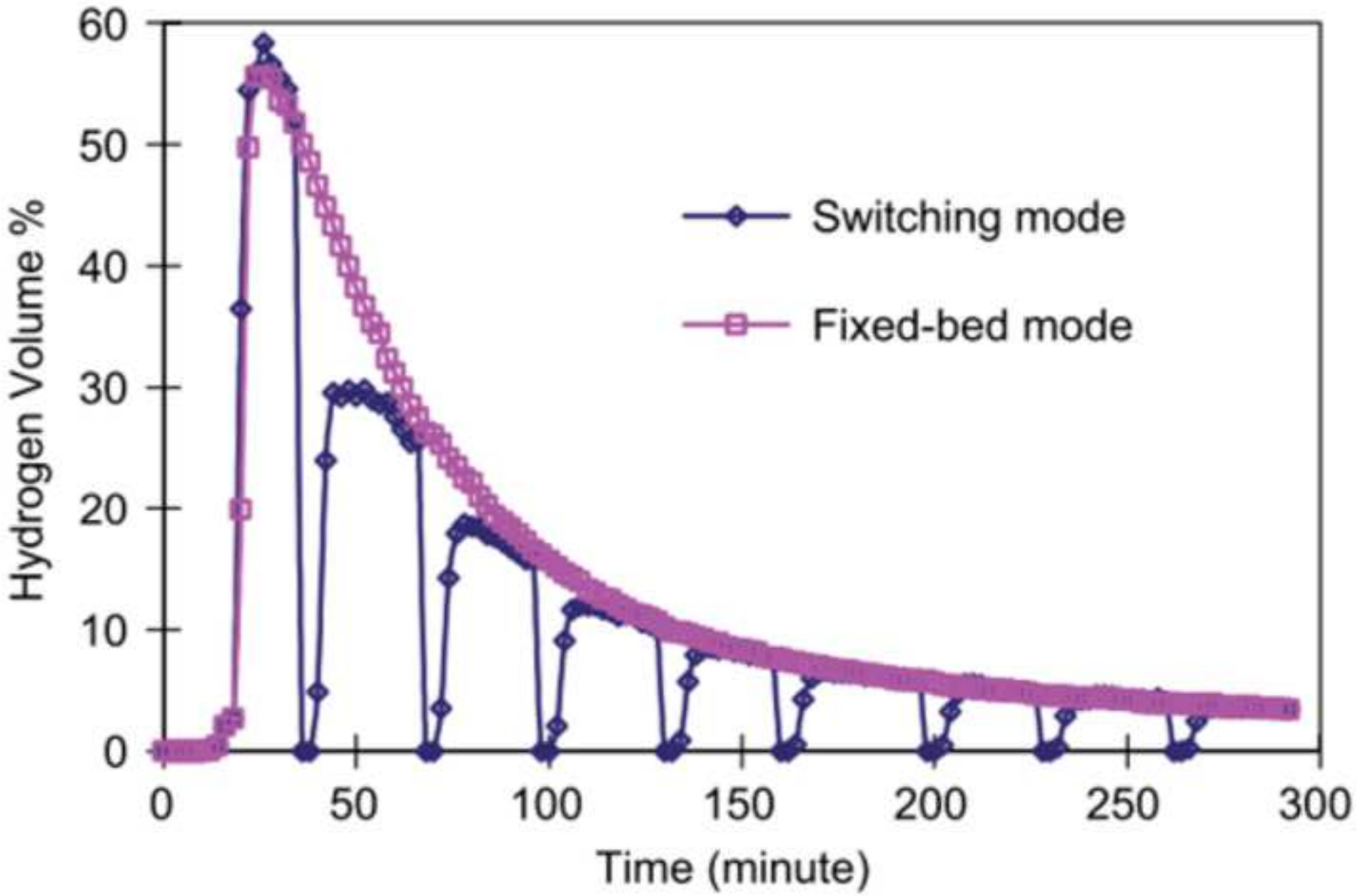

Figure 8

Click here to download high resolution image

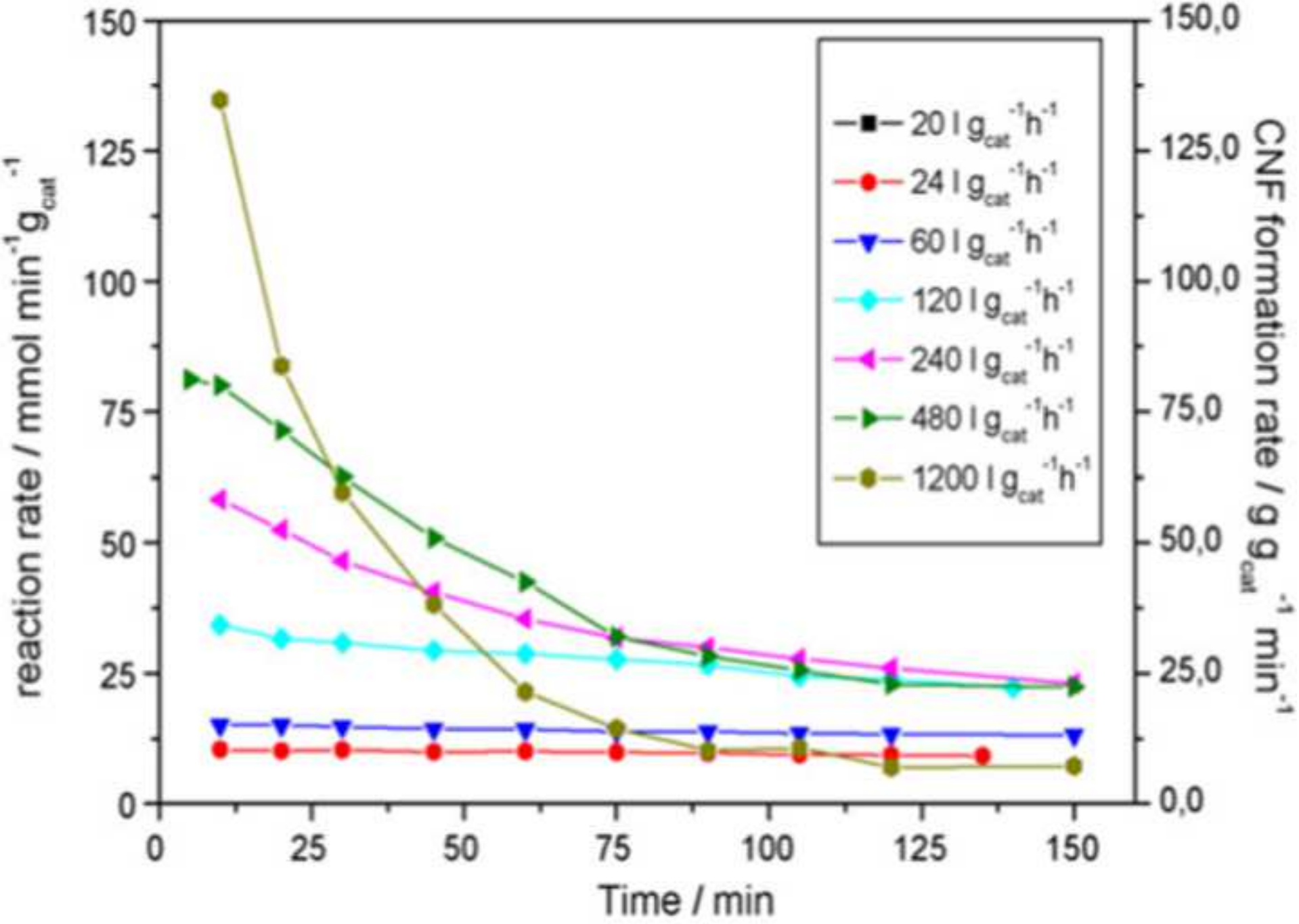

Figure 9

Click here to download high resolution image

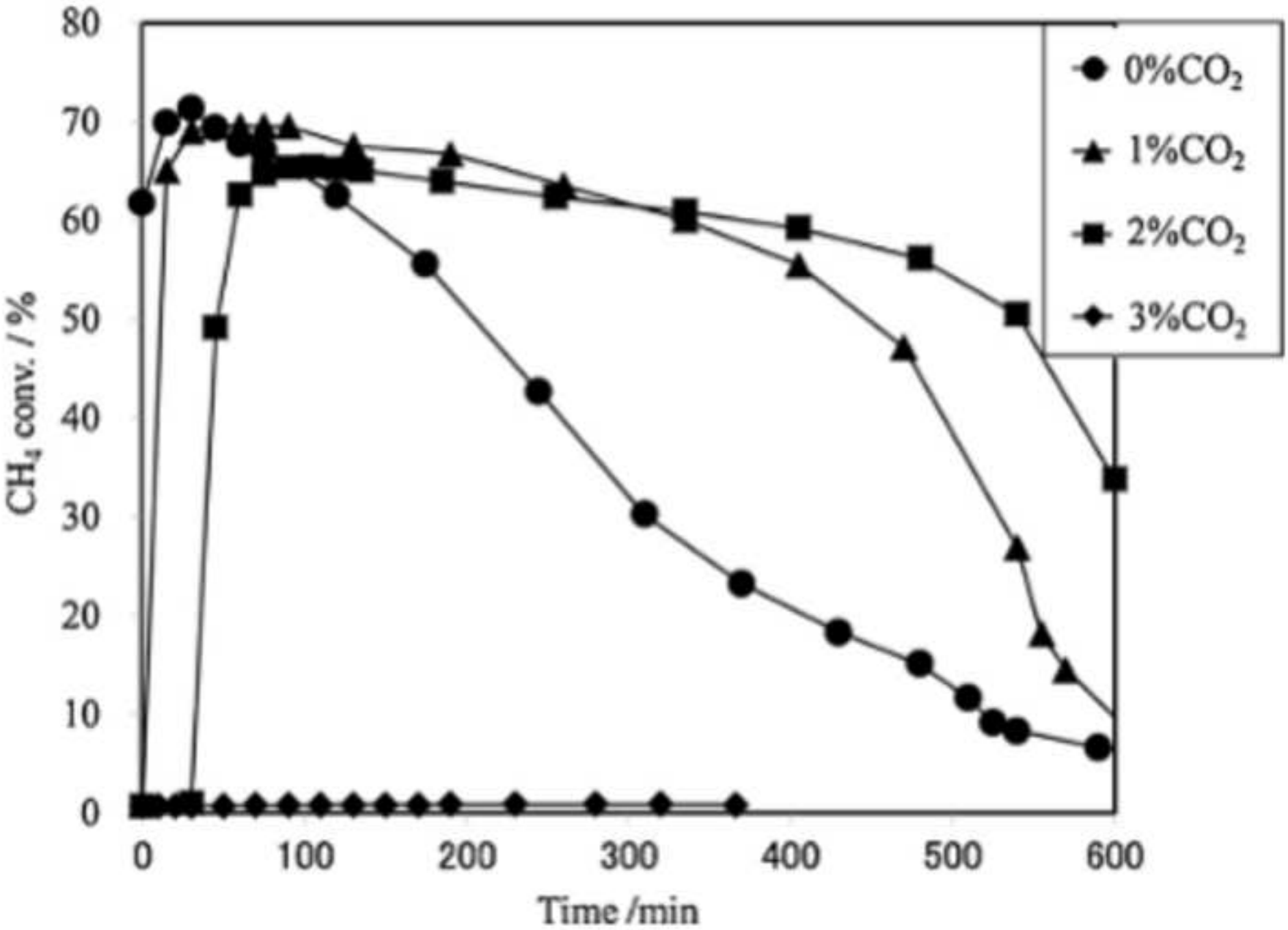

Figure 10
Click here to download high resolution image

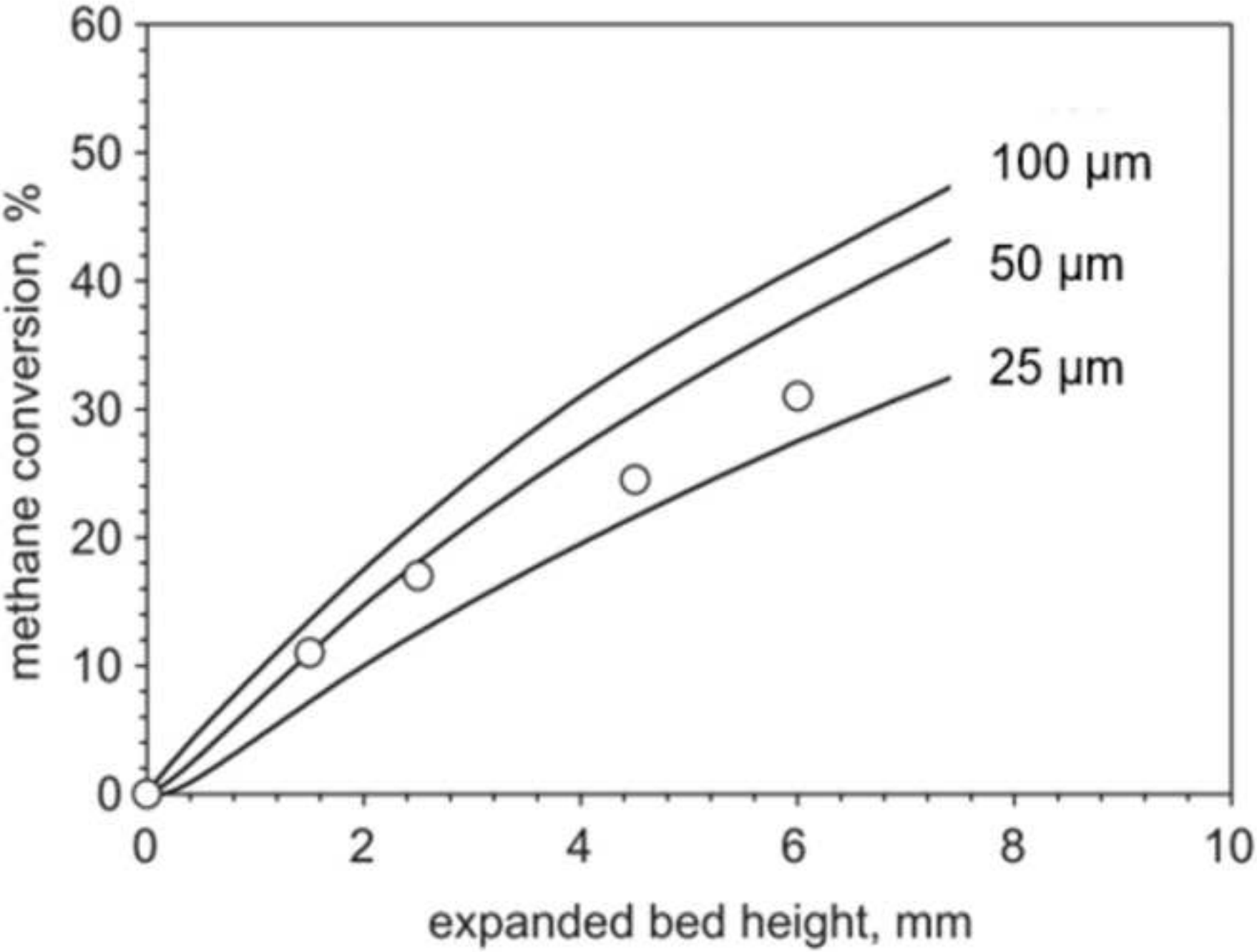

Figure 11

Click here to download high resolution image

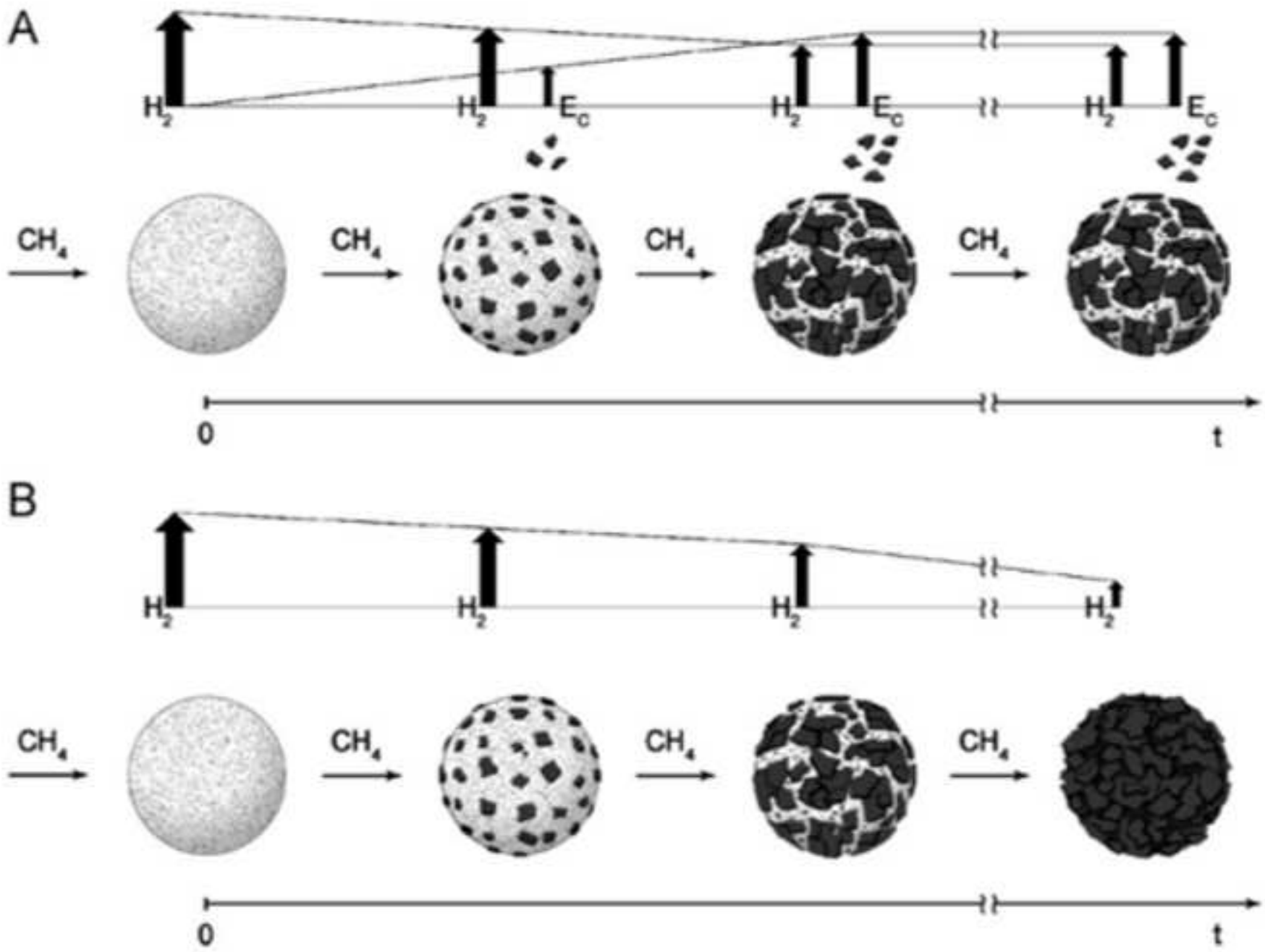

Figure 12

Click here to download high resolution image

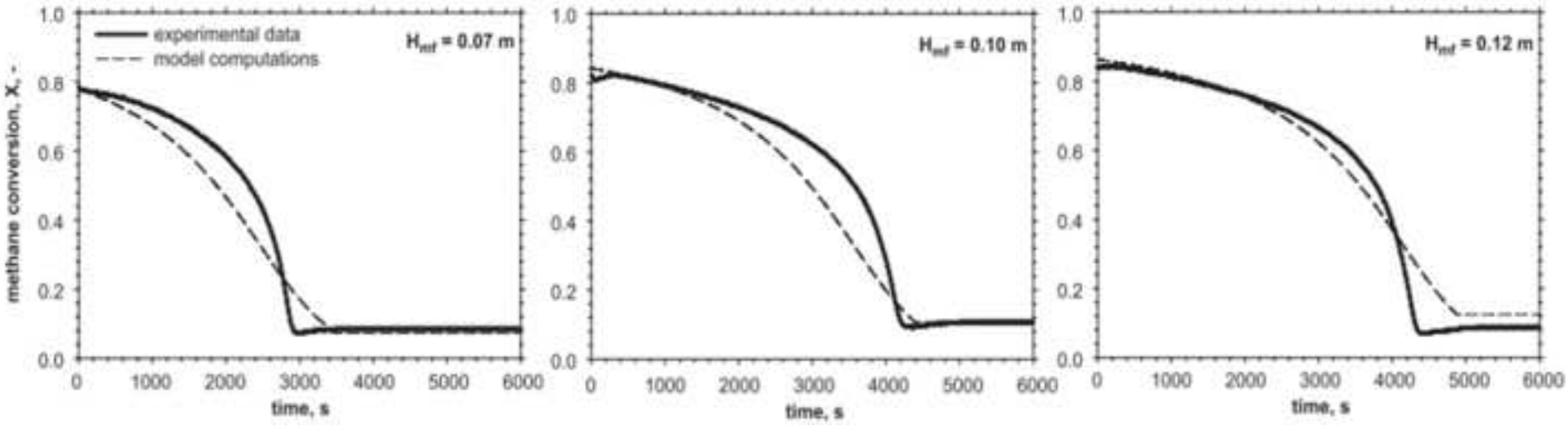

Figure 13

Click here to download high resolution image

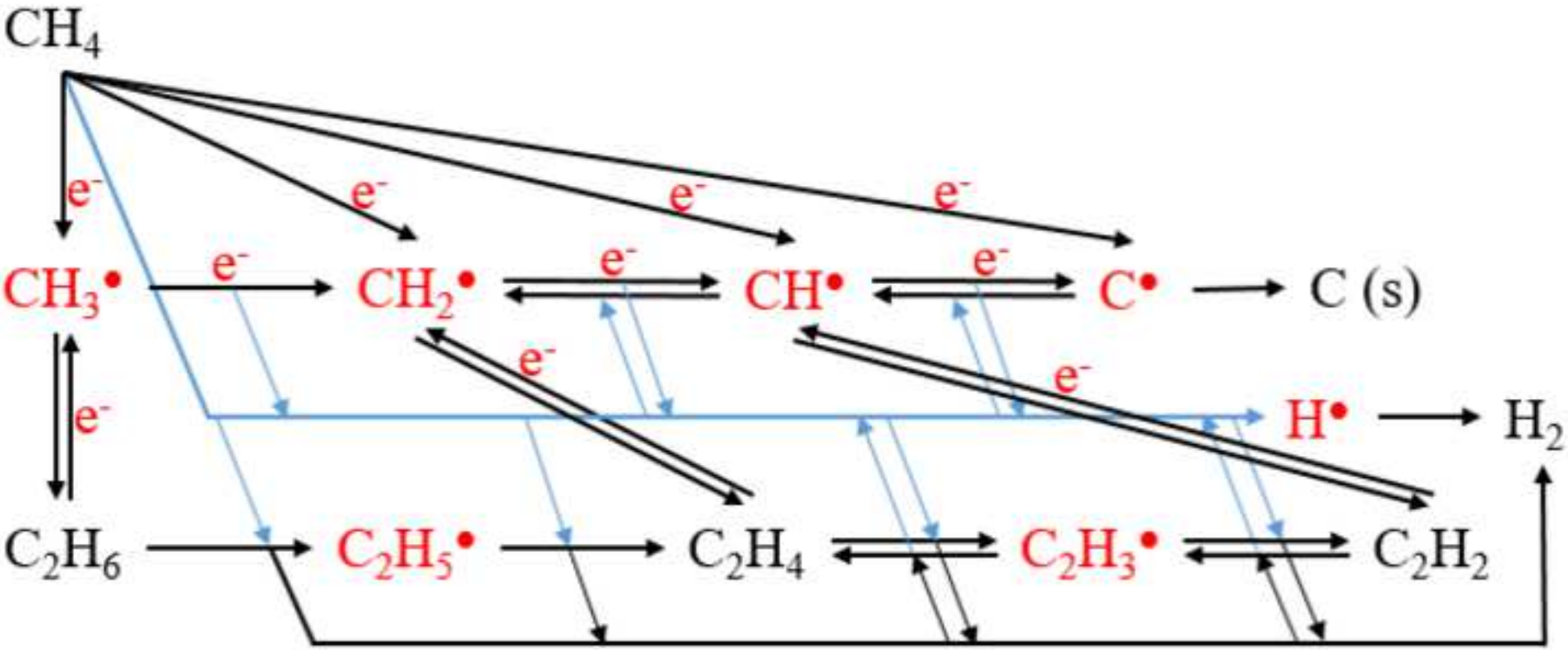

Figure 14

Click here to download high resolution image

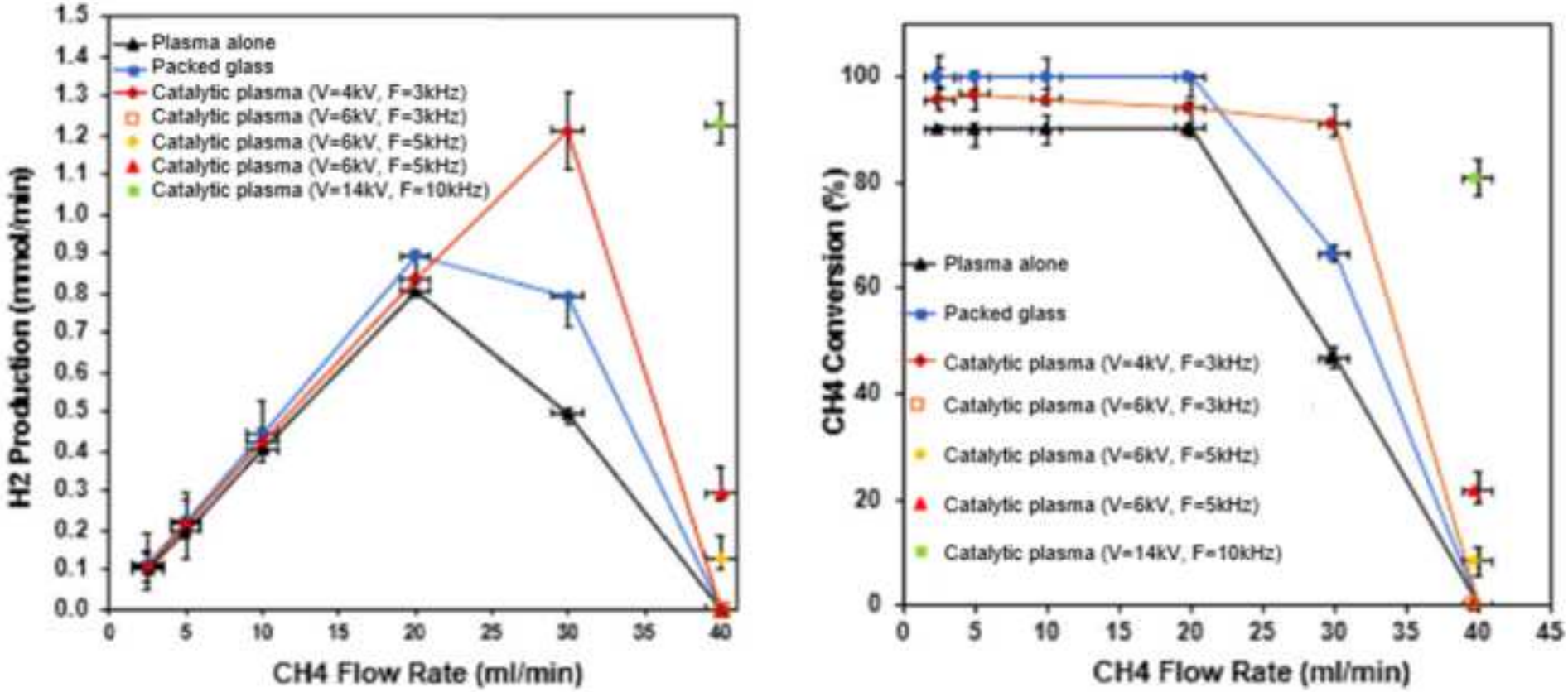

Figure 15

Click here to download high resolution image

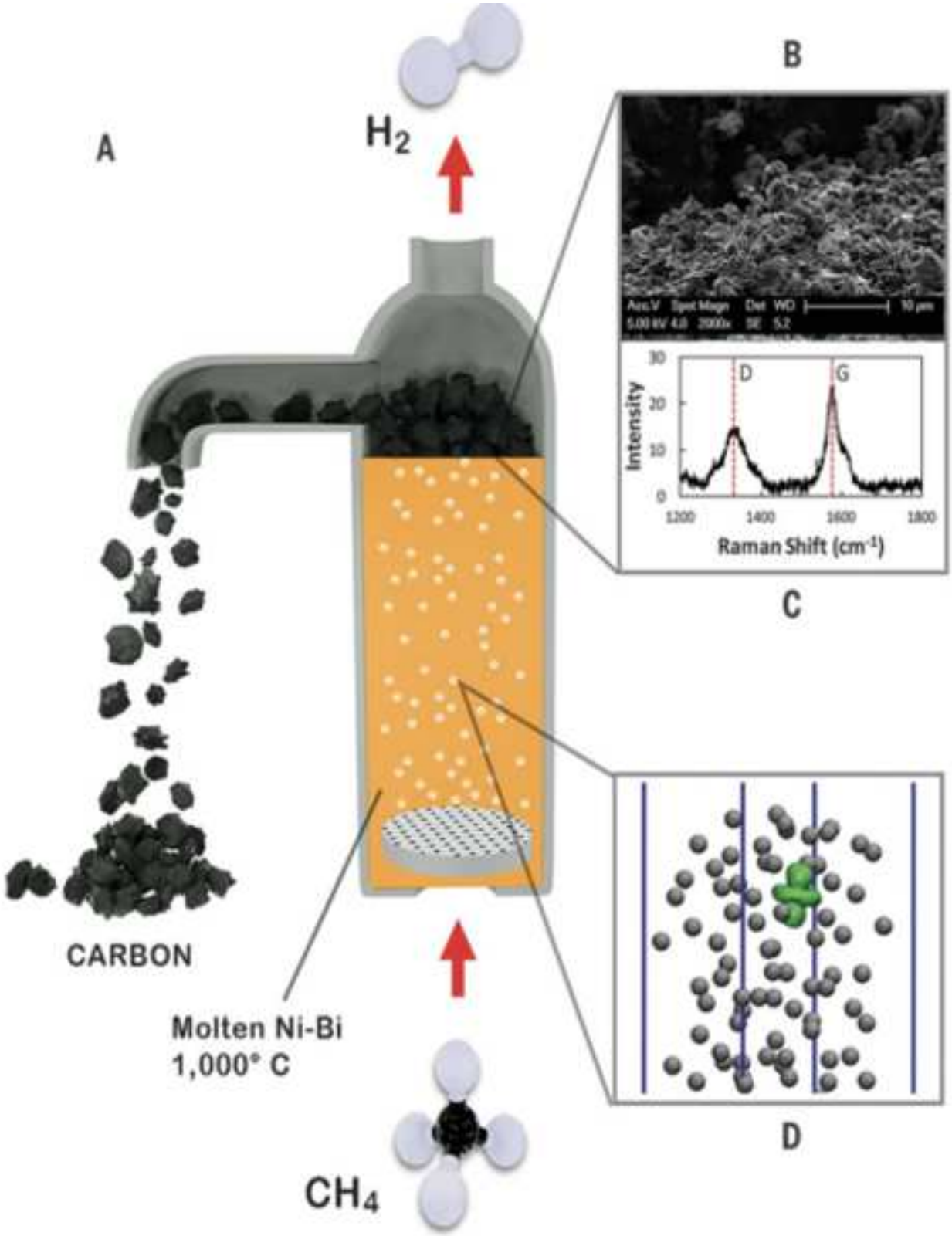

Figure 16

Click here to download high resolution image

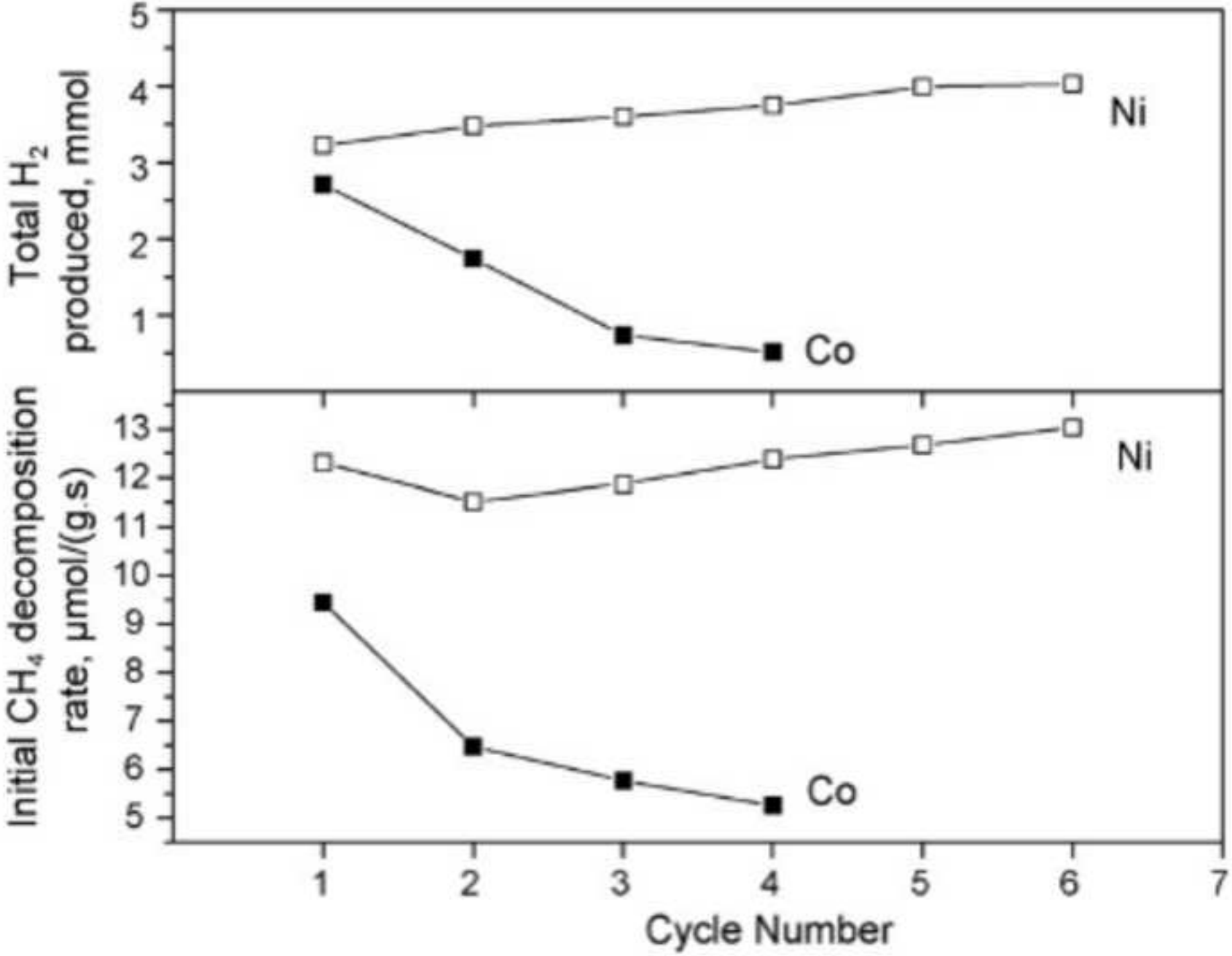

Figure 17

Click here to download high resolution image

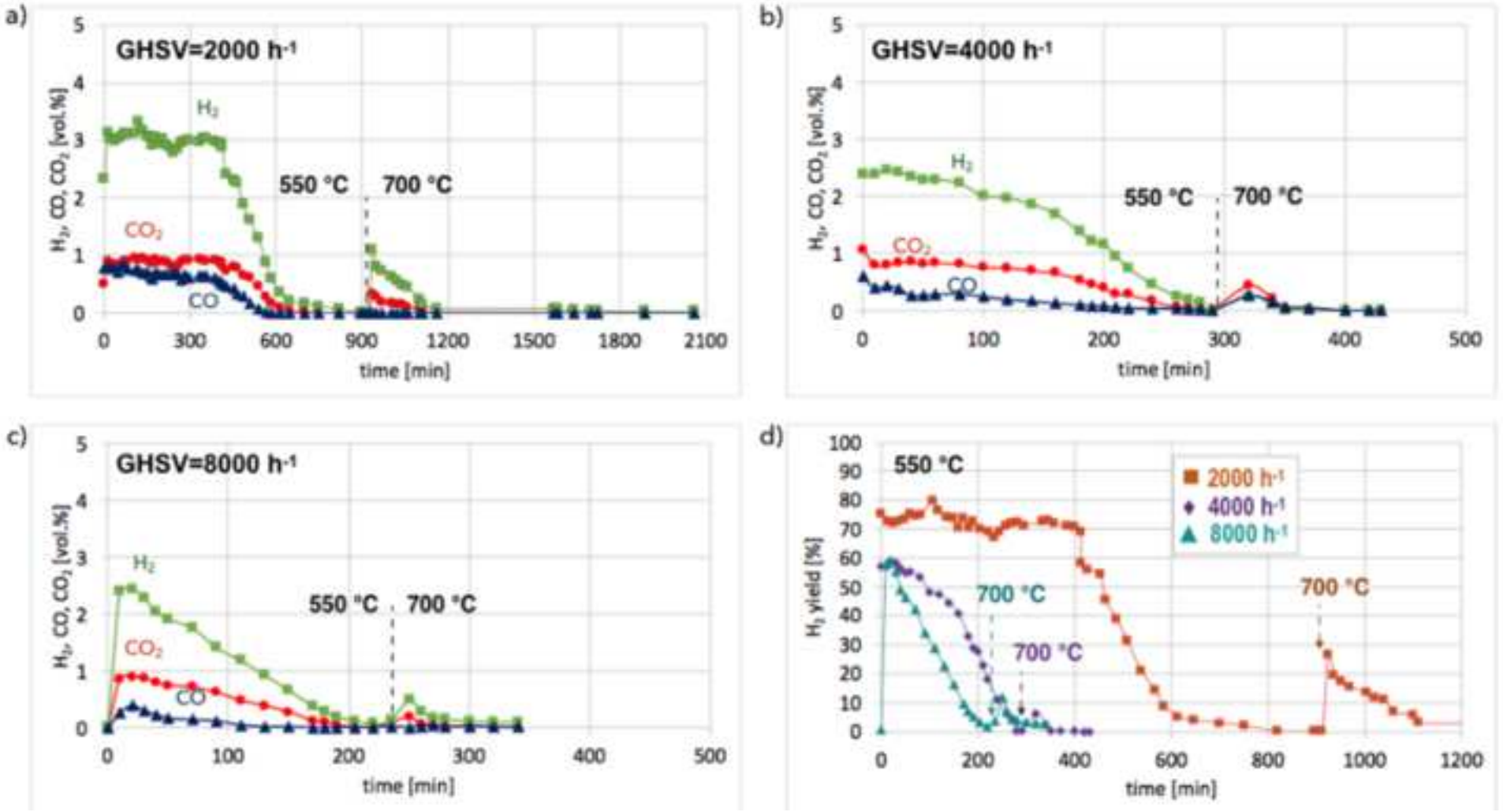

Figure 18

Click here to download high resolution image

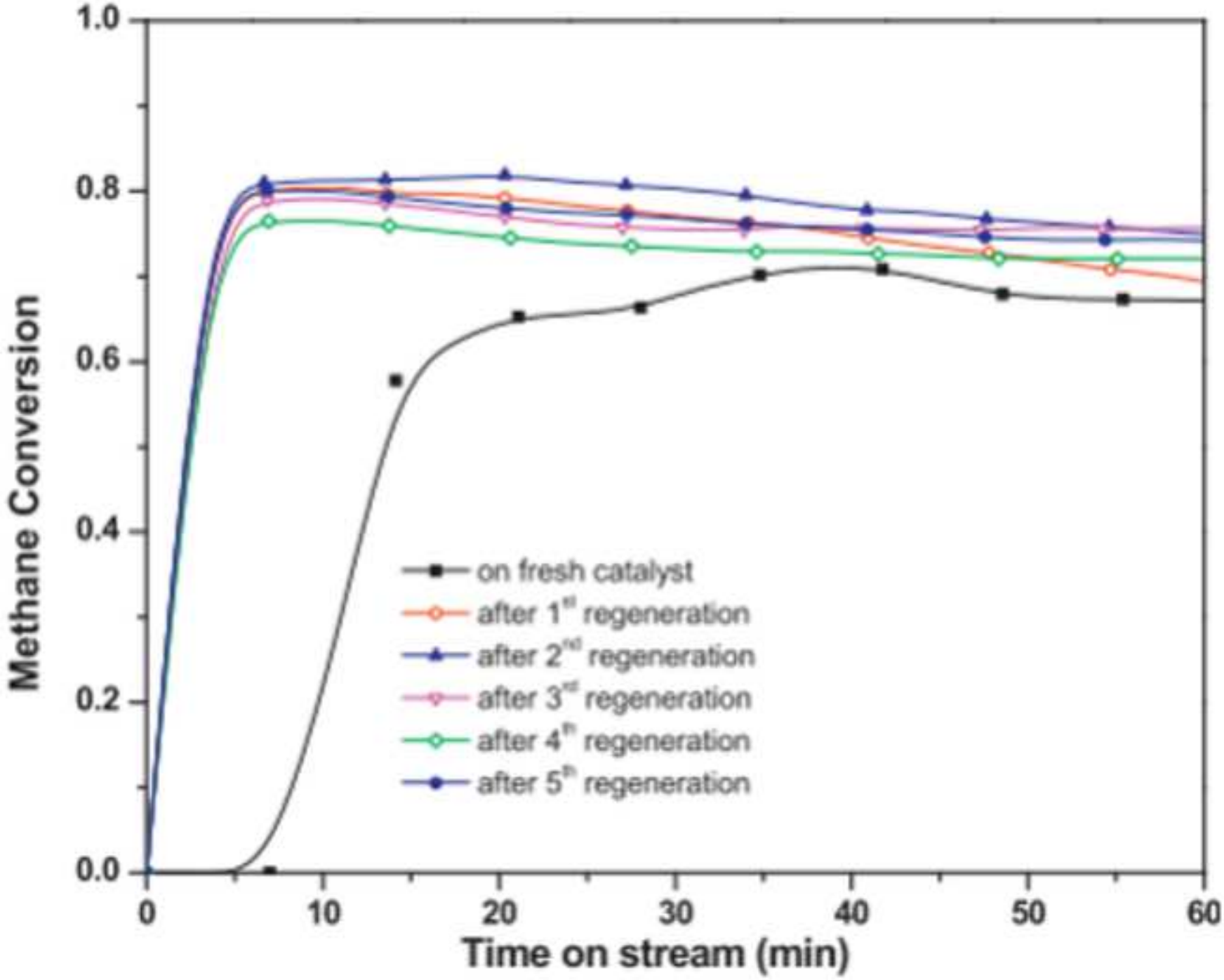

Figure 19
Click here to download high resolution image

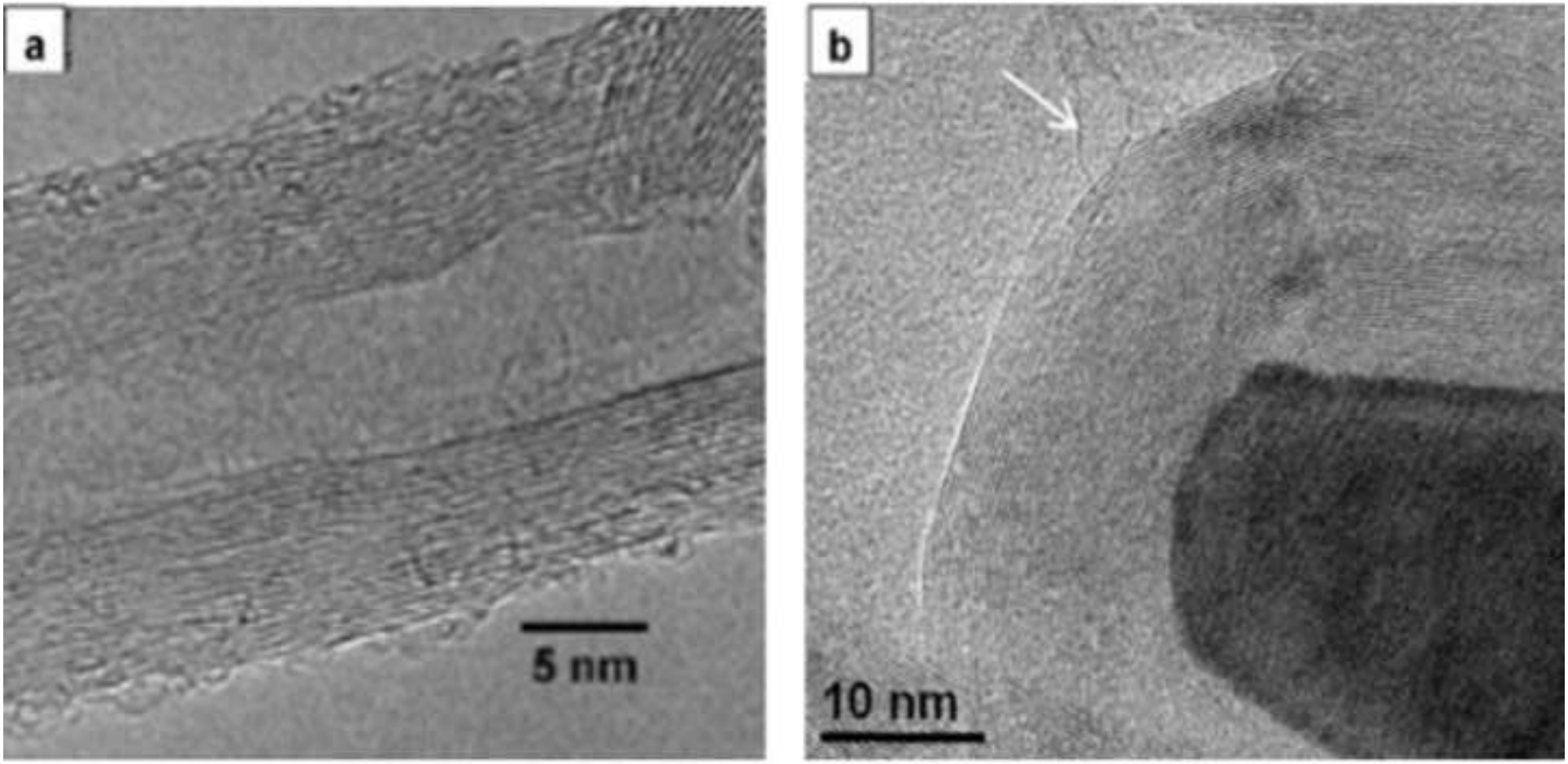

Figure 20
Click here to download high resolution image

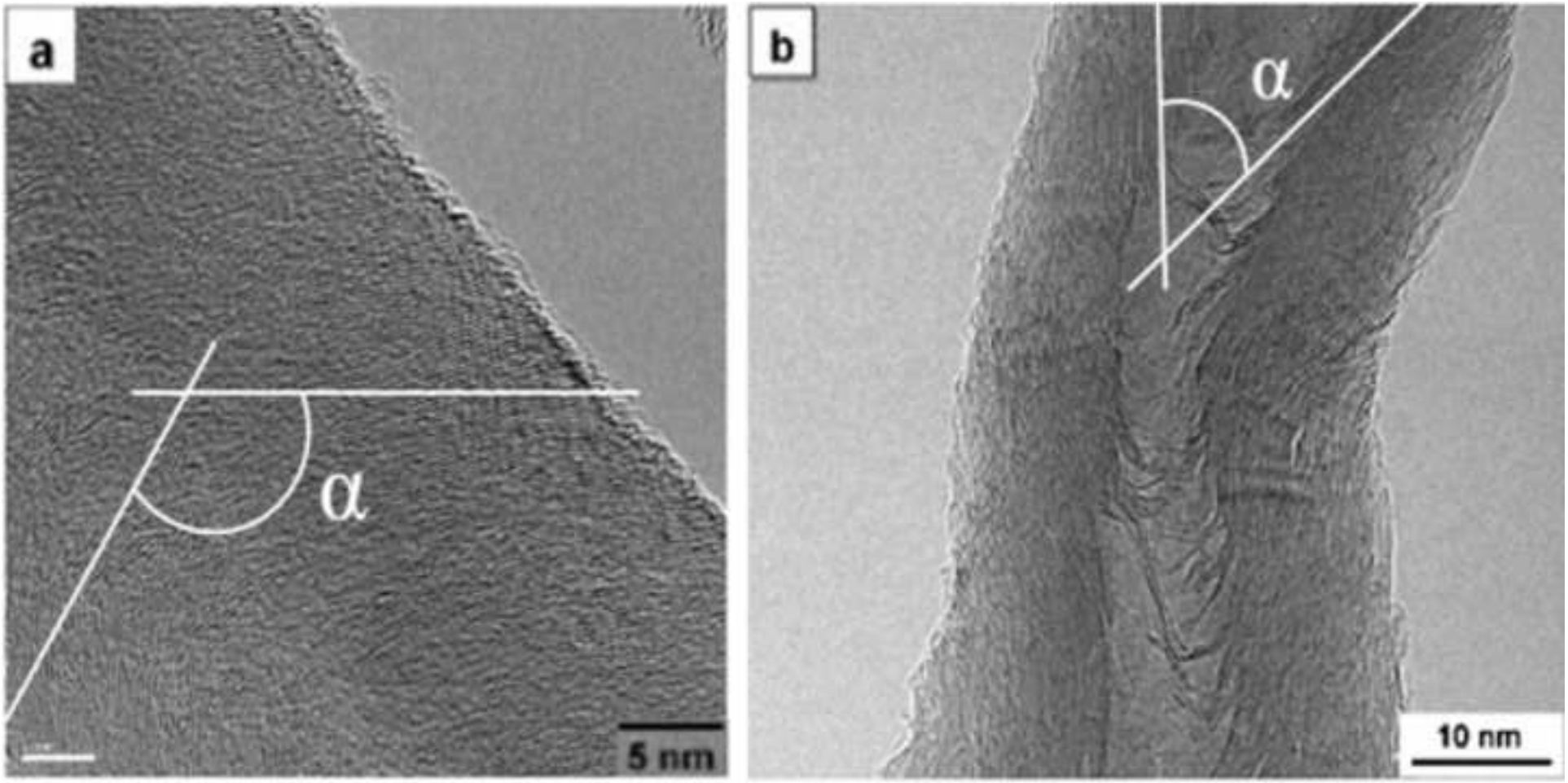

Figure 21
Click here to download high resolution image

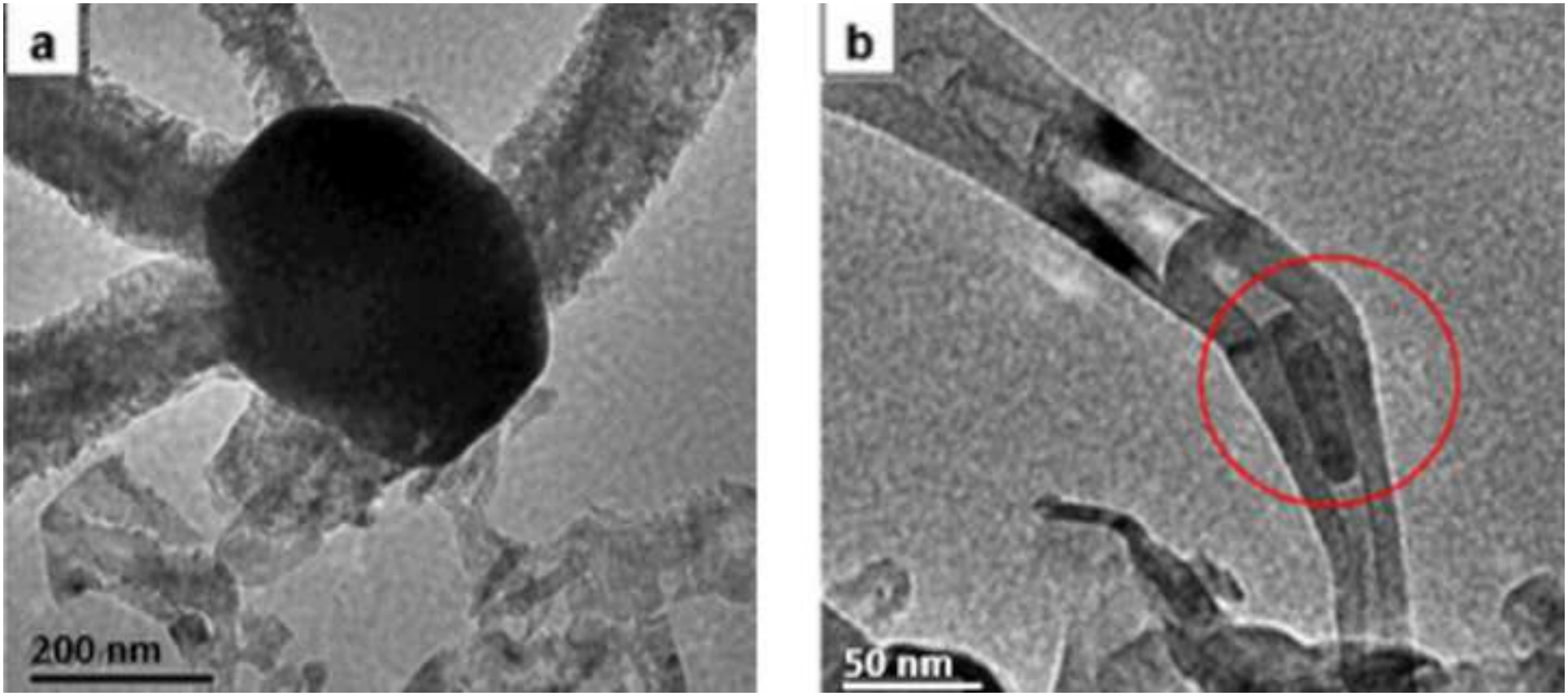

Graphical Abstract

Click here to download high resolution image

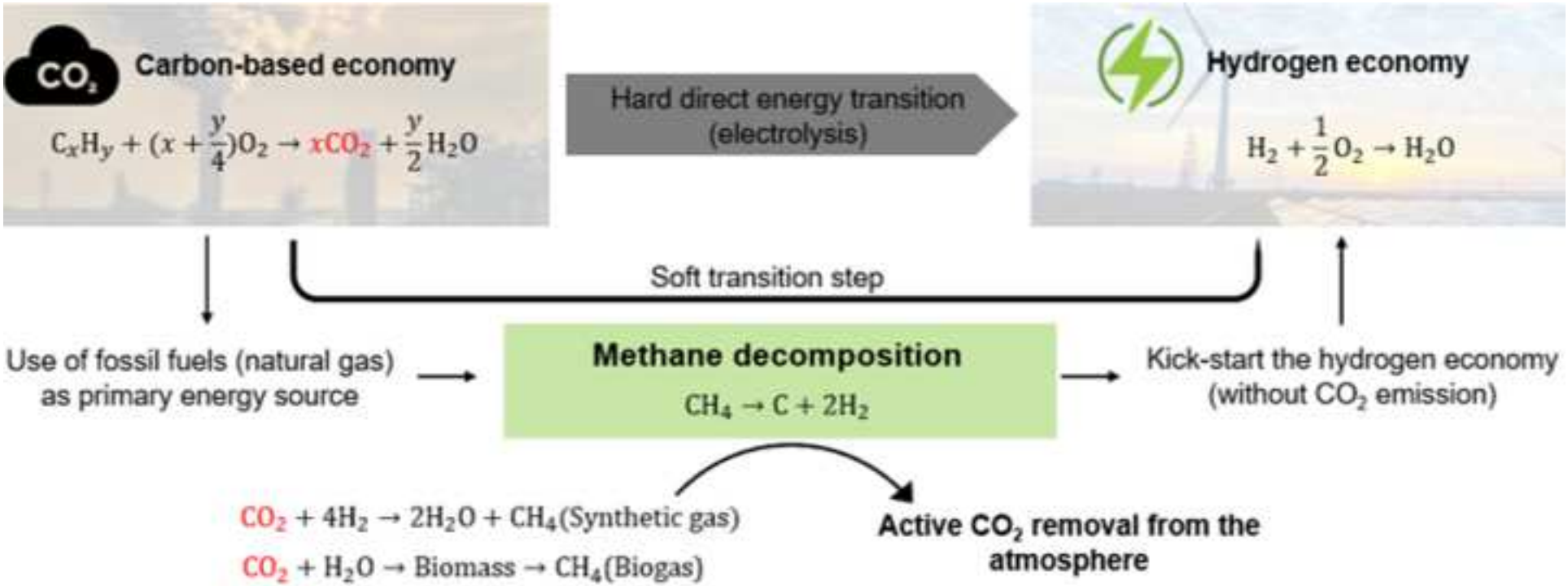

Table 1

Table 1 - Comparing bi and trimetallic metal catalysts.

Catalyst	6 / °C	Catalyst shape	@ / nm	Feed / $g_{CH4}·g_{Cat}^{-1}·h^{-1}$	Activity / $g_{H2}·g_{Cat}^{-1}·h^{-1}$	: G / %	P / h	I % / 9 / $g_C·g_{cat}^{-1}$
50Ni-25Fe/Al_2O_3[62]	650	Fine powder	40	8.58	0.892	42	>210	>562
75Ni-15Cu/ Al_2O_3[102]	625	n/a	20-25	64.29	3.241	20	54	525
82Ni-8Cu/ Al_2O_3[102]	625	n/a	20-25	64.29	2.791	17	62	515
60Ni-25Cu/SiO_2[109]	650	Fine powder	9	64.29	5.333	33	30	480
24Ni-6Cu/MgO[110]	665	Fine powder	38	51.43	3.378	26	45	456
62Fe-8Ni/Al_2O_3[93]	625	n/a	25-50	32.14	0.755	22	64	145
50Ni-10Fe-10Cu/Al_2O_3[108]	750	Slab	20	2.57	0.521	81	10	15.62
15Fe-3Ni/MgO[111]	700	Fine powder	3	2.14	0.386	72	3	3.47
30Fe-15Co/Al_2O_3[112]	700	Slab	5-40	2.14	0.380	71	3	3.42
30Fe-10Ni-5Co/Al_2O_3[112]	700	Slab	5-40	2.14	0.375	70	3	3.38
15Fe-6Co/MgO[111]	700	Fine powder	3	2.14	0.375	70	3	3.38
15Fe-6Mn/MgO[111]	700	Fine powder	5	2.14	0.375	70	3	3.38
30Fe-5Ni-10Co/Al_2O_3[112]	700	Slab	5-40	2.14	0.370	69	3	3.33
30Fe-7.5Ni-7.5Co/Al_2O_3[112]	700	Slab	5-40	2.14	0.359	67	3	3.23
25Ni-25Co/SBA-15[113]	700	Fine powder	20	3.57	0.171	19	5	2.57

Table 2

Table 1 - Pt and Pd doping on metal catalysts used in CMD.

Catalyst	6 / °C	Catalyst shape	@ / nm	Feed / $g_{CH4}·g_{Cat}^{-1}·h^{-1}$	Activity / $g_{H2}·g_{Cat}^{-1}·h^{-1}$	: G / %	P / h	$\frac{I\ \%}{9}$ / $g_C·g_{cat}^{-1}$
Ni/CeO_2[105]	700	Fine powder	50-100	3.21	0.183	23	6	3.30
0.2%wt Pt-Ni/CeO_2[105]	700	Fine powder	30-70	3.21	0.197	25	6	3.55
55Ni-15Cu[106]	600	Fine powder	20	5.14	0.746	58	10	22.37
55Ni-15Cu-4Pd[106]	600	Fine powder	25	5.14	0.771	60	10	23.14

CRediT

Luís Alves: Writing – Original draft preparation. **Vítor Pereira:** Writing – Original draft preparation. **Tiago Lagarteira:** Writing – Reviewing and Editing. **Adélio Mendes:** Writing – Reviewing and Editing, Supervision.

Highlights

- Catalytic methane decomposition is a promising pathway for the energy transition;
- Catalysts and reactor designs have been optimized to increase reaction stability;
- Carbon is a valuable by-product with the potential creation of new markets;
- Catalyst regeneration must be employed and optimized for long-term stability.

RSER Author Checklist Table

Item	Check	Important notes for Authors/Requirement
Article type	Select the single correct article type here and state in brackets the paper word count. x Review article (9898)	Papers will be indexed as Full-length articles, Review articles, Retractions, Corrigendum, Addendum or Editorials as explained above in this GFA.
Manuscript	This is the óentire eô a authors will assess. It is used later to prepare the published article, so it is important that all details required by the GFA are included.	The manuscript should be a single MS Word file or pdf that includes the cover letter, the RSER Author Checklist table and the paper as per the layout in the GFA.
Cover letter	A maximum of two pages, dated and addressed to the Editors stating the name and affiliation of the authors, it should state the following clearly; x Title paper, key findings and why novel and meets the journal scope, x Article type and if relates to a conference special issue. x Any details relating to elements of the work already published as a Preprint/Archiv/Working paper/conference paper etc. or as a thesis or other with a precise explanation, x Any details of funding agencies etc., x Provide a declaration of interest, x List any recommended reviewers, x The corresponding author must sign the Cover letter as the person held responsible for all aspects of the paper during and after the publication process.	Note that the role of the corresponding author is very important as they are responsible for the article ultimately in terms of Ethics in Publishing, making sure that the GFA is adhered to, informing readers of any relationships with organisations or people that may influence the work inappropriately as discussed in the GFA, all the content of the article and that the Proof is correct. It is very difficult if not impossible to edit a paper once published. Most mistakes in articles occur when corresponding authors are changed after/during acceptance; examples include leaving out acknowledgements of funding agencies and the full and correct author affiliations.
Layout of paper	The elements/headings listed below should appear in the order below in the paper: x Title x Author details x Abstract x Highlights x Keywords x Word Count x List of abbreviations including units and nomenclature x 1.0 Introduction x 2.0 Material and methods x 3.0 Theory/calculation x 4.0 Results x 5.0 Discussion x 6.0 Conclusion x Acknowledgements x List of References	Note read carefully the specific details of each element/heading in this GFA. The main headings i.e. 2.0 to 6.0 can vary from article to article, but all articles must include the title, author details, abstract, keywords, highlights, word count and list of abbreviations on page 1 of the paper.
English, grammar and syntax	Yes	The authors must proof read and check their work. This is NOT the role of the editorial team, reviewers or the publishing team. Some guidance on English, grammar and syntax is provided in this GFA below, but it is ultimately the authorôs
Title	Yes	The title should not include acronyms or abbreviations of any kind. Excessive use of capitals letters should also be avoided.
Author names and affiliations	Yes	The names of the authors in order of contribution or supervision or seniority depending on the funding agency/field requirements should be presented below the title of the article as follows: Last, First by initial e.g. Foley, A.M.[1], Leahy, P.[2] 1 = School of Mechanical & Aerospace Engineering, Queenôs University Belfa 2 = School of Engineering, University College Cork, Ireland
Corresponding author	Beside the name of the corresponding author there is an asterix and footnote.	The corresponding author must be denoted in the article by an asterix superscript beside their name and a

		footnote, as follows: Foley, A.M.[1,*] * = corresponding author details, a.foley@qub.ac.uk Note that only one corresponding author can be identified.
Highlights	These should be inserted as requested in the article and uploaded as a separate file.	Details on highlights are in the GFA below.
Graphical abstract	Yes	Note submitting a graphical abstract is at the discretion of the authors. It this is not required by RSER.
Copyright	Yes Figure 3 ïFigure 16 Figure 18 ïFigure 21	Authors are responsible for arranging copyright for any already published images, figures, graphs and tables borrowed from third parties. Citing a source is not enough, in fact this is an Ethics in Publishing issue. Guidance on arranging copyright is provided in the GFA below.
Referencing style	Yes ñR e n e w a b l e a n d S u s t a i n	The preferred journal style is Vancouver (i.e. [1], [2] etc., see details on using in this GFA. All references must be numbered chronologically starting at 1 in square brackets in the paper and the list of references. All references mentioned in the Reference List are cited in the text, and vice versa.
Single column	Yes	Note an article submitted in two column format will be automatically rejected.
Logos/emblems etc.	Yes	A paper must NOT be submitted with Elsevier logos/layout as if already accepted for publication.
Embed graphs, tables and figures/other images in the main body of the article	Yes	Although you will be required to submit all images, images MUST appear embedded in the main body of the article where they are to appear in the final published article.
Figures/Graphs/other images	Yes	Any captions for graphs should be below the graph in the Manuscript. Note that all figures must be individually uploaded as separate files in the correct format, check format requirement in this GFA. Ensure all figure citations in the text match the files provided.
Tables	Yes	Any captions for tables should be above the graph in the Manuscript. Note that all figures must be individually uploaded as separate files in the correct format, check format requirement in this GFA. Ensure all table citations in the text match the files provided.
Line numbering	Yes	RSER journal uses automatic line numbering, so authors must submit their source files without line numbers.
Acknowledgements	Yes	The questions authors need to ask themselves, when preparing their acknowledgement are as follows: Was this work funded by a government agency, industry or other philanthropic organisation? If yes, the corresponding author must check and include any grant/award/funding details. Were any data sources, models, images used or provided by others, who did not contribute to the article? If yes, then it is to good practice to name and thank them individually. Did any colleagues, friends or family proof read your work? If yes then it is also polite to mention them.
Ethics in Publishing	Yes	It is vital that all authors read our requirements for Ethics in Publishing. Once your name is on the article you all are responsible for any plagiarism issues. Note that a corresponding author must email the Editor in Chief to get approval for any changes in authorship before any Proof is finalised. A change in name of the corresponding author must also be done with the written consent of the author and the Editor in Chief nominated by the existing corresponding author.
Ethical Statement	Upload an Ethical Statement or alternatively state in the Cover Letter.	Read details in this GFA,

***Declaration of Interest Statement**